New Book Cover Design for JOSTT 8

Journal of Science & Technology in the Tropics

Volume 8 Number 1 June 2012

Journal of Science & Technology in the Tropics

JOSTT

DEDICATED TO THE ADVANCEMENT OF SCIENCE AND TECHNOLOGY RELATED TO THE TROPICS

Journal of Science & Technology in the Tropics

Volume 8 Number 1 June 2012

Volume 8 Number 1
June 2012

ISSN 1823-5034

9 771823 503009

AKADEMI SAINS MALAYSIA

COSTAM

Journal of
Science &
Technology
in the Tropics
Volume 8 Number 1 June 2012

CONTENTS

INSTRUCTIONS TO CONTRIBUTORS

JOSTT is a multi-disciplinary journal. It publishes original research articles and reviews on all aspects of science and technology relating to the tropics. All manuscripts are reviewed by at least two referees, and the editorial decision is based on their evaluations.

Manuscripts are considered on the understanding that their contents have not been previously published, and they are not being considered for publication elsewhere. The authors are presumed to have obtained approval from the responsible authorities, and agreement from all parties involved, for the work to be published.

Submission of a manuscript to JOSTT carries with it the assignment of rights to publish the work. Upon publication, the Publishers (COSTAM and ASM) retain the copyright of the paper.

Manuscript preparation

Manuscripts must be in English, normally not exceeding 3500 words. Type double spaced, using MS Word, on one side only of A4 size with at least 2.5 cm margins all round. Number the pages consecutively and arrange the items in the following order: title page, abstract, key words, text, acknowledgements, references, tables, figure legends.

Title page

Include (i) title, (ii) names, affiliations and addresses of all authors, (iii) running title not exceeding five words, and (iv) email of corresponding author.

Abstract and key words

The abstract, not more than 250 words, should be concise and informative of the contents and conclusions of the work. A list of not more than five key words must immediately follow the abstract.

Text

Original research articles should be organized as follows: Introduction, Materials and Methods, Results, Discussion, Acknowledgement, References. The International System of Units (SI) should be used. Scientific names and mathematical parameters should be in italics.

References

References should be cited in the text as numbers enclosed with square [ ] brackets. The use of names in the text is discouraged. In the reference section, the following examples should be followed:

1. Yong H.S., Dhaliwal S.S. and Teh K.L. (1989) A female Norway rat, *Rattus norvegicus,* with XO sex chromosome constitution. *Naturwissenschaften* **76**: 387-388.
2. Beveridge W.I.B. (1961) *The Art of Scientific Investigation*. Mercury Book, London.
3. Berryman A.A. (1987) The theory and classification of outbreaks. In Barbosa P. and Schultz J.C. (eds.) *Insect outbreaks* pp. 3-30. Academic Press, San Diego.

Tables

Tables should be typed on separate sheets with short, informative captions, double spacing, numbered consecutively with Arabic numerals, and do not contain any vertical lines. A table should be set up to fit into the text area of at most the entire page of the Journal.

Illustrations

Black-and-white figures (line drawings, graphs and photographs) must be suitable for high-quality reproduction. They must be no bigger than the printed page, kept to a minimum, and numbered consecutively with Arabic numerals. Legends to figures must be typed on a separate sheet. Colour illustrations can only be included at the author's expense.

Proofs and reprints

Authors will receive proofs of their papers before publication. Order for reprints must be made when returning the proofs.

Submission

Manuscripts (including all figures but not original artwork), together with a CD version of the text, should be submitted to:

The Editorial Office
Journal of Science and Technology in the Tropics
Academy of Sciences Malaysia
902-4 Jalan Tun Ismail
50480 Kuala Lumpur, Malaysia

E-mail: jostt@akademisains.gov.my

JOSTT is listed in Scopus

EDITORIAL

The International Year of Science

The year 2012 is the United Nations International Year of Science. What does this mean? It means that the United Nations Assembly had declared that 2012 shall be an International Year of Science when science would be celebrated by all nations under the United Nations. It is the hope of the United Nations that all its agencies related to science and technology shall develop programmes to promote awareness and appreciation of science as well.

UN Agencies such the United Nations Educational, Scientific and Cultural Organization (UNESCO), the Food and Agricultural Organization (FAO) and the United Nations Environmental Programme (UNEP) have pledged to give greater attention to the scientific aspects of their respective mandates. Whether this will translate to greater funding for programmes that can benefit member states remain to be seen.

Malaysia also has announced its pledge to give greater emphasis to science this year and the Ministry of Science, Technology and Innovations (MOSTI) is expected to launch the year officially soon. Institutions under MOSTI as well as in other Ministries, particularly the Ministry of Education and Ministry of Higher Education, should develop programmes to promote awareness of science in a more concerted manner. However, as science permeates all activities of human population, MOSTI should set up a coordinating mechanism to ensure that all programmes are coordinated between all Ministries and Departments.

At the same time Non-Governmental Organizations should also develop programmes that highlight science within their own activities and Government should consider giving seed money to NGOs to encourage their involvement. Finally there is the private sector that should be harnessed to promote this Year of Science. Together we all can make an impact in creating greater awareness of the importance of science in our everyday lives, the need to invest more into R&D and to inculcate greater interest amongst school children to study science and to take up science as a career.

It is equally important that whatever programmes that we have initiated in 2012, in conjunction with the International Year of Science, should not stop when the year ends. The efforts to encourage school children to study science and to take up science as a career, to encourage public to appreciate the importance of science in nation building and to encourage both public and private sectors to invest more into R&D must continue. The fact that only 32% of school going children take up science is a case of serious concern. Whatever programmes initiated must be well monitored and be sustainable. We, in the Academy of Sciences Malaysia and COSTAM will be most willing to play our part in this important mission.

Dr Salleh Mohd. Nor and Dr Ong Eng Long
Co-Chairman JOSTT

Journal of Science and Technology in the Tropics (2012) 8: 5-19

Redescriptions of *Armigeres annulipalpis* and *Armigeres flavus* (Diptera: Culicidae) from Sarawak, Malaysia

Takako Toma[1], Ichiro Miyagi[1, 2*], Takao Okazawa[3], Yukiko Higa[4], Siew Fui Wong[5], Moi Ung Leh[5] and Hoi Sen Yong[6]

[1] Laboratory of Medical Zoology, School of Health Sciences, Faculty of Medicine, University of the Ryukyus, Nishihara, Okinawa, 903-0215 Japan
[2] Laboratory of Mosquito Systematics of Southeast Asia and Pacific, c/o Ocean Health Corporation, 4-21-11, Iso, Urasoe, Okinawa, 901-2132 Japan
[3] International Student Center, Kanazawa University, Kakuma, Kanazawa, Ishikawa, 920-1192 Japan
[4] Department of Vector Ecology and Environment, Institute of Tropical Medicine (NEKKEN), Nagasaki University, Sakamoto 1-12-4, Nagasaki, 852-8523 Japan
[5] Sarawak Museum, Department, 93566, Kuching, Sarawak, Malaysia
[6] Institute of Biological Sciences, University of Malaya, 50603 Kuala Lumpur, Malaysia
(*E-mail: topmiyagii@ybb.ne.jp)

Received 29-02-2012; accepted 01-04-2012

Abstract Redescriptions and illustrations of the pupae and larvae of *Armigeres* (*Leicesteria*) *annulipalpis* (Theobald) and *Ar.* (*Lei.*) *flavus* (Leicester) were made based on the specimens collected in Sarawak, Malaysia. Illustrations of abdominal ornamentation of adults and male genitalia were also given. The larvae of *Ar. annulipalpis* were found mainly in water accumulation of green bamboo stumps and splits. *Armigeres flavus* was commonly found in bamboo stumps and containers with very turbid water in mountain forests.

Keywords *Armigeres annulipalpis* – *Armigeres flavus* – subgenus *Leicesteria* – redescription – immature stages

INTRODUCTION

The subgenus *Leicesteria* of genus *Armigeres* is represented by 18 species in the Oriental region, with 13 species recorded from Malaysia. They are mostly well defined and can be easily identified by the male genitalia and colorations of adult abdominal segments [1-3]. However, most of the pupae and larvae of the species were described without detailed illustrations, hence difficult to identify accurately. The subgenus is characterized by postspiracular area without setae, but covered with flat white and black scales. Female palpus is long, from 1/2 to 3/4 the length of proboscis. Scutum is more or less compressed laterally and produced forwards over the head and postnotum without scales and setae (with the exception of *Ar. flavus*). Abdomen has lateral tergal patches of white and sometimes yellow scales.

Several collections of *Armigeres* species were made during our survey in Sarawak 2005-2011, resulting in a fairly large series of adults, pupae and larvae

and associated larval and pupal excuviae being available for descriptions of immature stages of *Ar.* (*Lei.*) *annulipalpis* and *Ar.* (*Lei.*) *flavus* [4]. We describe and illustrate the immature stages of these two species in this paper. With existing descriptions of adult male and female of the species [1-3, 5, 6], redescriptions of the important adult characters are given briefly by current standards with illustrations of general appearances of adults, abdominal ornamentations and male genitalia.

MATERIALS AND METHODS

Specimens examined

Specimens of *Ar. annulipalpis* were collected as larva from green bamboo stumps, at Sampadi, about 70 km from Kuching, Sarawak by Miyagi, Okazawa and Toma in 2005, 2008 and 2011: 2♀♀ (050915-24); 3♀♀ (080909-1) with L (Larva) and P (Pupa) exuviae mounted on slide (435, 437, 468); 5♀♀, 4♂♂ (080909-1); 1♂ (080909-2) with L and P on slide (447) and G (Genitalia) on another slide (166); 1♂ (080909-1 with L and P (396); 4 ♀♀ (080909-1) with L and P on slide (430, 471, 473, 474); 2 ♀♀ (080909-2); 1♂ (080909-2) with L (402) and G (158); 4 ♀♀ (080909-2); 1♀, 1 ♂ (080909-3) with L and P (422, 402), G (158); 2♂♂ (080909-4) with L, P on slide (242, 403), G (170, 157); 1♂ (080909-4) with G (87); 3♂♂(20110902-2) with L and P (77, 181, 191); 10 whole larvae (20110902).

Specimens of *Ar. flavus* were collected as larva from green bamboo stumps, Matang National Park and Bario, Sarawak by Miyagi, Okazawa and Toma in 2006-2008: 2♂♂ (060914-9, -14) with L and P (420, 392), G (107, 36); 1♂ (080820-6) with L and P (189) with G (79); 1♀ (060914-14) with L, P (341); 2♂♂ (060828-11) with L, P (36,74); 13♀♀, 26♂♂ (20070907-08); 6 whole larvae (20060828-10); 12 whole larvae (20080829-9).

The illustrations of the abdominal ornamentation in the species were based mainly on fresh specimens, as deformity in the colorations of the sterna occurs in dry specimens [7]. The terminology used for the adults and immature stages mainly follows Harbach and Knight [8, 9]. The specimens examined are deposited in the collection of Sarawak Museum.

DESCRIPTIONS AND DISCUSSION

***Armigeres* (*Leicesteria*) *annulipalpis* (Theobald)**
(Fig. 1A-E, G, H, Fig. 3, Tables 1, 2)
Armigeres (*Leicessteria*) *annulipalpis* (Theobald). Thurman, 1959, Univ.

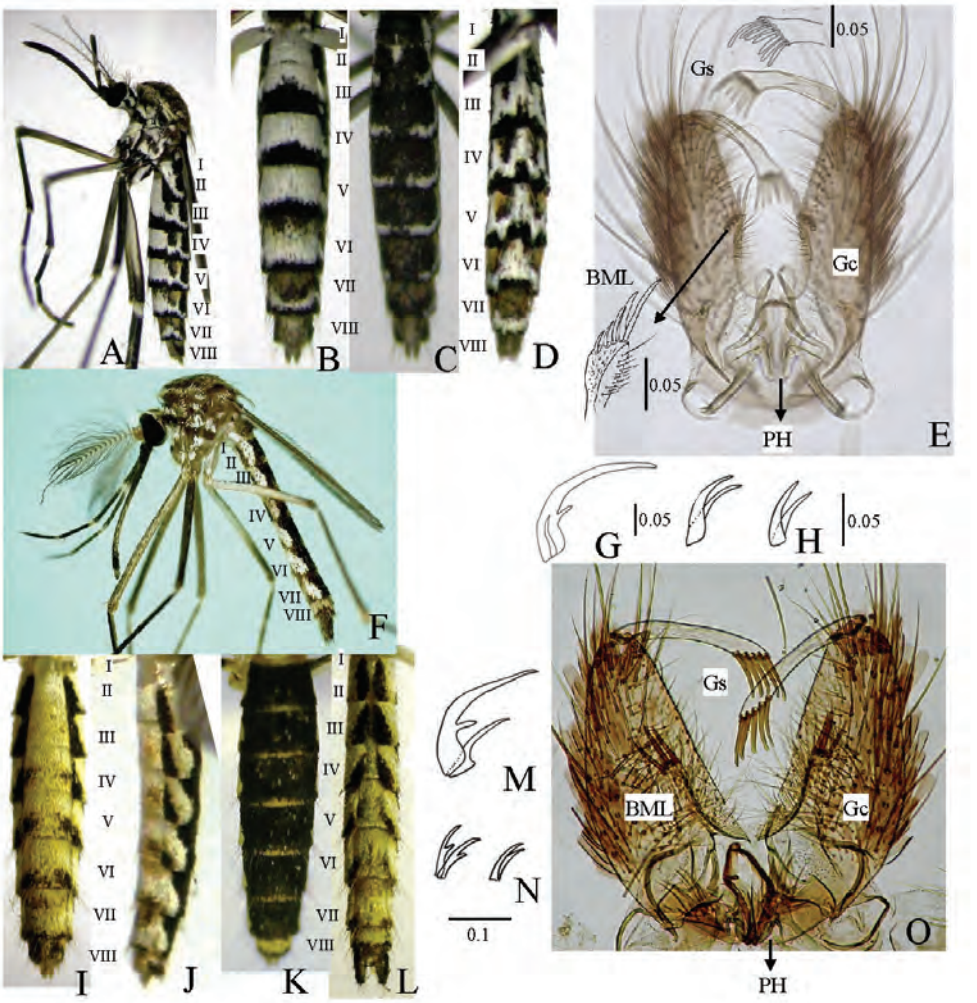

Figure 1. *Armigeres annulipalpis* (A-E, G, H) and *Armigeres flavus* (F, I-O): A, adult female (lateral aspect); B, female abdominal sterna ; C, female abdominal terga; D, male abdominal sterna; E, structure of male genitalia (ventral aspect); F, adult male (lateral aspect); G, male foreunguis; H, male mid (left) and hindunguis; I, female abdominal sterna ; J, female abdomen (lateral aspect); K, female abdominal terga; L, male abdominal sterna; M, male foreunguis; N, male mid (left) and hindunguis; O, structure of male genitalia; Gs, gonostylus; Gc, gonocoxite; BML, basal mesal lobe; PH, phalosome. Scales: mm.

Maryland Agr. Exp. Sta. Bull. A-100; 100 ♀, ♂, L; Macdonald, 1960, Stud. Inst. Med. Res. Malaya no. 29: 126 (♀, ♂, L).

Description

Female (Fig. 1A-C) — *Head***:** Occiput and vertex covered with flat, broad, dark scales, with a central patch of pale broad scales. Two dull yellow inter-ocular

setae and 3, 4 dark setae on ocular line. Postgena (in lateral view) with pale scale patch, divided by dark scale patch. Proboscis, ca 1.75 mm. Maxillary palpus ca 1.0 mm with pale scales on dorsum of the 2nd segment and with a distinct ring of white scales at the base of 3rd segment. Clypeus with pale scale patches on outer surface; inner surface of pedicel and first segment of flagellomere with pale scales. Anntena ca 2.0 mm long. *Thorax*: Integument dark brown. Scutum covered with narrow, curved, light brown and golden scales, produced somewhat forwards over the head (Fig. 1A). Median prescutellar with several white scales. All lobes of scutellum with patch white and dull yellow broad scales. Antealar area from lateral scutal fossal to wing root with a line of white broad patch. Antepronotal lobe covered closely with white broad scales and with several well developed setae; postpronotal lobe with dull yellow broad scales above and white broad scales below. Paratergite with several brown setae and white scales. Upper proepisternal, subspiracular and postspiracular areas, mesokatepisternum and mesanepimeron with patch of white scales; all these areas with 1-3 dull yellow setae. *Legs*: Forefemur, ca 1.75 mm. All coxae with a patch of white scales and yellowish setae on anterior side; all femora (Fe-I－III) dark dorsally with white scales on both basal and apical ends; hind femur with a dull white ventral line on basal 0.74. All tibiae (Ti-I－III) dark with white basal scale spots on both anterior and posterior parts. All tarsal segments (Ta-I－III_{1-5}) with narrow basal rings, faintly on Ta-$I_{4, 5.}$ All ungues (U-I－III) equal in size, without submedian teeth. *Wing:* Length ca 3.00 mm. Cell R_2 ca 1.8 times the length of its stem; alula with a row of small scales; upper calypter with a row of hair-like scales; halter, capitellum dark, rest light in colour. *Abdomen*: Length ca 3.25 mm. Sterna (Fig. 1A, B) I, II all white; III－VI white basally with black apical band; VII yellow basal and white mingled with black apical parts; VIII mostly yellow scaled. Terga (Fig. 1A, C) II with white scale spot on dorso-central part; lateral white markings on terga II－VII curved to the dorsum but do not join to form complete bands; lateral yellow brown scales on base of IV－VIII; VI－VIII almost covered with yellow scales dorsally.

Male (Fig. 1D, E, G, H) － Resembles the female except in the following characters. *Head*: Proboscis, ca 1.9 mm. Palpus, ca 2.1 mm, longer than proboscis. 2nd segment long with narrow basal white ring and wide median white ring; 3rd and 4th segments each with baso-ventral white spot. Antenna, ca 1.75 mm. *Thorax*: Postpronotum with numerous narrow pale scales on upper half; pale scales in lower half are slightly broader. Paratergites are entirely covered with white scales. *Abdomen*: Ornamentation as in female (Fig. 1D). *Legs*: Forefemur, ca 1.75 mm. Foreunguis (U-I) much larger than mid (U-II)- and hindungues (U-III), unequal, larger one with submedian small tooth; mid and hindungues small, equal, without submedian tooth (Fig. 1G, H). *Wing*: Length ca 2.75mm. *Genitalia* (Fig. 1E): Tergum IX with apical area partly sclerotized and divided

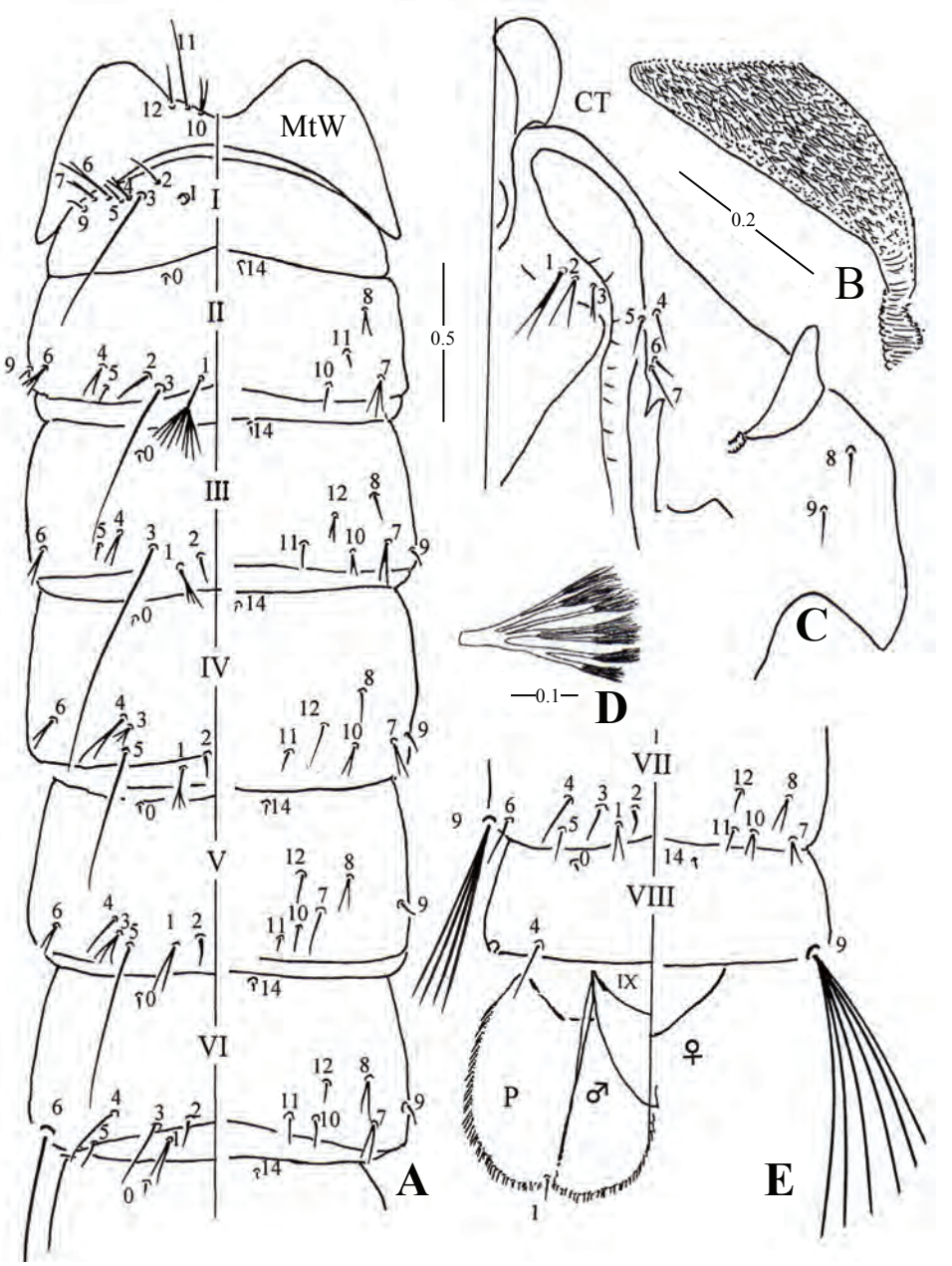

Figure 2. Pupa of *Armigeres annulipalpis*. A, metathoracic wing (MtW) and abdomens I—VI; B, trumpet; C, part of cephalothorax (CT); D, seta 1 of segment I; E, abdominal segments VII —IX and paddle (P). Scales: mm.

Table 1. Numbers of branches for pupae of *Armigeres annulipalpis* (Theobald)

Seta no.	Cephalo-thorax	Abdominal segments							
		I	II	III	IV	V	VI	VII	VIII
0	-	-	1	1	1	1	1	1	1
1	1, 2	M	8-15	2-6	2-4	1-4	1-3	2-4	-
2	1-3	1	1	1	1	1	1	1	-
3	2, 3	1	1	1	1-3	1-3	1 (1, 2)	1, 2	-
4	1-3	2, 3	2-4	1-3	2, 3	1-4	1, 2	1	1
5	1 (1, 2)	1	1 (1, 2)	1 (1, 2)	1	1 (1, 2)	1	1, 2	-
6	1 (1, 2)	1-4	2-5	1-3	1-3	1-3	1 (1, 2)	1, 2	-
7	1 (1, 2)	2, 3	2-6	2, 3	2-4	2, 3	1-3	1-3	-
8	1, 2	-	1, 2	1, 2	1 (1-3)	1-3	2 (1, 2)	1-3	-
9	1, 2	1	1	1 (1, 2)	1	1	1	2-6*	5-11*
10	1-3	-	1 (1, 2)	2	1, 2	1 (1, 2)	1	1, 2	-
11	1	-	1 (1, 2)	1	1	1	1	1	-
12	1 (1, 2)	-	-	1-3†	1†	1†	1†	1	-
14	-	-	1	1	1	1	1	1	1

M: dendritic with many branches. *weakly aciculated. †present, sometimes obsolete.
Obsolete and missing setae are shown with a hyphen (-).
Specimens examined: 5 pupal exuviae from Sampadi, Sarawak, Malaysia
Numbers in front and in parentbesia are shown frequent setal branches and range of variation respectively

into two lobes by a shallow U shaped depression with 8-15 fine setae on each lobe. Sternum IX broad with many scales entirely and with 20-25 fine setae on apical margin. Gonocoxite (Gc): 3.2 as long as its breadth at center, lateral and ventral aspects with many long setae and scales; basal dorsomesal lobe (BML) with a row of 4 or 5 graded spines, the inner apical one longest; gonostylus (Gs) ca 0.5 as long as the gonocoxite, comb of 7 teeth in a row, apical one spinelike larger than the other blant teeth. Phallosome (PH) round.

Pupa (Fig. 2, Table 1) — *Cephalothorax* (Fig. 2C): Yellow to light brown pigmentation. Trumpet (Fig. 2B), 0.5 mm, index 3.3. Setae 1-CT single or double, longer than others. *Abdomen*: Length ca 4.25 mm; segments I—VIII with very fine spicules; seta1-I (Fig. 2D) long, fanlike with 4 main branches; 1-II conspicuous forked with several branches; 3-II, III and 5-IV, V long, single; seta 6-VI long, usually single; 9-VII, VIII long with fine aciculate branches. *Paddle*: Length ca 0.75 mm lightly pigmented except at base, with midrib from base to apex and with marginal filamentous spicules; seta 1-P single, very fine. *Genital lobe*: Extending to ca 0.57 of paddle in male, to 0.25 of paddle in female.

Fourth-instar Larva (Fig. 3, Table 2) — *Head* (Fig. 3A): 0.96 mm as long as the width; light yellow-brown in colour except area around mouth and collar which are slightly darker; dorsomentum (Fig. 3D) with a strong median tooth and with 7 or 8 teeth on each side. Seta 1-C small, single, tapering; 9-C long with usually 2 branches. *Antenna*: Integument smooth, yellow in colour, length about 0.26 of head; shaft about the same breadth from base to apex, seta 1-A single at 0.6 from base. *Thorax* (Fig. 3C): Seta 1-P long, usually single; 3-M usually long

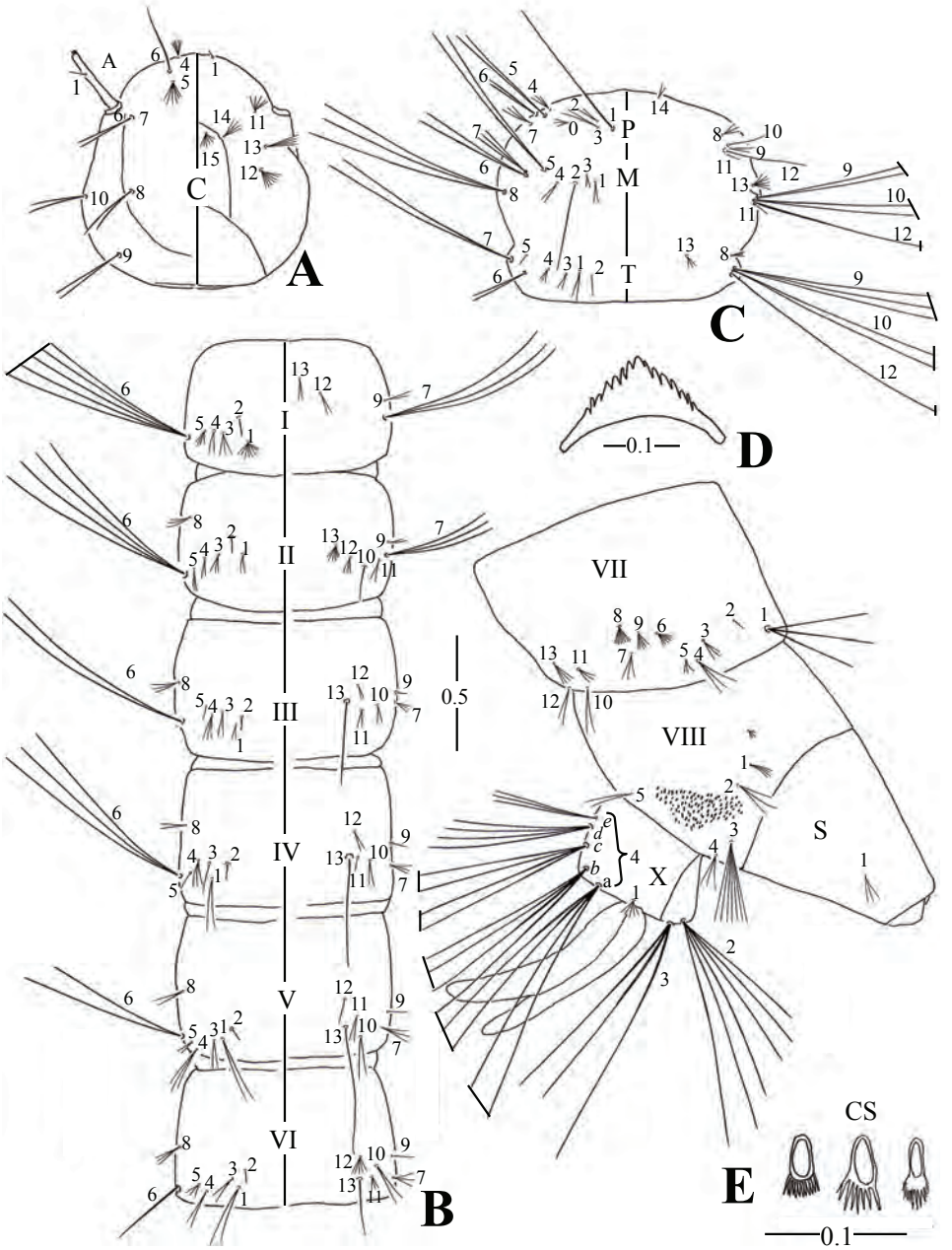

Figure 3. Fourth-instar larva of *Armigeres annulipalpis*. A, head; B, abdominal segments I—VI; C, thorax; D, dorsomentum; E, abdominal segments VII, VIII, X and siphon (S), and comb scales (CS). Scales: mm.

Table 2. Numbers of branches for fourth-instar larvae of *Armigeres annulipalpis* (Theobald)

Seta	Head	Thorax			Abdominal segments							
no.		P	M	T	I	II	III	IV	V	VI	VII	VIII
0	-	3-6	-	-	-	-	-	-	-	-	-	-
1	1	1 (1, 2)*	1, 2	1-3	4-9	1-6	1-6	1-3	2 (1-3)	1, 2	2-5*	4-12
2	-	1, 2	1-3	1-3	1, 2	1	1, 2	1, 2	1, 2	1, 2	1, 2	2-6
3	-	1 (1-3)	1, 2	1-4	3-7	2-6	2-4	1-3	2-5	2 (2, 3)	3-6	5-7*
4	5-13	2, 3	2, 3	1-4	2-6	2-7	3-5	2-4	2-6	2-4	2-4	1-4
5	4-9	2 (1-3)*	1, 2*	1	2-4	1-3	1-3	1-4	2-3	3-6	3-6	1, 2
6	1	1,2	1, 2*	1-3	3-6*	3-5*	2*	2, 3*	1, 2*	1 (1, 2)*	4-6	-
7	2 (1-3)*	2-6*	1-3	2-5*	2, 3*	2-4*	3-6	3-6	3-6	2, 3	3-5	1-X=3-7
8	2 (1-3)	2-4	2-5*	3-8	-	3, 4	2, 3	2	1, 2	3-5	6-11	
9	2*	2 (1, 2)	2*	2, 3*	1-4	1-3	1	1, 2	1, 2	1 (1, 2)	5, 6	2-X=4-6*
10	2 (1, 2)	1	2*	2, 3*	-	1, 2	2, 3	2, 3	2 (1-3)	1, 2	2, 3	
11	3-7	1	1, 2	-	-	2, 3	1-3	1, 2	2, 3	1-3	2-6	3-X=3-5*
12	4-9	1	1, 2*	1, 2*	2-4	3-8	2, 3	2	1, 2	4-9	2, 3	
13	1-4	-	6-9	3-7	1 (1, 2)	6-12	1-3	1	1	1 (1, 2)	4-10	4-X*a-e*=2-5*
14	4-11	2 (1-3)	-	-	-	-	-	-	-	-	-	-
15	5-10	-	-	-	-	-	-	-	-	-	-	-

*Weakly aciculated.

Obsolete and missing setae shown with a hyphen (-).

Specimens examined: 5 fourth-instar larvae from Matang and Sampadi, Sarawak., Malaysia.

and single, sometimes short with 2 or 3 branches; 5-M long, single or double; 8-M long, 2－5 branched; setae 9, 10-M long, double; 9, 10-T long double or triple branched; 7-T long, 2－5 branched. All these setae more or less aciculated. *Abdomen* (Fig. 3B, E): Setae 1-I conspicuous, forked with 4－9 branches; 6-I, II large, usually 3－6 branched; 6-III double; 6-IV, 3, 4 branched; 7-I long, 2, 3 branched; 7-II long, 2－4 branched; 13-IV, V long, single; 3-VIII well developed with 5－7 branches. All these setae more or less aciculated. Comb scales (SC) 60-100 in a triangular patch; individual scales paddle-shaped with spicules on apical margin (Fig. 3E). Saddle incomplete, pigmented brown; anal papilla long-oval with rounded apices. Siphon: Length 0.8 mm, index 1.5; seta 1-S 1－3 branched arising about 0.32 from apical end.

Taxonomic Discussion

In larva, seta 1-C is small, single or double; antennal seta 1-A is single, inserted slightly beyond the midway point; thoracic seta 3-M is small, single or double; abdominal seta 6-I are 3－6 branched, 6-II 3－5 branched. Comb teeth are arranged in a patch of more than 60, each is uniformly fringed apically.

The adult of the species is characterized by abdominal terga II with a median basal white patch and female palps with clear central white ring. On the basis

of the male genitalic characters, this species resembles *Armigeres* (*Leicesteria*) *traubi* Macdonald from Selangor Malaysia. We examined holotype (♂), No. 0555/8, Selangor, Ulu Gombak, 18 March, 1953 (W.W. Macdonald) of *Ar. traubi* in the British Museum in 1996. It can be distinguished from *Ar. annulipalpis* by the thorax moderately laterally compressed forwards over the head and the ornamentation of abdominal terga and sterna.

Biological notes

The larvae of *Ar. annulipalpis* were found often associated with *Armigeres pectinatus* (Edwards) in green living bamboo stumps and splits in lowland bamboo forest in Sarawak. Nothing is known of biting habits.

Distribution

China, India, Indonesia, Myanmar, Thailand and Malaysia.

***Armigeres* (*Leicesteria*) *flavus* (Leicester)**
(Figs. 1F, I-O, Figs. 4, 5; Tables 3, 4)
Armigeres (*Leicesteria*) *flavus* (Leicester). Thurman, 1959, Univ. Maryland Agr. Exp. Sta. Bull. A-100; 100 (♀, ♂, L); Macdonald, 1960, Stud. Inst. Med. Res. Malaya no. 29: 126 (♀, ♂, L).

Female (Fig. 1I－K) － *Head:* Occiput and vertex covered with flat, broad, dark scales, with a central small patch of pale broad scales and with many upright scales; a row of several yellowish ocular and inter ocular setae. Proboscis uniformly dark, ca 3.0 mm, with a ventral line of dull pale scales on the whole length. Maxillary palpus ca 1.25 mm, ca 0.44 length of proboscis, dark, without pale spot and ring. Clypeus dark without pale scale; pedicel and first segment of flagellomere yellowish with pale scales. Anntena ca 3.0 mm long. *Thorax:* Integument dark brown. Scutum not produced forwards over the head, covered with closely narrow, curved, pale scales. Median prescutellar and all lobes of scutellum covered with white scales; anterior pronotal with white scales and pale setae; postpronotal lobe with pale narrow scales above and white broad scales below; paratergite with a patch of white scales; upper proepisternal, subspiracular and postspiracular areas, mesokatepisternum and mesanepimeron with large patch of white scales; upper and lower mesokatepisteral areas with a vertical row of about 20 pale setae; prealar knob with about 10 pale setae. Postnotum with setae and pale scales. *Legs:* All coxae with a patch of white scales and yellowish setae on anterior side. Forefemur, ca 3.5 mm. All femora dark dorsally and white ventrally. Tibiae with a line of pale scales on underside; hind tibia distinctly shorter than fore and midtibiae; hind tarsus with clear rings, fore and mid tarsi with faint pale

rings at the basal segments, indistinct on the more distal segments. Fore and mid ungues equal and toothed, hind unguis smaller, equal and simple. *Wing*: ca 4.50 mm; cell R_2 ca 1.8 times the length of its stem. *Abdomen*: Length ca 4.0 mm. Sterna yellowish-white scaled, with few scattered brownish scales on posterior segments (Fig. 1I). Terga II—VI dark brown, each segment with a narrow apical patch of pale yellow scale band, VIII covered mostly with pale yellow scales; lateral patches of white scales which do not extend to the dorsum (Fig. 1J, K).

Male (Fig. 1F) — Resembles the female except in the following characters. *Head:* Proboscis, ca 3.0 mm; palpus, ca 3.4 mm, with 3 clear pale rings. Antenna, ca 2.3 mm. *Abdomen*: ca 6.5 mm with many fine setae on sternal segments; coloration and banding as in female. *Wing*: Length ca 4.6 mm. *Legs*: Forefemur, ca 3.2 mm. Foreunguis unequal, the larger one toothed; midunguis equal and toothed; hindunguis equal and simple (Fig. 1M, N). *Genitalia* (Fig.1O): Tergum IX shaped depression with usually 10-15 setae on each lobe. Gonocoxite (Gc) long, ca 2.3 as long as its breadth at center, with long setae and scales on lateroventral surface. Basal dorsomesal lobe (BML) with a row of 3 or 4 blunt spines. Gonostylus (Gs) slightly expanded apically, with 5 or 6 long blunt teeth. Phallosome (PH) long oval.

Pupa (Fig. 4, Table 3) — *Cephalothorax* (Fig. 4C): Yellow to light brown pigmentation. Trumpet (Fig. 4B), 0.55 mm, brown pigmentation, index 2.5. Setae 1, 3-CT usually single, 7-CT 2— 4 branched, longer than others; 11-MtW single, longer than 10, 11-MtW. *Abdomen* (Fig. 4A, E): Length ca 6.0 mm. Dorsal integuments in segments I—VIII with very fine wrinkles. Seta 1-I long, fanlike with 7-17 main branches (Fig. 4D); 1-II—IV conspicuous with many branches; 3-II, III and 5-IV, V long, usually single; seta 6-VI well developed single or double, rarely small with 8 branches; position of setae 1, 2, 3-VI variable, usually 1, 2 and 3 but rarely 2-VI laterad of 3 and mesad of 1; 9-VII and -VIII long with 7—12 and 7—17 aciculate branches. *Paddle*: Length 1.5 mm, lightly pigmented except at base, with midrib from base to apex and with marginal filamentous spicules; seta (1-P) single, very fine, filamentous. *Genital lobe:* Extending to ca 0.58 of paddle in male, to 0.4 in female.

Fourth-instar Larva (Fig. 5, Table 4) — *Head* (Fig. 5D): 1.0-1.2 mm, as long as or little shorter than the width. Light yellow-brown in colour except area around mouth and collar which are dark; dorsomentum (Fig. 5C) with a strong median tooth and with 5 or 6 teeth on each side. Seta 1-C long, single, arising from a stout tubercle (Fig. 5E); 9-C long, double branched; Antenna: Integument smooth, yellow in colour, length about 0.20 of head; shaft about the same breadth from base to apex; 1-A at 0.32 from the base. Additional seta (no number) with 5—10

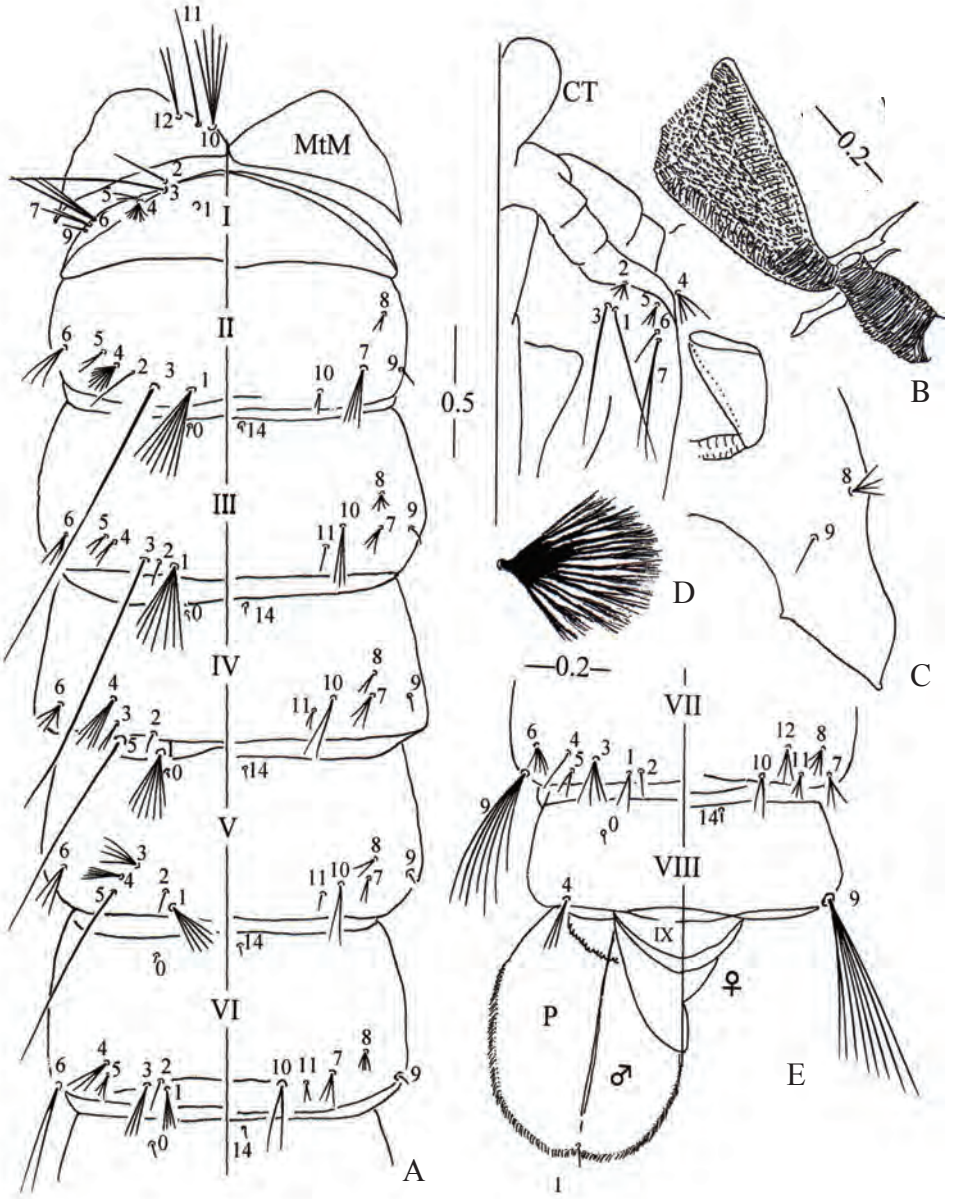

Figure 4. Pupa of *Armigeres flavus*. A, metathoracic wing (MtW) and abdomens I—VI; B, trumpet; C, part of cephalothorax (CT); D, seta 1 of segment I; E, abdominal segments VII—IX and paddle (P). Scales: mm.

Table 3. Numbers of branches for pupae of *Armigeres flavus* (Leicester)

Seta	Cephalo-	Abdominal segments							
no.	thorax	I	II	III	IV	V	VI	VII	VIII
0	-	-	-	1	1	1	1	1	1
1	1 (1, 2)	M	7-11	4-12	5-14	5-10	3-9	1-8	-
2	2-9	1 (1, 2)	1	1	1	1	1	1	-
3	1 (1, 2)	1 (1, 2)*	1*	1*	1-5	4-6	2-7	2-6	-
4	3-8	7-14	8-15	2-7	5-11	4-10	2-6	1-7	1-6
5	3-12	1-3	2-8	2-5	1*	1*	2-5	1-5	-
6	1	3-7	3-9	3-7	3-11	1-7	1, 2	4-9	-
7	2-4	2-6	3-9	2-11	2-11	3-16	2-8	2-8	-
8	4-7	-	2, 3†	2-7	2-7	2-6	3-7	4-11	-
9	1-3	1, 2	1 (1, 2)	1 (1, 2)	1	1	1	7-12*	7-16*
10	3-10	-	1-4	3, 4	2-8	2-4	1-3	1-4	-
11	1	-	-	1, 2	1, 2	1, 2	1, 2	3-7	-
12	1-4	-	-	-	-	-	-	3-10†	-
14	-	-	-	1	1	1	1	1	1

M: dendritic with many branches. *long, weakly aciculated. †present, sometimes obsolete.
Obsolete and missing setae are shown with a hyphen (-).
Specimens examined: 5 pupal exuviae from Matang, Pa Umur, and Pa Ukat of Sarawak, Malaysia

Table 4. Numbers of branches for fourth-instar larvae of *Ar. flavus* (Leicester)

Seta	Head	Thorax			Abdominal segments							
no.		P	M	T	I	II	III	IV	V	VI	VII	VIII
0	-	6-17	-	-	-	-	-	-	-	-	-	-
1	1	1*	1-5	4-8	2 (2-4)*	1*	1*	1*	1*	1, 2*	1-3*	12-22
2	-	1-3	2-6	1, 2*	1-4	2	1-3	1-4	1-4	1, 2	1-3	2-4
3	-	2-4	1 (1, 2)*	4-8	3-7	10-23	3-7	2-7	3-16	2-8	5-23	5-9*
4	11-17	8-13	1-6	4-16	9-19	5-10	5-11	4-10	2-11	5-9	2-6	4-6
5	2-8	1*	1, 2*	1, 2	3-7	5-9	7-9	6-11	4-13	5-11	3-13	1-11
6	1	1 (1, 2)*	1*	2*	2, 3*	2 (1-3)*	1, 2*	1 (1, 2)*	1*	1*	9-17	-
7	2 (2, 3)	1 (1, 2)*	1-3*	2 (2, 3)*	2*	2*	8-24	7-18	9-16	5-8	3-9	1-X=6-12
8	2-5	2-8	2, 3*	10-20	-	4-12	3-8	2-6	2-6	5-10	15-29	
9	2*	2-7	2*	1-3*	2-4	1-5	2-5	2-6	2-6	3, 4	8-15	2-X=3, 4*
10	1-3	1	1*	1, 2*	1-4	1-4	2-6	2-8	3-5	2-5	4-6	
11	3-5	1-4	-	-	10-18	3-7	3-7	3-7	5-7	3-6	11-26	3-X=2, 3*
12	7-13	1	1 (1, 2)*	1*	-	5-16	3-5	2-5	1-3	2-4	2-6	
13	1-4	-	11-23	10-17	5-13	7-31	1, 2*	2*	2*	13-26	14-23	4-X*a-e*=1-3*
14	8-15	2-6	10-16	-	-	-	-	-	-	-	-	-
15	5-8	-	-	-	-	-	-	-	-	-	-	-

*Weakly aciculated.
Obsolete and missing setae shown with a hyphen (-).
Specimens examined: 5 fourth-instar larvae from Pa Umur and Pa Ukat, Bario, Sarawak, Malaysia.

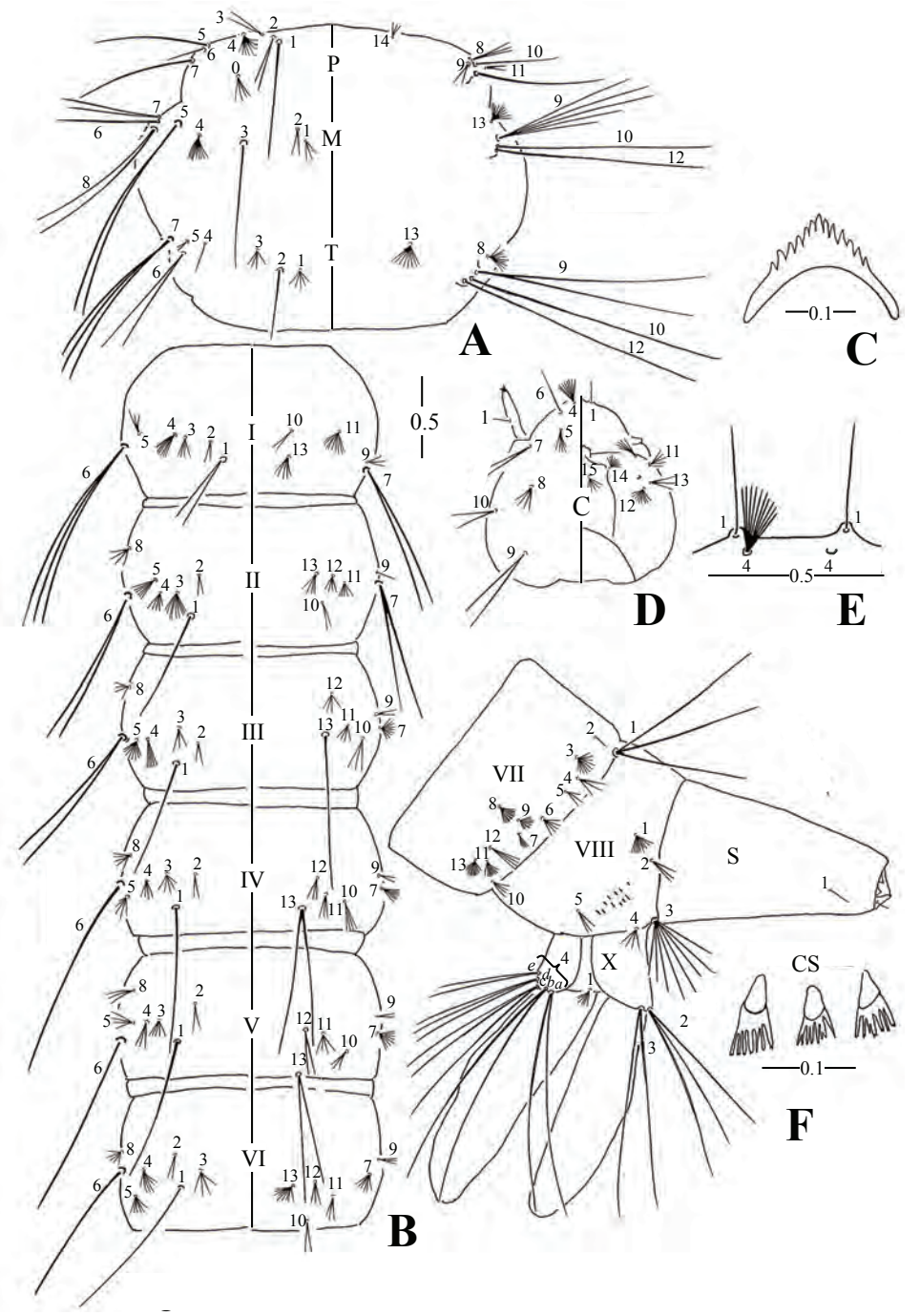

Figure 5. Fourth-instar larva of *Armigeres flavus*. A, thorax; B, abdominal segments I–VI; C, dorsomentum; D, head; E, arrangement of head setae 1; F, abdominal segments VII, VIII, X and siphon (S), and comb scales (CS). Scales: mm.

branches situated near seta 11 (Fig. 5D). *Thorax* (Fig. 5A): Seta 1-P long, single; 5-M long, single; 8-M long, 2, 3 branched; 7-T long, usually double branched. All these long setae more or less aciculated. *Abdomen* (Fig. 5B, F): Setae 1-II—V long, single; 1-VI 2, 3 branched; 1-VII 1—3 branched; 6-I long, 2, 3 branched; 6-II long, 1-3 branched; 6-III, IV single or double; 6-V, VI single; 7-I, II long double; 13-IV, V long double. All these setae more or less aciculated. Comb scales (SC) 6—15 in an irregular row, each scale frayed evenly towards the tip (Fig. 5F). A large dorsal plate (saddle) and an additional ventral sclerotized plate in segment X. Anal papilla long-oval with rounded apices. *Siphon*: Short and stout, 0.6 mm, index 1.35; seta 1-S fine 1 or 2 branched arising about 0.27 from apical end.

Distribution

India, Bangladesh, Myanmar, China (Yunnan), Cambodia, Laos, Vietnam, Thailand, Indonesia, Malaysia (East and West), Philippines and Taiwan.

Taxonomic discussion

Armigeres flavus is unique, easily distinguished from other members of the subgenus *Leicesteria*. In the adults, thorax is not markedly compressed laterally nor produced forwards over the head. Hind tibia is distinctly shorter than fore tibia and hind tarsi with narrow basal pale rings. Upper and lower mesokatepisteral areas have a vertical row of about 20 pale setae. Abdominal terga II—VI have median yellowish-white scale patches at apical margins and white lateral patches; the sterna is white with scattered brownish scales on posterior segments. Postpronotum has several minute pale setae on the apex. In male genitalia, the basal dorsomesal lobe has a row of 3 or 4 blunt spines and the gonostylus has 5 or 6 long blunt teeth. In pupa, abdominal setae 9-VII and -VIII are well developed with 7—12 and 7—16 aciculated branches. In larva, seta 1-C is long and single arising from a stout tubercle and comb with 6—15 teeth arranged in a patch (or irregular row), each expanded into many thin points. Abdominal segment X has dorsal (saddle) and additional small ventral sclerotized plates.

Thurman [1] recognized the subgenus *Leicesteromyia* Brunett for *Armigeres flavus* (Leicester, 1908) = *Chaetomyia flavus* Leicester, 1908 but *Ar. flavus* is treated as one of the members of *Leicesteria* by Macdonald [2] and Delfinado [3].

Biological notes

The larva of the species is large, fat and creamy white. We commonly found the larvae in great numbers at accumulation of very turbid water in young bamboo stumps, and frequently associated with *Armigeres kuchingensis* Edwards and *Armigeres confusus* Edwards in fallen split bamboos and artificial containers with

foul water at Bario and Matang National Park, Sarawak. The unusual egg-laying behaviour of *Ar. flavus* has been described [2, 10, 11] in Gombak, Malaysia. The female held an egg raft tightly between her tibiae and the 1st tarsomeres of both hid legs with the junction of tibiae and 1st tarsi bent down during the incubation period. It is a daytime biter in the forest.

Acknowledgments —We thank the Sarawak Forestry Department for granting permission for sampling of two-winged flies (Diptera) in the Bario highland and Matang National Park, Sarawak.

REFERENCES

1. Thurman E.B. (1959) *A contribution to a revision of the Culicidae of Northern Thailand. Bulletin A-100.* University of Maryland Aguriculture Experiment Station, Maryland.
2. Macdonald W.W. (1960) On the systematics and ecology of *Armigeres* subgenus *Leicesteria* (Diptera; Culicidae). *Studies from the Institute for Medical Research Federated Malay States* **29**: 110-159.
3. Delfinado M.D. (1966) The culicine mosquitoes of the Philippines. Tribe Culicini (Diptera: Culicidae). *Memoirs of the American Entomological Institute* **7**: 1-252.
4. Miyagi I. and Toma T. (2009) Culicidae and Corethrellidae (Diptera) collected in Sarawak, Malaysia from 2005-2008. *Sarawak Museum Journal* **66** (87): 313-331.
5. Barraud P.J. (1934) *The fauna of British India, including Ceylon and Buruma. Diptera, Culicidae. Tribes Magarhinini and Culicini.* Vol. **5**.
6. Brug S.L. (1939) Notes on Dutch East-Indian mosquitoes. *Tijdschrift voor Entomologie* **82**: 91-113.
7. Toma T., Miyagi I., Okazawa T., Higa Y. and Leh C. (2010) Redescriptions of five species of the genus *Armigeres*, subgenus *Armigeres* (Diptera: Culicidae) collected from fallen coconut fruits at the coastal plains of Sarawak, East Malaysia. *Medical Entomology and Zoology* **3** (4): 281-308.
8. Harbach R.E. and Knight K.L. (1980) *Taxonomists' glossary of mosquito anatomy.* Plexus Publishing Inc., Marlton.
9. Harbach R.E. and Knight K. L. (1981) Corrections and additions to taxonomists' glossary of mosquito anatomy. *Mosquito Systematics* **13** (2): 201-217.
10. Okazawa T., Miyagi I. and Yong H.S. (1992) Oviposition and eggs of *Armigeres* (*Leicesteria*) *flavus* (Diptera, Culicidae). *Japanese Journal Entomology* **60** (1): 54-58.
11. Miyagi I., Toma T., Okawawa T., Mogi M. and Hashim R. (2005) Female *Armigeres* (*Leicesteria*) *flavus* holding and egg raft with her hind legs. *Journal of the American Mosquito Control Association* **21**(4): 466-468.

Journal of Science and Technology in the Tropics (2012) 8: 21-27

Sex-chromosome constitution and supernumerary chromosome in the large bandicoot rat, *Bandicota indica* (Rodentia, Muridae) from Peninsular Malaysia

Hoi Sen Yong[1], Praphathip Eamsobhana[2,*] and Phaik Eem Lim[1,3]
[1] Institute of Biological Sciences, University of Malaya, 50603 Kuala Lumpur, Malaysia
[2] Department of Parasitology, Faculty of Medicine Siriraj Hospital, Mahidol University, Bangkok 10700, Thailand
[3] Institute of Ocean and Earth Sciences, University of Malaya, 50603 Kuala Lumpur, Malaysia
(*Corresponding author e-mail: sipes@mahidol.ac.th)

Received 20-12-2011; accepted 27-01-2012

Abastract The Peninsular Malaysia taxon of *Bandicota indica* has a standard complement of 44 chromosomes, with medium-sized subacrocentric X and small submetacentric Y chromosomes. The present study reveals variation in the size and morphology of the X-xhromosome in *B. indica* with 2n = 44. The difference in size of the X-chromosome is attributed to variation in constitutive heterochromatin. Excepting the X-chromosome, the karyotype of the Malaysian taxon is similar to the Indian *B. indica nemorivaga* with 2n = 44. It differs from the Thailand taxon in the number of biarmed and uniarmed autosomes. A male specimen (with 45 chrosomes) of the Malaysian taxon possessed a supernumerary (B) chromosome which is identical to that reported in *B. indica nemorivaga*.

Keywords B-chromosome – sex-chromosome – mammal – constitutive heterochromatin – *Angiostrongylus cantonensis* – rat lungworm

INTRODUCTION

The large bandicoot rat, *Bandicota indica* (Bechstein) is a member of the Muridae [1]. It occurs in Sri Lanka, India, Bangladesh, lowlands of Nepal through Myanmar, southern China, Hong Kong, Laos, Vietnam, Thailand, Peninsular Malaysia, Taiwan and Java [2]. The populations in Peninsualr Malaysia (states of Perlis and Kedah), Java and Taiwan are probably introductions.

Bandicota indica is one of some 17 species of murid rodents which are the final or definitive hosts of the rat lungworm *Angiostrongylus cantonensis*, the causative agent of human angiostrongyliasis in Southeast Asia and the Asia Pacific [3]. It has been incriminated in China [4], India [5], Indonesia [6], Sri Lanka [7], Taiwan [8] and Thailand [9]. It is also a carrier of other pathogens such as hantavirus [10, 11] and *Leptospira* [12].

Bandicoot rats are an important food source among some people in Thailand. In view of its importance in public health, we investigated various aspects of the genetics of the host (*B. indica*) and the parasite. We report here the sex-chromosome

constitution and supernumerary chromosome in *B. indica* from Peninsular Malaysia.

MATERIALS AND METHODS

The large bandicoot rat *B. indica* was trapped in the rice fields of Kedah, Peninsular Malaysia. Two male and one female specimens were used for chromosome study. The bandicoot rats were treated with 0.01% (w/v) colchicine in RPMI for 1 h. Bone marrow of tibia and femur was used for chromosome preparation by the air drying technique [13]. Briefly, the colchicine-treated bone marrow cells were treated with 0.56% KCl solution for 30 min, then fixed in 3:1 ethanol:acetic acid preservative (three changes). The final cell suspension was used for immediate chromosome preparation or stored in deep freezer until needed. The metaphase chromosomes were stained with 2% Giemsa for conventional karyoptype, or treated with trypsin for G-banding and C-banding [14, 15]. At least 20 well-spread metaphases of each specimen were photographed under oil immersion for karyotype analysis [16].

RESULTS AND DISCUSSION

The bandicoot rats, genus *Bandicota*, are represented by three species – *B. bengalensis*, *B. indica* and *B. savilei* [1, 2]. The Peninsular Malaysia taxon of the large bandicoot rat belongs probably to *B. indica siamensis* [17].

In the large bandicoot rat, the subspecies *B. indica indica* has 2n = 42, with large submetacentric X and Y chromosomes [18, 19]. The subspecies *B. indica nemorivaga* has 2n = 44, with large submetacentric X and small submetacentric Y chromosomes [19, 20]. *B. i. nemorivaga* has also been reported to possess as many as three supernumerary (B) chromosomes [20].

The Thailand taxon of *B. indica* had been reported to possess 2n = 46 [21]. More recently, a female *B. indica* was reported to possess 44 chromsomes, and a male with 45 chromosomes [22]. The X-chromosome was submetacentric and the Y acrocentric. There were 26 biarmed autosomes with the rest acrocentric. Due to the poor quality of the chromosome preparation, the extra chromosome in the male could not be determined and was suggested to be due to Robertsonian translocation, X-autosome translocation or B-chromosome.

In the present study of the Peninsular Malaysia taxon of *B. indica*, one male and one female had 44 chromosomes, while one male had 45 chromosomes. The extra chromosome in the 45-chromosome complement was a small biarmed (metacentric) element (Fig. 1). This supernumerary (B) chromosome is identical to that reported in *B. i. nemorivaga* [20]. It therefore renders support to the assumption

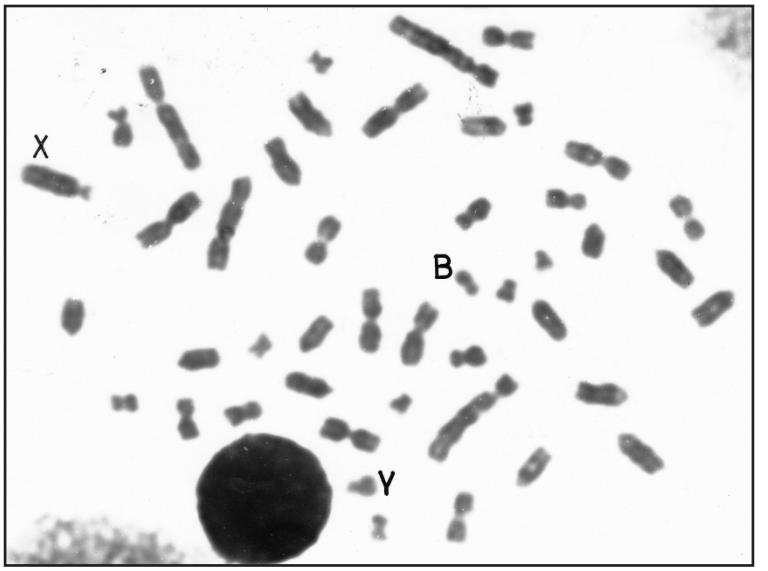

Figure 1. Metaphase of a male *Bandicota indica* from Peninsular Malaysia with 44 + 1B chromosomes. The subacrocentric X-chromosome is distinctive in the complement.

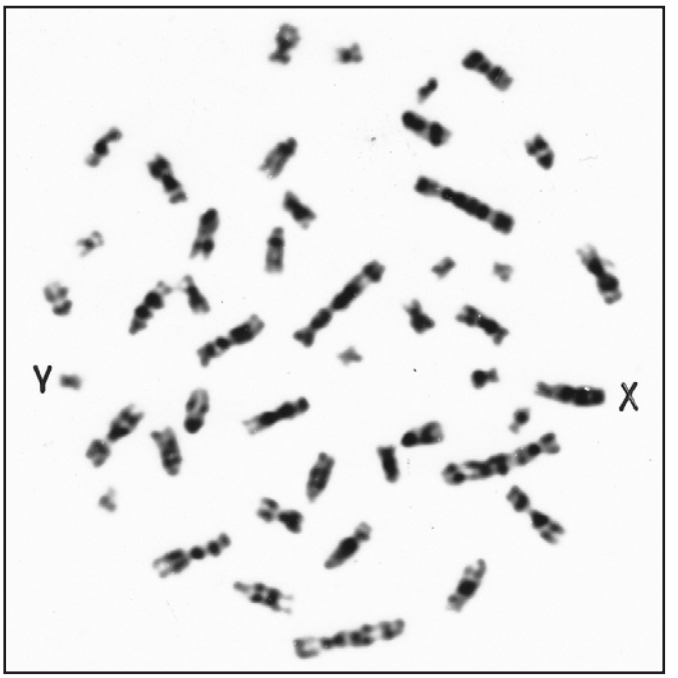

Figure 2. Trypsin G-banded metaphase of a male *Bandicota indica* with 44 chromosomes from Peninsular Malaysia. Three distinct bands are present on the X-chromosome.

that the 46-chromosome complement reported for the Thailand taxon consisted of two supernumerary chromosomes [19, 21]. In view of this, the 45-chromosome complement of the Thailand specimen [22] could be reasonably attributed to the occurrence of B-chromosome. However population study is needed to resolve this. For example, the occurrence of B-chromosomes in the house rat *Rattus rattus* was clearly demonstrated through population cytogenetic study [23]. Likewise, population study could also reveal the occurrence of Robertsonian translocation, e.g. in *R. rattus* [24] and *Suncus murinus* [25].

The autosome complement of the Peninsular Malaysia taxon of *B. indica* is similar though not identical to that of *B. i. nemorivaga* from India, with 14 pairs of biarmed and 7 pairs uniarmed (acrocentric) elements (Fig. 1). It is quite different from the Thailand taxon with 10 pairs [21] or 8 pairs [22] of acrocentric autosomes. The difference between biarmed and uniarmed chromosomes could be due to pericentric inversion, for example, in the house rat *R. rattus* [26].

In the present Malaysian material, the X-chromosome is a medium-sized subacrocentric element (Fig. 1). It differs from the large submetacentric X reported in the Indian taxon *B. i. nemorivaga* [19, 20]. C-banding also does not show a heterochromatic block in the very short arm of the subacrocentric X. Whether it is identical to the X-chromosome of the Thailand taxon of *B. indica* cannot be ascertained as the published karyotype was rather poor.

It is tempting to infer that the long arm of the X-chromosome in the Malaysian *B. indica* corresponds to the long arm (non-heterochromatic arm) of the submetacentric X in the Indian *B. i. nemorivaga*. G-banding of the Malaysian specimens shows three dark bands (Fig. 2). Whether the X-chromosome of *B. i. nemorivaga* consists of two or three bands cannot be discerned in the published karyotypes [19, 20].

The Y-chromosome in the present Malaysian material is a biarmed element (Fig. 1, 2). It is similar to that reported for the Indian *B. i. nemorivaga*. It is uniformly stained in C- and G-banded metaphase (Fig. 2). The Y-chromosome in the Thailand *B. indica* is, however, acrocentric [21, 22]. The difference between the biarmed and uniarmed Y-chromosome could be due to pericentric inversion.

It is evident that *B. indica* with 2n = 44 exhibits variation in the size and morphology of the X-chromosome. The larger size in the Indian *B. i. nemorivaga* is due to the presence of a totally heterochromatic short arm in its submetacentric X-chromosome [20]. Such variation in the size and morphology of the X-chromosome as a result of variation of constitutive heterochromatin, has also been reported in *B. bengalensis* [27]. Geographic and intraspecific variation in the sex chromosomes have been reported in other mammals, e.g. *B. bengalensis* [27, 28] and *S. murinus* [29].

It is noteworthy that the 2n = 44 *B. indica* is characterized by the presence of supernumerary chromosomes, while no such accessory chromosome has been

reported for the 2n = 42 taxon. In the present study, a pair of the small biarmed autosomes in the Malaysian taxon is heterochromatic when C-banded and darkly stained when G-banded (Fig. 2). Assuming taxonomic identification of all the taxa is correct, this calls for more thorough investigation to determine whether the 2n = 44 taxa of *B. indica* have arisen due to the incorporation of a pair of supernumerary chromosomes into the standard complement with 2n = 42. In addition, other approaches such as DNA sequences, should be pursued to determine the genetic relationship of the various taxa.

Acknowledgements – This work is supported by a University of Malaya research grant (H-00000 5620009). We thank the University of Malaya and Mahidol University for supporting our collaborative research on various aspects of the Rat lungworm *Angiostrongylus cantonensis* and its hosts.

REFERENCES

1. Corbet G.B. and Hill J.E. (1992) *The mammals of the Indomalayan Region: a systematic review*. British Museum (Nat. Hist.), London.
2. Musser G.G. and Brothers E.M. (1994) Identification of bandicoot rats from Thailand (*Bandicota*, Muridae, Rodentia). *American Museum Novitates* No. 3110: 1-56.
3. Eamsobhana P. (2006) *The Rat Lungworm* Parastrongylus (=Angiostrongylus) cantonensis: *parasitology, immunology, eosinophilic meningitis, epidemiology and laboratory diagnosis*. Wankaew (IQ) Book Center Co. Ltd., Bangkok.
4. Zhu T.C., Shen H.X., Ye X.G. and Ting B.L. (1993) The survey on *Angiostrongylus cantonensis* in rats, definitive host, in You-hao farm, Xu-wen county, Guangdong province. *Chinese Journal of Zoonoses* **9**: 36-37. (in Chinese)
5. Parmeter S.N. and Chowdhury A.B. (1966) *Angiostrongylus cantonensis* in India. *Bulletin Calcutta School of Tropical Medicine* **14**: 38.
6. Carney W.P. and Stafford E.E. (1979) Angiostrongyliasis in Indonesia: a review. In: Cross J.H. (ed.) *Studies on angiostrongyliasis in Eastern Asia and Australia*. NAMRU-2-SP-44 pp. 14-25. U.S. Naval Medical Research Unit No. 2, Taipei.
7. Alicata J.E. (1966) The presence of *Angiostrongylus cantonensis* in islands of the Indian Ocean and probable role of the giant African snail, *Achatina fulica*, in dispersal of the parasite to the Pacific islands. *Canadian Journal of Zoology* **44**: 1041-1049.
8. Cross J.H. (1967) Review of angiostrongyliasis in Taiwan. *Seminar on helminthiasis and eosinophilic meningitis* pg. 7. South Pacific Commission, Noumea, New Caledonia.
9. Punyagupta S., Bunnag T., Juttiyudata P. and Rosen L. (1970) Eosinophilic meningitis in Thailand. Epidemiologic studies of 484 typical cases and the etiologic role of *Angiostrongylus cantonensis*. *American Journal of Tropical Medicine and Hygiene* **19**: 950-958.

10. Hugot J.-P., Plyusnina A., Herbreteau V., Nemirov K., Laakkonen J., Lundkvist A., Supputamongkol Y., Henttonen H. and Plyusnin A. (2006) Genetic analysis of Thailand hantavirus in *Bandicota indica* trapped in Thailand. *Virology Journal* **3**: 72-80.
11. Xiao S.Y., LeDuc J.W., Chu Y.K. and Schmaljohn C.S. (1994) Phylogenetic analysis of virus isolates in the genus *Hantavirus*, family Bunyaviridae. *Virology* **198:** 205-217.
12. Wangroongsarb P., Petkanchanapong W., Yasaeng S., Imvithaya A. and Naigowit P. (2002) Survey of leptospirosis among rodents in epidemic areas of Thailand. *Journal of Tropical Medicine and Parasitology* **25**: 55-58.
13. Yong H.S. (1968) Karyotype of four Malayan rats (Muridae, genus *Rattus* Fischer). *Cytologia* (*Tokyo*) **33**: 174-180.
14. Sam C.K., Yong H.S. and Dhaliwal S.S. (1979) The G- and C-bands in relation to Robertsonian polymorphism in the Malayan house shrew, *Suncus murinus* (Mammalia, Insectivora). *Caryologia* **32**: 355-363.
15. Yong H.S. (1983) Heterochromatin blocks in the karyotype of the pencil-tailed treemouse, *Chiropodomys gliroides* (Rodentia, Muridae). *Experientia* **39**: 1039-1040.
16. Yong H.S. (1969) Karyotypes of Malayan rats (Rodentia-Muridae, genus *Rattus* Fischer). *Chromosoma* **27**: 245-267.
17. Medway Lord (1983). *The wild mammals of Malaya (Peninsular Malaysia) and Singapore*. Oxford University Press, Malaysia.
18. Avirachan T.T., Mehta H.J. and Sugandhi M.R. (1971) Chromosomes of the genus *Bandicota*. *Mammalian Chromosomes Newsletter* **12**: 62-67.
19. Gadi I.K. and Sharma T. (1983) Cytogenetic relationships in *Rattus*, *Cremnomys*, *Millardia*, *Nesokia* and *Bandicota* (Rodentia: Muridae). *Genetica* **61**: 21-40.
20. Gadi I.K., Sharma T. and Raman R. (1982) Supernumerary chromosomes in *Bandicota indica nemorivaga* and a female individual with XX/XO mosaicism. *Genetica* **58**: 103-108.
21. Markvong A., Marshall J.T. and Gropp A. (1973) Chromosomes of rats and mice of Thailand. *Natural History Bulletin of Siam Society* **25**: 23-40.
22. Badenhorst D., Herbreteau V., Chaval Y., Pagès M., Robinson T.J., Rerkamnuaychoke W., Morand S., Hugot J.-P. and Dobigny G. (2009) New karyotypic data for Asian rodents (Rodentia, Muridae) with the first report of B-chromosomes in the genus *Mus*. *Journal of Zoology* **279**: 44-56.
23. Yong H.S. and Dhaliwal S.S. (1972) Supernumeray (B-) chromosomes in the Malayan house rat, *Rattus rattus diardii* (Rodentia, Muridae). *Chromosoma* **36**: 256-262.
24. Yong H.S. (1971) Centric fusion in the Malayan house rat, *Rattus rattus diardii* (Rodentia, Muridae). *Experientia* **27**: 467-468.
25. Yong H.S. (1972) Robertsonian translocations in the Malayan house shrew, *Suncus murinus* (Insectivora, Soricidae). *Experientia* **28**: 585-586.
26. Yong H.S. (1972) Population cytogenetics of the Malayan house rat, *Rattus rattus diardii*. *Chromosomes Today* **3**: 223-227 (with 1 plate).
27. Sharma T. and Raman R. (1973) Variation of constitutive heterochromatin in

the sex chromosomes of the rodent *Bandicota bengalensis bengalensis* (Gray). *Chromosoma* **41**: 75-84.

28. Pathak S. (1972) Intraspecific sex chromosome polymorphism in the *Bandicota bengalensis bengalensis* (Gray) collected from India. *Cellular and Molecular Life Sciences* **28**: 221-223.
29. Yong H.S. (1974) Geographic variation in the sex chromosomes of the West Malaysian house shrew. *Caryologia* **37**: 65-71.

Journal of Science and Technology in the Tropics (2012) 8: 29-40

Dust acoustic dressed solitons in a four component dusty plasma with superthermal electrons

Prasanta Chatterjee[1], Ganesh Mondal[2], Gurudas Mondal[3] and C. S. Wong[4*]

[1] Department of Mathematics, Siksha Bhavana, Visva Bharati University, Santiniketan-731235, India
[2] Department of Mathematics, Siksha-Satra, Visva Bharati University, Santiniketan-731236, India
[3] Department of ECE, East West University, Mohakhali, Dhaka-1212, Bangladesh
[4] Plasma Technology Research Centre, Physics Department, University of Malaya, 50603 Kuala Lumpur, Malaysia
(*E-mail: cswong@um.edu.my)

Received 22-12-2011; accepted 12-02-2012

Abstract Nonlinear dust acoustic dressed soliton is studied in a four component dusty plasma. Superthermal distributions for electrons are considered. The Korteweg-de Vries (KdV) equation is derived by using reductive perturbation technique. A higher order inhomogeneous differential equation is obtained for the higher order correction. The expression for dressed soliton is obtained by the renormalization method. The expressions for higher order correction are determined by using a truncated series solution technique.

Keywords Korteweg-de Vries equation – reductive perturbation technique – inhomogeneous differential equation – renormalization method – dressed soliton

INTRODUCTION

Dusty plasma research is one of the most rapidlly growing areas in plasma physics. Usually the dust grains are of micron or sub micron size but their masses are very large. Non-linear phenomena like solitons, shocks and vortices in dusty plasma have been studied theoretically and experimentally by several investigators [1-11]. Recently, it is reported that dust acoustic waves (DAW) [4-5] and dust ion acoustic waves (DIAW) [6-7] are also present in dusty plasma and these wave phenomena attract many researchers to work in these fields. Most of the investigators consider three component dusty plasma system for their research and these three components are electrons, ions, and negatively charged dust grains[12-14]. However, it has been found that positively and negatively charged dust grains can co-exist in space [15-17] and in laboratory plasmas [18]. Therefore, it is suggested to investigate the nonlinear behaviours of DAW and DIAW by considering four component dusty plasma that consists of electrons, ions, and positively and negatively charged dust grains.

Most studies of waves in dusty plasmas are based on assumption of a Maxwellian distribution function for the plasma particles. The Maxwellian distribution is the most popular plasma particle distribution and has become the default distribution when the detailed distribution function is unknown. However, it has been observed that in real plasma systems the particles distribution deviate from Maxwellian distributions [19-21]. In theoretical models, when Maxwellian distribution is used to explain or to predict different waves and instabilities, the results do not give quantitative fits with observations [22-24]. This means that Maxwellian distribution is not a realistic distribution under all circumstances and other distribution such as kappa [25] fits better for observed results in the space plasmas. A series of observations [26-28] of space plasmas indicate clearly the presence of superthermal electron and ion stuctures in astrophysical plasma environments; due to the effect of external forces acting on the natural space environmental plasmas, or due to the wave-particle interaction that ultimately leads to kappa like distributions. As a consequence, a high energy tail appears in the distribution function of the particles.

It is well known that solitons in plasma are mostly studied with the framework of Korteweg-de Varies (KdV) equation or (Kodomstev-Petviasville) KP equation. Tailor *et al*. [29] have shown that ion acoustic solitons in the KdV or KP description do not match very well with the experimental observations. Several modifications in theory have been proposed [30-31] in order to give a more accurate prediction of the dynamics of the soliton. One such modification is to include the higher order perturbation corrections in velocity, amplitude, and width to the KdV soliton [32-38]. This gives an improved solution called the dressed soliton which is supposed to give a better agreement with experimental observations. It appears that in order to obtain the non secular solution of dressed soliton by the renormalization method [38] most authors [32-35] have used the method of variation of parameters to obtain the particular solution.

Recently, a new method of truncated series solution has been developed to obtain the solution of the dressed soliton [36]. Chatterjee *et al*. [37-39] have also obtained the dressed soliton for different quantum plasma models. In our present work, we have used the same procedure to obtain the expression for dressed soliton. Here we consider a four component unmagnetized dusty plasma system consisting of superthermal electrons, Boltzmann distributed ions, and also positively and negatively charged dust grains. Using the reductive perturbation technique (RPT), we derive the KdV equations and a linear inhomogeneous equation (higher order KdV type), which govern the evolution of the first and second order potentials, respectively. The nonsecular solution is obtained using the renormalization method of Kodama and Taniuti [40].

BASIC EQUATIONS

The basic equtions are:

$$\frac{\partial n_1}{\partial t}+\frac{\partial (n_1 u_1)}{\partial x}=0, \quad (1)$$

$$\frac{\partial u_1}{\partial t}+u_1\frac{\partial u_1}{\partial x}=\frac{\partial \psi}{\partial x}, \quad (2)$$

$$\frac{\partial n_2}{\partial t}+\frac{\partial (n_2 u_2)}{\partial x}=0, \quad (3)$$

$$\frac{\partial u_2}{\partial t}+u_2\frac{\partial u_2}{\partial x}=-\alpha\beta\frac{\partial \psi}{\partial x}, \quad (4)$$

$$\frac{\partial^2 \psi}{\partial x^2}=n_1-(1-\mu_i+\mu_e)n_2+\mu_e\frac{1}{(1-\frac{\sigma\psi}{\kappa_e-\frac{1}{2}})^{\kappa_e+1/2}}-\mu_i e^{-\psi}, \quad (5)$$

where n_1 and n_2 are the number densities of the negatively and positively charged dust grains normalized by their equilibrium values n_{10} and n_{20} respectively, u_1 and u_2 are negative and positive dust field speed normalized by $C_1=\sqrt{Z_1 k_B T_i/m_i}$. ψ, the electric potential is nomalized by $k_B T_i/e$. x and t are normalized by $\lambda_D=\sqrt{Z_1 k_B T_i/4\pi Z_1^2 e^2 n_{10}}$ and $\omega_{p1}^{-1}=\sqrt{m_1/4\pi Z_1^2 e^2 n_{10}}$ respectively. Define $\alpha=Z_1/Z_2$, $\beta=m_1/m_2$, $\mu_e=n_{e0}/Z_1 n_{10}$, $\sigma=T_i/T_e$, where Z_1 and Z_2 are the number of electrons or protons residing on a negative and positive dust particle respectively. κ_e is kappa distribution of electrons, T_i and T_e are ion and electron temparatures respectively, k_B is the Boltzmann contant and e is the charge of the electrons.

Now, we derive the Korteweg-de Vries (KdV) eqaution from Eqs. (1)-(5) employing the reductive perturbation technique. The independent variables are stretched as $\xi=\varepsilon^{1/2}(x-v_o t)$, $\tau=\varepsilon^{3/2}t$ and the dependent variables are expanded as:

$$n_1=1+\varepsilon n_1^{(1)}+\varepsilon^2 n_1^{(2)}+\varepsilon^3 n_1^{(3)}+\cdots, \quad (6)$$

$$n_2=1+\varepsilon n_2^{(1)}+\varepsilon^2 n_2^{(2)}+\varepsilon^3 n_2^{(3)}+\cdots, \quad (7)$$

$$u_1=0+\varepsilon u_1^{(1)}+\varepsilon^2 u_1^{(2)}+\varepsilon^3 u_1^{(3)}+\cdots, \quad (8)$$

$$u_2=0+\varepsilon u_2^{(1)}+\varepsilon^2 u_2^{(2)}+\varepsilon^3 u_2^{(3)}+\cdots, \quad (9)$$

$$\psi = 0 + \varepsilon\psi^{(1)} + \varepsilon^2\psi^{(2)} + \varepsilon^3\psi^{(3)} + \cdots \quad (10)$$

Here ε is a small nonzero parameter proportional to the amplitude of the perturbation. Now, considering the stretched variables and subtituting Eqs. (6)-(10) into Eqs. (1)-(5) we obtain in the lowest order of ε the distorsion relation as:

$$V_0^2 = \frac{[1+(1-\mu_i+\mu_e)\alpha\beta](2\kappa_e-1)}{\mu_i(2\kappa_e-1)+\mu_e\sigma(2\kappa_e+1)} \quad (11)$$

In the next higher order of ε, we eliminate the second order perturbed quantities from a set of equations to obtain the required KdV equation.

$$\frac{\partial\psi^{(1)}}{\partial\tau} + A\psi^{(1)}\frac{\partial\psi^{(1)}}{\partial\xi} + B\frac{\partial^3\psi^{(1)}}{\partial\xi^3} = 0 \quad (12)$$

where the nonliner coefficient A and the dispersion coefficient B are given by

$$A = \frac{1}{2V_0[1+(1-\mu_i+\mu_e)\alpha\beta]}(1-(1-\mu_i+\mu_e)\alpha^2\beta^2 + \frac{V_0^4\mu_e(2\kappa_e+1)^2\sigma^2}{2\kappa_e-1)^2} - V_0^4\mu_i), \quad (13)$$

$$B = \frac{V_0^3}{2[1+(1-\mu_i+\mu_e)\alpha\beta]}. \quad (14)$$

Equation (12) describes the nonlinear propagation of DASWs in a four component dusty plasmas in the presene of superthermal electrons.

Next we determine the higher order nonlinear and dispersion effects of the KdV equation. We start by equating the next higher order terms in ε and after some standard algebra, we obtain the differential equation for the higher order correction $\psi^{(2)}$:

$$\frac{\partial\psi^{(2)}}{\partial\tau} + A\frac{\partial(\psi^{(1)}\psi^{(2)})}{\partial\xi} + B\frac{\partial^3\psi^{(2)}}{\partial\xi^3}$$

$$= L(\psi^{(1)})^2\frac{\partial\psi^{(1)}}{\partial\xi} + M\psi^{(1)}\frac{\partial^3\psi^{(1)}}{\partial\xi^3} + N\frac{\partial^5\psi^{(1)}}{\partial\xi^5} + P\frac{\partial}{\partial\xi}(\frac{\partial\psi^{(1)}}{\partial\xi})^2, \quad (15)$$

where *L*, *M*, *N* and *P* are given in the appendix. Equation (15) is a linear inhomogeneous differential equation in $\psi^{(2)}$ whose source term is given as a function of $\psi^{(1)}$. In the next section, we determine the non-secular solution for $\psi^{(2)}$ (for details see [36]).

SOLUTIONS

We use the method of renormalization developed by Kodama and Taniuti [40] to obtain a nonsecular solution for $\psi^{(2)}$. Equation (12) is modified as:

$$\frac{\partial \tilde{\psi}^{(1)}}{\partial \tau} + A\tilde{\psi}^{(1)}\frac{\partial \tilde{\psi}^{(1)}}{\partial \xi} + B\frac{\partial^3 \tilde{\psi}^{(1)}}{\partial \xi^3} + \delta\lambda\frac{\partial \tilde{\psi}^{(1)}}{\partial \xi} = 0, \quad (16)$$

while the inhomogeneous Eq. (15) for $\psi^{(2)}$ becomes

$$\frac{\partial \tilde{\psi}^{(2)}}{\partial \tau} + A\frac{\partial(\tilde{\psi}^{(1)}\tilde{\psi}^{(2)})}{\partial \xi} + B\frac{\partial^3 \tilde{\psi}^{(2)}}{\partial \xi^3} + \delta\lambda\frac{\partial \tilde{\psi}^{(2)}}{\partial \xi} = S(\tilde{\psi}^{(1)}) + \delta\lambda\frac{\partial \tilde{\psi}^{(1)}}{\partial \xi}. \quad (17)$$

The parameter $\delta\lambda$ in Eqs. (16) and (17) is introduced in such a way that the secular (resonant) term in $S(\tilde{\psi}^{(1)})$ is canceled by the term $\delta\lambda(\partial\tilde{\psi}^{(1)}/\partial\xi)$. A new stationary frame variable η is introduced as:

$$\eta = \xi - (\lambda + \delta\lambda)\tau, \quad (18)$$

where $(\lambda+\delta\lambda) = X - 1$, and X is the Mach number. Using (18) in (16) and integrating using boundary conditions that $\tilde{\psi}^{(1)}$ and its derivatives vanish as $\eta \to \pm\infty$, we obtain the stationary renormalized solitary wave solution of Eq. (16), given by (up to 1st order in λ) as:

$$\tilde{\psi}^{(1)} = \psi_0 \, sech^2(\tilde{D}\eta), \quad (19)$$

where

$$\psi_0 = \frac{3\lambda}{A}, \quad (20)$$

$$\tilde{D} = D = \left(\frac{\lambda}{4B}\right)^{1/2}. \quad (21)$$

Now using (18)-(21) in (17), integrating with respect to η, under the boundary conditions that $\tilde{\psi}^{(2)}$ and its derivatives vanish as $\eta \to \pm\infty$ and removing the secular terms, we obtain a second order inhomogeneous differential equation for $\tilde{\psi}^{(2)}$ which is

$$B\frac{d^2\tilde{\psi}^{(2)}}{d\eta^2} + \lambda(3\,sech^2(\tilde{D}\eta) - 1)\tilde{\psi}^{(2)} = A_2 sech^4\tilde{D}\eta + A_3 sech^6\tilde{D}\eta, \quad (22)$$

where A_2, A_3 are given in the appendix and $\delta\lambda$ is given by

$$\delta\lambda = -\frac{N\lambda^2}{B^2}. \quad (23)$$

Equation (22) is a second-order inhomogeneous differential equation whose solution can be written as:

$$\tilde{\psi}^{(2)} = \tilde{\psi}_{comp} + \tilde{\psi}_p, \quad (24)$$

where $\tilde{\psi}_{comp}$ is the complementary function and $\tilde{\psi}_p$ is the particular solution. Following Refs [32-39], it can be shown easily that the complementary function $\tilde{\psi}_{comp}$ has no role in the second order correction $\tilde{\psi}_2$, while the particular integral does. A series solution method developed by Chatterjee *et el*. [36] is adopted to determine $\tilde{\psi}_p$, where $\tilde{\psi}_p$ is defined as a truncated power series

$$\tilde{\psi}_p = \sum_{i=1}^{K} a_i sech^{2i}(\tilde{D}\eta) = a_1 sech^2(\tilde{D}\eta) + a_2 sech^4(\tilde{D}\eta) + \cdots \quad (25)$$

and it is a particular solution of the Eq. (22). The matching parameter K can be determined after equating the highest power of $sech\xi$ that arises in the left and right hand side of Eq. (22) after substitution. A simple calculation would show that $K = 2$. Therefore, the appropriate series that solves Eq. (25) is expressed as:

$$\tilde{\psi}_p = a_1 sech^2(\tilde{D}\eta) + a_2 sech^4(\tilde{D}\eta), \quad (26)$$

where a_1 and a_2 are given by

$$a_1 = \frac{1}{\lambda}\left(\frac{2}{3}A_2 + A_3\right), \quad (27)$$

$$a_2 = -\frac{A_3}{2\lambda}. \quad (28)$$

Using Eqs. (19), (24) and (26), the stationary one soliton solution up to second order in λ for a four component superthermal dusty plasma is finally given by:

$$\tilde{\psi} = \tilde{\psi}^{(1)} + \tilde{\psi}^{(2)} = \tilde{\psi}_0\ sech^2(\tilde{D}\eta) + a_1 sech^2(\tilde{D}\eta) + a_2 sech^4(\tilde{D}\eta). \quad (29)$$

The amplitude of the KdV soliton that includes the second order contribution $\tilde{\psi}_0$, the amplitude of the dressed soliton that includes the second order contribution $\tilde{\psi}_0^*$ and the width $\tilde{W}$ of the dressed soliton are then given below:

$$\tilde{\psi}_0 = \frac{3(\lambda + \delta\lambda)}{A}, \quad (30)$$

$$\tilde{\psi}_0^* = \frac{3(\lambda + \delta\lambda)}{A} + a_1 + a_2, \quad (31)$$

$$\tilde{W} = \left(\frac{4B}{\lambda + \delta\lambda}\right)^{1/2}. \quad (32)$$

RESULTS AND DISCUSSION

Equation (19) gives the renormalized KdV soliton whose amplitude and widths are given by Eqs. (20) and (21), respectively. Equation (26) represents the higher order correction to KdV soliton whose speed is $\lambda + \delta\lambda$ and amplitude and width are given by Eqs. (31) and (32). The solutions of Eqs. (16) and (17) are obtained by the method of renormalization [38]. Although several investigators ([32-35]) have used the method of variation of parameters to find the particular solution of the higher order correction, we chose a simpler technique by considering the particular solution as a truncated power series of $sech^2(\tilde{D}\eta)$, [36].

The dust acoustic dressed soliton in four component plasma with superthermal electron is considered. The effects of higher order nonlinear terms on solitons are illustrated by plotting the KdV soliton (dotted line), $\tilde{\psi}^{(1)}$ the higher order correction (dashed line) $\tilde{\psi}^{(2)}$ and the dressed soliton (solid line) $\tilde{\psi}$ vs η as shown in Figure 1(a). The other parameters are $\lambda = 0.3$, $\mu_i = 0.5$, $\mu_e = 0.5$, $\sigma = 0.15$, $\alpha = 1$, $\beta = 1$, and $\kappa = 1.5$. It is seen that the amplitude of the higher order correction (dashed line) is smaller than the the amplitude of KdV soliton (dotted line). The dressed soliton (solid line) $\tilde{\psi}$ vs η for $\kappa = 1000$ is as shown in Figure 1(b). The other parameters are same as in Figure 1(a). The amplitude of the dressed soliton (solid line) $\tilde{\psi}$ is found to be larger than the amplitude of the KdV soliton (dotted line) $\tilde{\psi}^{(1)}$ Also the amplitude of KdV soliton is larger than the amplitude of higher order correction (dashed line). From the perturbation theory it is known that one can only consider the higher order correction if $|a_1 + a_2| < |\tilde{\psi}_0|$. On the contrary, non-physical solution is obtained if $|a_1 + a_2| \geq |\tilde{\psi}_0|$. So Figure 1(a) and (b) are physical.

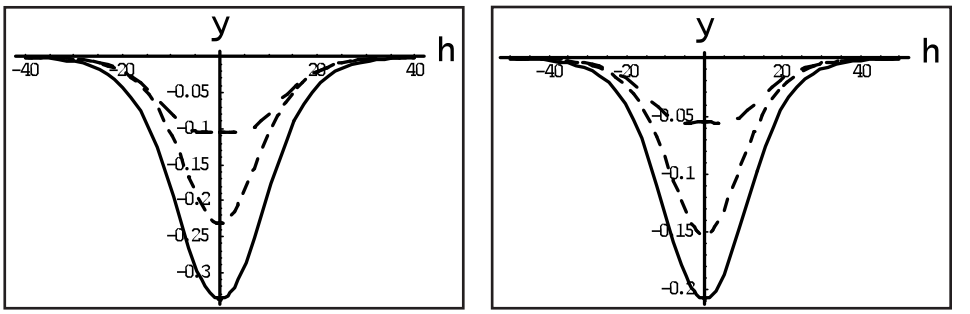

Figure 1. The KdV soliton (dotted line) $\psi^{(1)}$, the higher order correction (dashed line) $\psi^{(2)}$ and the dressed soliton (solid line) ψ are plotted against η. Top: 1(a) $\kappa = 1.5$ $\lambda = 0.3$, $\mu_i = 0.5$, $\mu_e = 0.5$, $\sigma = 0.15$, $\alpha = 1$ and $\beta = 1$ Bottom: 1(b) $\kappa = 1000$, $\lambda = 0.3$, $\mu_i = 0.5$, $\mu_e = 0.5$, $\sigma = 0.15$, $\alpha = 1$ and $\beta = 1$.

Figure 2(a) has been plotted to observe the effect of different parameters on the amplitudes of solitons. In this figure the amplitude of KdV soliton (dotted line) $\tilde{\psi}^{(1)}$, the amplitude of dressed soliton (solid line) $\tilde{\psi}$ and the amplitude of higher order correction(dashed line) $\tilde{\psi}^{(2)}$ are drawn aganist κ. The other parameters are $\lambda = 0.3$, $\mu_i = 0.5$, $\mu_e = 0.5$, $\sigma = 0.15$, $\alpha = 1$ and $\beta = 1$. It is seen that the amplitude of KdV, the amplitude higher order correction and the amplitude of dressed soliton decreses rapidly and then increses slowly with the increse of κ througout the region. But the amplitude of higher order correction never exceed the amplitude of the KdV soliton. So the dressed soliton is physical for all values of κ.

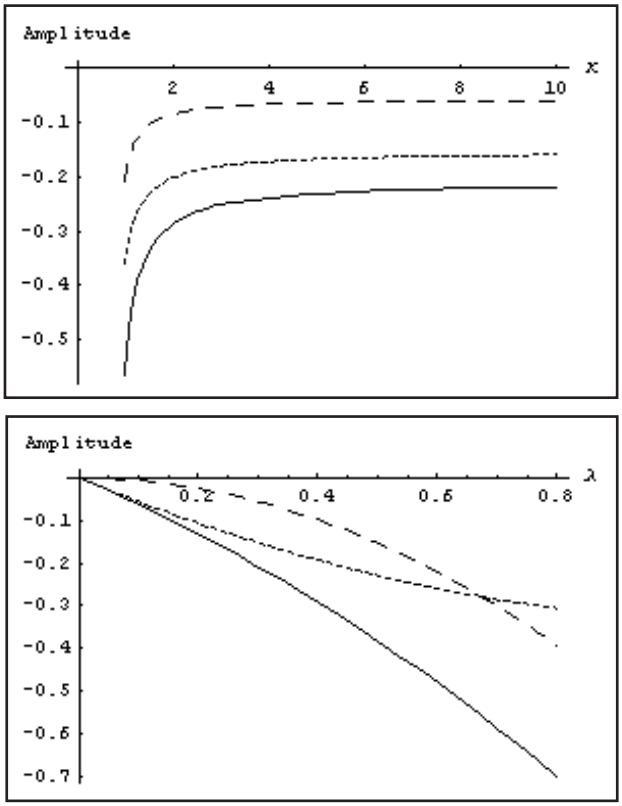

Figure 2. Top: 2(a) The amplitudes of the KdV soliton (dotted line) $\psi^{(1)}$, the higher order correction (dashed line) $\psi^{(2)}$ and dressed soliton (solid line) ψ are plotted against κ. The other parameters are $\lambda = 0.3$, $\mu_i = 0.5$, $\mu_e = 0.5$, $\sigma = 0.15$, $\alpha = 1$ and $\beta = 1$. Bottom: 2(b) The amplitude of KdV (dotted line), the amplitude of the higher order correction (dashed line) and the amplitude of the dressed soliton (solid line) is plotted against λ. The other parameters are, $\kappa = 1.5$, $\mu_i = 0.5$, $\mu_e = 0.5$, $\sigma = 0.15$, $\alpha = 1$ and $\beta = 1$.

In Figure 2(b), the amplitude of KdV soliton (dotted line), the dressed soliton (solid line) and the higher order correction (dashed line) have been plotted against λ by taking other parameters as $\mu_i = 0.5$, $\mu_e = 0.5$, $\sigma = 0.15$, $\alpha = 1$, $\beta = 1$, and $\kappa = 1.5$. It is seen that the amplitude of the different solitons increses with the increses of λ. It is also observed that if $\lambda \geq 0.607$ the amplitude of higher order correction exceed the amplitude of the amplitude of KdV soliton. So the dressed soliton exits if $\lambda < 0.607$.

In Figure 3 the width of the dressed soliton against κ has been plotted. Other parameters are same as in Figure 1(a). It is observed that the width of dressed soliton increses rapidly initially then slowly with the increase of κ.

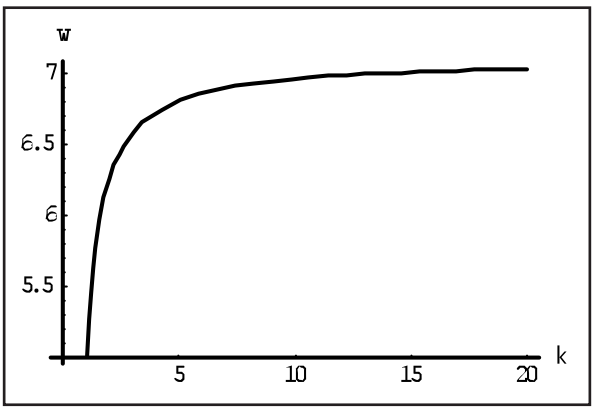

Figure 3. The width of dressed soliton is plotted against κ. The other parameters are $\lambda = 0.3$, $\mu_i = 0.5$, $\mu_e = 0.5$, $\sigma = 0.15$, $\alpha = 1$ and $\beta = 1$.

Finally we can remark that all the parameters have a singificant role on the width and the amplitude of dressed soliton.

CONCLUSION

We have studied dust acoustic KdV solitons, second order correction to KdV solitons and the dressed soliton in a four component dusty plasma. The KdV equation is obtained using RPT. Higher order nonlinear and dispersion terms are considered and a linear second order inhomogeneous differential equation is derived for the higher order correction. The derived dressed soliton solution is expected to give a better accuracy in matching the experimental data. The physical situation is considered where the electron distribution is superthermal (kappa distriduted). The renormalization method is used to get the stationary nonsecular solution. Following a technique described in [36], we have derived the particular solution by considering a finite term series for higher order potential. The range of parameters where the higher order correction is valid

are also described. Finally, we discussed the characteristics of the dressed soliton using graphs. It is interesting to note that the technique can be extended to higher order correction of KdV soliton in non planar geometry and to a shock wave solution.

Acknowledgements – The authors would like to thank the SAP(DRS) for finnancial support.

REFERENCES

1. Sheehan D.P., Carilo M. and Heidbrink W. (1990) Device for dispersal of micrometer and submicrometer sized particles in vacuum. *Rev. Sci. Instrum.* **61**: 3871-3875.
2. Carlile R.N., Geha S., O'Hanlon J.F. and Stewart J.C. (1991) Electrostatic trapping of contamination particles in a process plasma environment. *Appl. Phys. Lett*. **59**: 1167-1169.
3. Bliokh P.V. and Yarashenko V.V. (1985) Electrostatic waves in Saturans Rings. *Sov. Astro.* **29**: 330-336.
4. Rao N.N., Shukla P.K. and Yu M.Y. (1990) Dust-acoustic waves in dusty plasmas. *Planet Space Sci*. **38**: 543-546.
5. Barkan A. and Merlino R.L. and D'Angelo N. (1995) Laboratory observation of the dust acoustic wave mode. *Phys. Plasmas* **2**: 3563-3565.
6. Shukla P.K. and Silin V.P. (1992) Dust ion-acoustic wave. *Phys. Scripta* **45**: 508.
7. Merlino R.L., Barkan A., Thompson C. and D'Angelo N. (1998) Laboratory studies of waves and instabilities in dusty plasmas. *Phys. Plasmas* **5**:1607-1614.
8. Melandso F. (1996) Lattice waves in dust plasma crystals. *Phys. Plasmas* **3**: 3890-3901.
9. Farokhi B., Shukla P.K., Tsindsadze N.L. and Tskhakaya D.D. (1990) Linear and nonlinear dust lattice waves in plasma crystals. *Phys. Lett*. **A264**: 318-323.
10. Shukla P.K. and Verma R.K. (1993) Convective cells in nonuniform dusty plasmas. *Phys. Fluids* **B5**: 236-237.
11. Shukla P.K., Yu M.Y. and Bharuthram R. (1991) Linear and nonlinear dust drift waves. *J. Geophys. Res*. **96**: 21343-21346.
12. Mahmood S. and Saleem H. (2003) Dust acoustic solitary wave in the presence of dust streaming. *Phys. Plasmas* **10**: 47-52.
13. Maitra S. and Roychoudhury R. (2005) Gas dynamical approach to study dust acoustic solitary waves. *Phys. Plasmas* **12**: 064502.
14. Chatterjee P. and Jana R.K. (2005) Speed and shape of dust acoustic solitary waves in presence of dust streaming. *J. Naturforschung* **60a**: 275-281.
15. Nakamura Y. and Tsukabayashi I. (1984) Observation of modified Korteweg-de Vries solitons in a multicomponent plasma with negative ions. *Phys. Rev. Lett.* **52**: 2356-2359.
16. Watanabe S.J. (1984) Ion acoustic soliton in plasma with negative ion. *Phys. Soc. Japan* **53**: 950-956.
17. Sheridan T.E. (1998) Some properties of large-amplitude, negative-potential solitary waves in a three-component plasma. *J. Plasma Phys.* **60**: 17-28.

18. Shukla P.K. (1994) Shielding of a slowly moving test charge in dusty plasmas. *Phys. Plasmas* **1**: 1362-1363.
19. Lifshitz E.M. and Pitaevskii L.P. (1975) *Physical Kinetics*. Pergamon, New York.
20. Krapchev V.K. and Ram A.K. (1980) Adiabatic theory for a single nonlinear wave in a Vlasov plasma. *Phys. Rev.* **A22**: 1229-1242.
21. Steinacker J. and Miller J. (1992) Stochastic gyroresonant electron acceleration in a low beta plasma. I. Interaction with parallel transverse cold plasma waves. *The Astrophysical Journal* **393**: 764-781.
22. Xue S., Thorne R.M. and Summers D. (1993) Electromagnetic ion-cyclotron instability in space plasmas. *J. Geophys. Res.* **98**: 17475-17484.
23. Quereshi M.N.S., Shah H.A., Murtaza G., Schwartz S.J. and Mahmood F. (2004) Parallel propagating electromagnetic modes with the generalized (*r*,*q*) distribution function. *Phys. Plasma* **11**: 3819-3830.
24. Summers D. and Thorne R.M. (1991) The modified plasma dispersion function. *Phys. Fluids* **B3**: 1835-1847.
25. Treumann A. (1999) Kinetic theoretical foundation of Lorentzian statistical mechanics. *Phys. Scripta* **59**: 19-26.
26. Vasylinas V.M. (1968) A survey of low-energy electrons in the evening sector of the magnetosphere with OGO 1 and OGO 3. *J. Geophys. Res.* **73**: 2839-2884.
27. Leubner M.P.J. (1982) On Jupiter's whistler emission. *J. Geophys. Res.* **87**: 6335-6338.
28. Armstrong T.P., Paonessa M.T., Bell E.V. and Krimgis S.M. (1983) Voyager observations of Saturnian ion and electron phase space densities. *J. Geophys. Res.* **88**: 8893-8904.
29. Tailor R.J., Baker D.R. and Ikezi H. (1970) Formation and interaction of ion-acoustic solitons. *Phys. Rev. Lett.* **25**: 11-14.
30. Kato Y., Tajiri M. and Taniuti T. (1972) Precursor of Ion-Acoustic Quasishock Wave in Collisionless Plasma. *Phys. Fluids* **15**: 865-871.
31. Ichikawa Y.H., Mistu-Hashi T. and Komo K. (1976) Contribution of Higher order terms in the reductive perturbation theory .I. A case of weakly dispersive wave. *J. Phys. Soc. Japan* **41**: 1382-1386.
32. Tiwari R.S., Kaushik A. and Mishra M.K. (2007) Effects of positron density and temperature on ion acoustic dressed solitons in an electron–positron–ion plasma. *Phys. Lett.* **A365**: 335-340.
33. El-Shewy E.K. (2005) Effect of higher order nonlinearity to nonlinear electron-acoustic solitary waves in an unmagnetized collisionless plasma. *Chaos, Solitons & Fractals* **26**: 1073-1079.
34. Gill T.S., Bala P. and Kaur H. (2008) Higher order solutions to ion-acoustic solitons in a weakly relativistic two-fluid plasma. *Phys. Plasmas* **15**: 122309.
35. EL-Labany S.K., El-Shamy E.F. and El-Warraki S.A. (2009) Dressed ion-acoustic solitons in magnetized dusty plasmas. *Phys. Plasmas* **16**: 013703.
36. Chatterjee P., Mondal G., Roy K., Muniandy S.V., Yap S.L. and Wong C.S. (2009) Genaration of drassed soliton in four componant dusty plasma with non thermal ions. *Phys. Plasmas* **16**: 072102.
37. Chatterjee P., Das B., Mondal G., Muniandy S.V. and Wong C.S. (2010) Higher order corrections to dust-acoustic soliton in a quantum dusty plasma. *Phys. Plasmas* **17**: 103705.

38. Chatterjee P., Roy K., Muniandy S.V. and Wong C.S. (2009) Dressed soliton in quantum dusty pair-ion plasma. *Phys. Plasmas* **16**: 112106.
39. Chatterjee P., Roy K., Mondal G., Muniandy S.V., Yap S.L. and Wong C.S. (2009) Dresseed solitons in Quantum electron-positron-ion plasmas. *Phys. Plasmas* **16**: 122112.
40. Kodoma Y. and Taniuti T. (1978) Higher Order Approximation in the Reductive Perturbation Method. I. The Weakly Dispersive System. *J. Phys. Soc. Japan* **45**: 298-310.

APPENDIX: Expressions

$$L = L_1[(\frac{A^2}{V_0^4} - \frac{6A}{V_0^5} - \frac{9}{2V_0^6}) - (1-\mu_i+\mu_e)(\frac{3A^2\alpha\beta}{V_0^4}$$

$$-\frac{21A\alpha^2\beta^2}{2V_0^5} + \frac{3\alpha^3\beta^3}{V_0^6} - \frac{3\alpha^3\beta^3}{2V_0^5}) - \frac{\mu_e(2k_e+1)^3\sigma^3}{2(2k_e-1)^3}] \quad (33)$$

$$L_1 = \frac{V_0^3}{2(1+(1-\mu_i+\mu_e))} \quad (34)$$

$$M = L_1[(-\frac{5AB}{V-0^4} - \frac{6B}{V_0^5}) - (1-\mu_i+\mu_e)(\frac{6AB\alpha\beta}{V_0^4} - \frac{6B\alpha^2\beta^2}{V_0^5})] \quad (35)$$

$$N = L_1[-\frac{3B^2}{V_0^4} - (1-\mu_i+\mu_e)(\frac{3B^2\alpha^2\beta^2}{V_0^4})] \quad (36)$$

$$P = L_1[(-\frac{9AB}{V_0^4} - \frac{4B}{V_0^4}) - (1-\mu_i+\mu_e)(\frac{3AB\alpha\beta}{V_0^4} - \frac{4B\alpha^2\beta^2}{V_0^5})] \quad (37)$$

$$A_2 = -\frac{45N\lambda^3}{2AB^2} + \frac{9\lambda^3(M+2P)}{2A^2B}, \quad (38)$$

$$A_3 = \frac{45N\lambda^3}{2AB^2} - \frac{9(M+P)\lambda^3}{A^2B} + \frac{9L\lambda^3}{A^3} \quad (39)$$

$$a_1 = \frac{15N\lambda^2}{2AB^2} - \frac{3(2M+P)\lambda^2}{A^2B} + \frac{9L\lambda^2}{A^3} \quad (40)$$

$$a_2 = -\frac{45N\lambda^2}{4AB^2} + \frac{9(M+P)\lambda^2}{2A^2B} - \frac{9L\lambda^2}{2A^3}. \quad (41)$$

Journal of Science and Technology in the Tropics (2012) 8: 41-51

Effects of non-thermal ions on dust-ion-acoustic shock waves in a dusty plasma with heavy negative ions in non-planar geometry

A. Paul[1], G. Mandal[1,*], A. A. Mamun[2] and M. R. Amin[1]

[1] Department of Electronics and Communications Engineering, East West University, 43 Mohakhali, Dhaka 1212, Bangladesh
[2] Department of Physics, Jahangirnagar University, Savar, Dhaka 1342, Bangladesh
(*E-mail: gdmandal@ewubd.edu)

Received 20-12-2011; accepted 22-02-2012

Abstract Dust negative ion acoustic (DNIA) shock wave in a dusty multi-ion plasma consisting of electrons, light positive ions, heavy negative ions and extremely massive charge fluctuating negative dust in a non-planar geometry has been investigated by employing reductive perturbation technique. For this, a modified Burger's equation is derived and numerically solved it to get the envelope of the DNIA shock wave. The effect of the non-thermal ions on the DNIA shock waves is included in the dusty plasma with heavy negative ions. It is shown how the basic features of the nonlinear DNIA shock waves are modified by the presence of the charge fluctuating dust and the nonlinear nature of the positively charged light ions in the non-planer geometry. It has been observed that the developed shock heights are different for different geometries, and in the case of spherical geometry the shock wave has higher height compared to that of the cylindrical geometry. The results of the present work would be useful in understanding laboratory and space dusty plasmas.

Keywords dusty plasma – non-thermal ions – Burger's equation

INTRODUCTION

Studies of the dust ion acoustic (DIA) waves in multi-ion dusty plasmas have received a great deal of attention in recent years [1-11]. Dusty plasma exists in astrophysical and space environments [12-15], such as cometary tails, planetary rings and interstellar medium. Shukla and Silin [16] have first theoretically reported one of these waves as low frequency dust ion-acoustic (DIA) waves. The DIA waves of Shukla and Silin [16] have also been observed in laboratory experiments [1, 17-20]. Both in theoretical and experimental point of view the linear properties of DIA waves [15, 16, 21, 22] are now well understood. Recently there has been extensive research work on nonlinear waves associated with the DIA waves [23-26].

The presence of negative ions, which are present in space and laboratory dusty plasma situations [19, 20, 27], significantly modify the charging of dust particles

[28-30]. The non-linear DIA waves were studied by Mamun *et al.* [31], Mamun and Shukla [24], and Sayeed and Mamun [32], where they have considered the Boltzmann distributed electrons and ions. However, they have not considered any charge fluctuation on the dust grains. In their work, it is found that the DIA waves are solitary waves. Most of the studies [28, 29, 32, 33] on these nonlinear waves have been done where dust particles are considered stationary and the charges on dust particles are constant. But the charge on dust particles varies with time and space [29, 34-36], so this concept many not be realistic in space and laboratory plasmas, and the dusty plasma waves are always associated with the dust charge fluctuation.

Mamun *et al.* [31] have studied non-linear propagation of dust negative ion acoustic (DNIA) waves and have shown that the dust charge fluctuation is a source of dissipation, and is responsible for the formation of DNIA shock structures in such a dusty multi-ion plasma. It has been found that the basic features of such DNIA shock structure are different from those of the DIA shock structure of Mamun, *et al.*[29-31, 37]. In their work Paul *et al.* [38] have considered a one-dimensional, collisionless, unmagnetized dusty multi-ion plasma consisting of electrons, single charged light positive ions, heavy negative mobile ions, and extremely massive charge fluctuating dust. They have shown how the basic features of nonlinear DNIA shock waves are modified by presence of the charge fluctuating dust and the nonthermal nature of the mobile negatively charged heavy ions.

Most of the theoretical works on DNIA shock waves, for example [31] and [38], are based on the one-dimensional planar geometry which may not be a realistic situation for laboratory devices. Thus, in this paper, we have considered dusty multi-ion plasma as [38]; however, here we investigate it in the situation of non-planar cylindrical and spherical geometries.

GOVERNING EQUATIONS

We consider a one-dimensional, collisionless, unmagnetized dusty multi-ion plasma consisting of electrons, single charged light positive ions, heavy negative mobile ions, and extremely massive charge fluctuating dust. The equilibrium state of the dusty multi-ion plasma system under consideration is defined as $n_{i0} - n_{e0} - z_h n_{h0} + q_{d0} n_{d0} / e = 0$, where e is the magnitude of the electronic charge, n_{j0} is the equilibrium number density of plasma species j, z_h is the charge state of the heavy ions and q_{d0} is the equilibrium charge of a dust particle.

The nonlinear dynamics of DNIA shock waves in such a dusty multi-ion plasma system in a non-planar geometry is described by

$$\frac{\partial n_h}{\partial t}+\frac{1}{r^\nu}\frac{\partial}{\partial r}(r^\nu n_h u_h)=0, \tag{1}$$

$$\frac{\partial u_h}{\partial t}+u_h\frac{\partial u_h}{\partial r}=\frac{z_h e}{m_h}\frac{\partial \phi}{\partial r}-\frac{V_{Th}^2}{n_h}\frac{\partial n_h}{\partial r}, \tag{2}$$

and

$$\frac{1}{r^\nu}\frac{\partial}{\partial r}(r^\nu\frac{\partial \phi}{\partial r})=4\pi e\left(n_e-n_i+z_h n_h-\frac{Q_d}{e}n_{d0}\right), \tag{3}$$

where $\nu=1$ corresponds to cylindrical and $\nu=2$ corresponds to spherical geometry, n_h is the heavy ion number density, u_h is heavy ion fluid speed, z_h is the charge state of heavy ions, m_h is the heavy ion mass, ϕ is the electrostatic wave potential, V_{Th}^2 is the ratio of heavy ion thermal energy and the heavy ion mass $(=T_h/m_h)$, where T_h is the temperature of the heavy ions in energy units, n_e is electron number density, n_i is the light ion number density, and Q_d is the charge of the static dust particles. We consider Boltzmann distributed electrons and non-thermal light ions for the propagation of low phase speed electrostatic perturbation mode. We can express n_e and n_i as follows:

$$n_e=n_{e0}\exp\left(\frac{e\phi}{T_e}\right), \tag{4}$$

$$n_i=n_{i0}\exp\left(-\frac{e\phi}{T_i}\right)\left(1+\beta\frac{e\phi}{T_i}+\beta\frac{e^2\phi^2}{T_i^2}\right), \tag{5}$$

where T_e and T_i are respectively the electron and ion thermal energies respectively. If the electron, light ion collection current, and heavy ion collection current at equilibrium are represented by I_e, I_i and I_{h0} and respectively, then the variation of the dust grain charge Q_d can be written as

$$\frac{\partial Q_d}{\partial t}=I_e+I_i+I_{h0}. \tag{6}$$

For $Q_d<0$, I_e and I_i [30] are given by

$$I_e=-4\pi r_d^2 n_e e\left(\frac{T_e}{2\pi m_e}\right)^{1/2}\exp\left(\frac{eQ_d}{r_d T_e}\right), \tag{7}$$

and

$$I_i = 4\pi r_d^2 n_{i0} e\left(\frac{T_e}{2\pi m_i}\right)^{1/2} \exp\left(-\frac{e\phi}{T_i}\right)\left[1+\frac{24\alpha}{5}+\frac{16\alpha}{3}\left(\frac{e\phi}{T_i}\right)\right.$$
$$\left. + 4\alpha\frac{e^2\phi^2}{T_i^2}-\frac{eQ_d}{r_d T_i}\left(1+\frac{8\alpha}{5}+4\alpha\frac{e^2\phi^2}{T_i^2}+\frac{16\alpha}{3}\frac{e\phi}{T_i}\right)\right], \quad (8)$$

where r_d is the dust particle radius and $\beta = 4\alpha/(1+3\alpha)$. Here we consider that the heavy ion current fluctuation is much less than electron and light ion current fluctuation. Let us normalize different variables as follows:

$N = n_h/n_{h0},\ U = u_h/C_h,\ \Phi = e\phi/T_h,\ Q = Q_d/q_{d0},\ R = r/\lambda_{Dh},\ T = t\omega_{ph},$

where $\lambda_{Dh} = \left(T_h/4\pi z_h^2 e^2 n_{h0}\right)^{1/2},\ C_h = \left(T_h/m_h\right)^{1/2},$

and $\omega_{ph} = \left(4\pi z_h^2 e^2 n_{h0}/m_h\right)^{1/2}.$

By using these relations, Eqs. (1)-(3) and Eq. (6) can be written in the following form:

$$\frac{\partial N}{\partial T}+\frac{1}{R^\nu}\frac{\partial}{\partial R}\left(R^\nu NU\right)=0, \quad (9)$$

$$\frac{\partial U}{\partial T}+U\frac{\partial U}{\partial R}=z_h\frac{\partial Q}{\partial R}-\frac{1}{N}\frac{\partial N}{\partial R}, \quad (10)$$

$$\frac{1}{R^\nu}\frac{\partial}{\partial R}\left(R^\nu\frac{\partial\Phi}{\partial R}\right)=\mu_e\exp\left(\sigma_e\Phi\right)-\mu_i\exp\left(-\sigma_i\Phi\right)\left(1+\beta\sigma_i\Phi+\beta\sigma_i^2\Phi^2\right)$$
$$+\frac{N}{z_h}+\gamma Q, \quad (11)$$

and

$$\frac{\partial Q}{\partial T}=D+E\Phi+FQ+GQ^2+HQ\Phi+KQ^2, \quad (12)$$

where

$\sigma_e = T_h/T_e,\ \sigma_i = T_h/T_i,\ \mu_e = n_{e0}/z_h^2 n_{h0},\ \mu_i = n_{i0}/z_h^2 n_{h0},$

$\gamma = q_{d0}n_{d0}/ez_h^2 n_{h0},$

$A = \mu_e - \mu_i,\ B = \mu_e\sigma_e + (1-\beta)\mu_i\sigma_i,\ C = \mu_e\sigma_e^2/2 - \mu_i\sigma_i^2/2,$

$P = -4\pi r_d^2 n_{e0} e(T_e/2\pi m_e)^{1/2}/(q_{d0}\omega_{ph}),$

$S = 4\pi r_d^2 n_{i0} e(T_i/2\pi m_i)^{1/2}/(q_{d0}\omega_{ph}),$

$$J = I_{h0}/(q_{d0}\omega_{ph}),\ D = P + (1+24\alpha/5)S + J,\ E = \sigma_e P + (1-8\alpha/15)\sigma_i S,$$
$$F = Peq_{d0}/r_d T_e - (1+8\alpha/5)eS/r_d T_i,\ G = e^2 q_{d0}^2 P/2r_d^2 T_e^2,$$
$$H = Peq_{d0}\sigma_e/r_d T_e + (1-16\alpha/15)Seq_{d0}\sigma_i/r_d T_i,$$
$$K = (\sigma_e^2 P/2) + \left[(1/2) + (16\alpha/15)\right]\sigma_i^2 S.$$

DERIVATION OF BURGER'S EQUATION

To derive a dynamical equation for the nonlinear propagation of the DNIA shock waves in a non-planar geometry, we use Eqs. (9-12) and employ the reductive perturbation technique (RPT) [39]. We consider the following stretched coordinates [40]:

$$\xi = \varepsilon(R - V_p T), \tag{13}$$

and

$$\tau = \varepsilon^2 T, \tag{14}$$

where ε is a small parameter satisfying $0 < \varepsilon < 1$ that measures the weakness of the dispersion, and V_p is the phase speed of the perturbation mode normalized by C_d.

Now we expand the variables N, U, Φ and Q in the power series of ε,

$$N = 1 + \varepsilon N^{(1)} + \varepsilon^2 N^{(2)} + \ ..., \tag{15}$$
$$U = \varepsilon U^{(1)} + \varepsilon^2 U^{(2)} + \ ..., \tag{16}$$
$$\Phi = \varepsilon\Phi^{(1)} + \varepsilon^2\Phi^{(2)} + \ ..., \tag{17}$$
$$Q = 1 + \varepsilon Q^{(1)} + \varepsilon^2 Q^{(2)} + \ .... \tag{18}$$

Substituting these values in Eqs. (9-12), we get equations of different powers of ε. Equating the coefficients of ε from Eqs. (11) and (12), and the coefficients of ε^2 from Eqs.(9) and (10), we obtain:

$$Q^{(1)} = -\delta\Phi^{(1)}, \tag{19}$$
$$N^{(1)} = -z_h M\Phi^{(1)}, \tag{20}$$
$$U^{(1)} = -V_p z_h M\Phi^{(1)}, \tag{21}$$
$$V_p^2 = 1 + \frac{1}{M}, \tag{22}$$

where $\delta = (E+H)/(F+2G)$ and $M = \delta\left[(1/z_h)+A\right]+B$. Now, equating the coefficients of ε^2 from Eqs. (11) and (12), and the coefficients of ε^3 from Eqs. (9) and (10), we obtain:

$$\frac{\partial N^{(1)}}{\partial \tau} - V_p \frac{\partial N^{(2)}}{\partial \xi} + \frac{\partial U^{(2)}}{\partial \xi} + \frac{\partial}{\partial \xi}\left((N^{(1)}U^{(1)}\right) + \frac{\nu U^{(1)}}{V_p \tau} = 0, \tag{23}$$

$$\frac{\partial U^{(1)}}{\partial \tau} - V_p \frac{\partial U^{(2)}}{\partial \xi} + U^{(1)}\frac{\partial U^{(1)}}{\partial \xi} = z_h \frac{\partial \Phi^{(2)}}{\partial \xi} - \frac{\partial N^{(2)}}{\partial \xi} + N^{(1)}\frac{\partial N^{(1)}}{\partial \xi}, \tag{24}$$

$$B\Phi^{(2)} + \frac{N^{(2)}}{z_h} - \left(\frac{1}{z_h} + A\right)Q^{(2)} + C\left\{\Phi^{(1)}\right\}^2 = 0, \tag{25}$$

and

$$-V_p \frac{\partial \Phi^{(1)}}{\partial \xi} = (K + C\lambda)\left\{\Phi^{(1)}\right\}^2 + G\left\{Q^{(1)}\right\}^2 + HQ^{(1)}\Phi^{(1)} + (E + H + B\lambda)\Phi^{(2)} + \frac{\lambda}{z_h}N^{(2)}, \tag{26}$$

where $\lambda = (F+2G)/(A+1/z_h)$.

From the set of Eqs. (23) - (26) for $N^{(2)}$, $U^{(2)}$, $\Phi^{(2)}$ along with another set of Eqs. (19) - (21) for $N^{(1)}$, $U^{(1)}$, $\Phi^{(1)}$, we can easily derive the following non-linear dynamical equation:

$$\frac{\partial \Phi^{(1)}}{\partial \tau} + \frac{\nu}{2\tau}\Phi^{(1)} + A_1\Phi^{(1)}\frac{\partial \Phi^{(1)}}{\partial \xi} = C_1\frac{\partial^2 \Phi^{(1)}}{\partial \xi^2}, \tag{27}$$

where

$$A_1 = \left[2\left(1-V_p^2\right)(K + C\lambda + G\delta^2 - H\delta) + \lambda z_h M^2\left(1-3V_p^2\right)\right]/2\lambda V_p M$$

and

$$C_1 = \left(1-V_p^2\right)\delta/2\lambda M$$

are respectively the nonlinear coefficient and dissipative coefficient of Eq. (27). Equation (27) is the well-known modified Burger equation. The term $(\nu/2\tau)\Phi^{(1)}$ in Eq. (27) is due to the effect of non-planar geometry [41, 42].

NUMERICAL SOLUTION OF THE MODIFIED BURGER'S EQUATION AND GRAPHICAL REPRESENTATION

As mentioned earlier the one-dimensional planar case $(\nu = 0)$ has already been studied by Paul *et al.* [38]. In this case, we introduced $\zeta = \xi - U_0\tau'$ and $\tau' = \tau$,

where in the reference frame U_0 is the shock wave speed. This leads us to write Eq. (27) under the steady state condition $\partial / \partial \tau' = 0,$ as

$$-U_0 \frac{\partial \Phi^{(1)}}{\partial \zeta} + A_1 \Phi^{(1)} \frac{\partial \Phi^{(1)}}{\partial \zeta} = C_1 \frac{\partial^2 \Phi^{(1)}}{\partial \zeta^2} \qquad (28)$$

As shown in Paul *et al.* [38], the solution of the above equation, Eq. (28) describes the shock waves, whose speed U_0 is related to the extreme values $\Phi(-\infty)$ and $\Phi(\infty)$ by $\Phi(\infty) - \Phi(-\infty) = 2U_0 / A_1$. Therefore Φ is bounded at $\zeta = \pm\infty$ under this condition, the shock wave solution of Eq. (28) is [16, 17]:

$$\Phi(\nu = 0) = \Phi_0 \left[1 - \tanh\left(\frac{\zeta}{\Delta} \right) \right] \qquad (29)$$

where $\Phi_0 = U_0 / A_1$ is the height of the DNIA shock waves and $\Delta = 2C_1 / U_0$ is the thickness of the DNIA shock waves.

It is to be noted here that in the present case of the non-planar geometry, an exact analytic solution of Eq. (27) is not possible. Therefore, we have numerically solved Eq.(27) and have studied the effects of cylindrical $(\nu = 1)$ and spherical $(\nu = 2)$ geometries on time-dependent non-linear structure for the typical dusty plasma parameters as in [38], namely $\mu_e = n_{e0} / z_h^2 n_{h0} = 0.2 - 0.4,\ \mu_i = n_{i0} / z_h^2 n_{h0} = 1.0 - 1.4,\ \sigma_e = T_h / T_e = 0.125,$ $\sigma_i = T_h / T_i = 0.1 - 0.25,\ T_e \sim T_i = 0.2$ eV, $z_h = 1,\ z_d = 10^3,\ r_d = 5\mu m,$ $m_i = 39 m_p,\ T_h = 0.125 T_i,\ m_h = 146 m_p,$ where m_p is the proton mass.

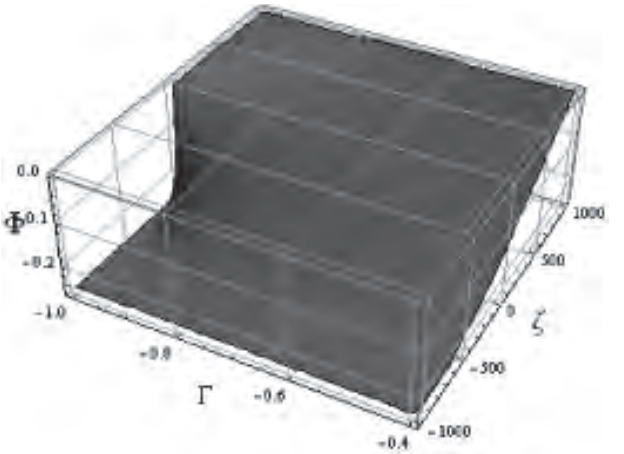

Figure 1. Time evolution of the cylindrical $(\nu = 1)$ shock wave potential Φ versus spatial coordinate ξ and time Γ for $\beta = 0.4,\ \mu_i = 0.5,\ \mu_e = 0.8,\ \sigma_i = 0.125.$

In the numerical analysis, the following initial condition is used: $\Phi(\nu = 0) = \Phi_0 \left[1 - \tanh(\zeta / \Delta)\right]$. The results are displayed in Figures 1 and 2. Figure 1 shows the effect of the cylindrical $(\nu = 1)$ geometry of DNIA shock waves whereas Figure 2 shows the effect of the spherical $(\nu = 2)$ geometry. The numerical solution of Eq. (27) shows that for large value of $\tau(= -2)$, cylindrical, spherical and one dimensional planar shocks structures are similar. For a large τ the value of $(\nu / 2\tau)$ is very small, thus the term $(\nu / 2\tau)\phi$ is negligible for both the cases.

But in case of small τ the term $(\nu / 2\tau)\phi$ is not negligible, and it plays a significant role in the formation of the shock structures. Both the figures (Figs. 1 and 2) show the shock structure evolution at $\tau = -2$. It is clear that the developed shock heights are different from each other in different geometry. In case of spherical geometry, the shock wave has higher height than that of the cylindrical geometry.

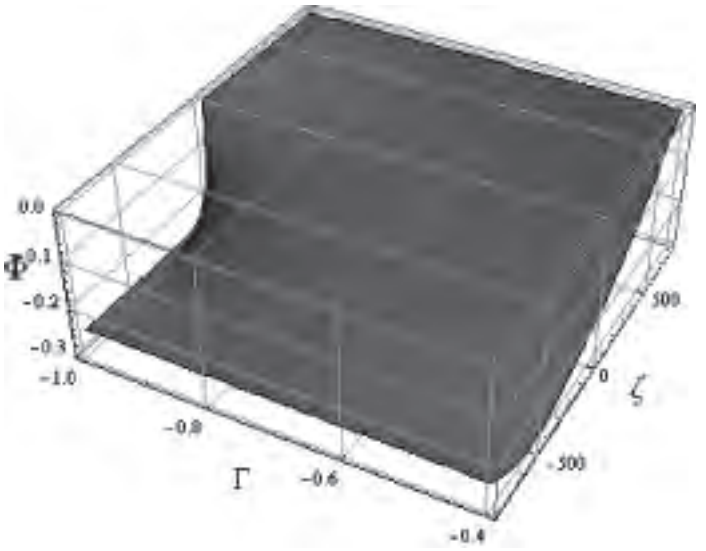

Figure 2. Time evolution of the spherical $(\nu = 2)$ shock wave potential Φ versus spatial coordinate ξ and time Γ for $\beta = 0.4$, $\mu_i = 0.5$, $\mu_e = 0.8$, $\sigma_i = 0.125$.

CONCLUSION

We have studied the nonlinear propagation of DNIA (dust negative ion acoustic) shock waves in an unmagnetized dusty plasma consisting of charge fluctuating stationary dust, mobile negatively charged heavy ions, Maxwellian electrons and

nonthermal light ions in a non-planar geometry. The propagation of the small amplitude nonlinear DNIA shock wave in the multi-ion dusty plasma is considered by analyzing the solution of the Burger's equation. The Burger's equation is derived by using the standard perturbation method. A detailed numerical analysis of the amplitude of the DNIA shock wave is performed in terms of the parameter β which accounts for the nonthermal nature of the positively charged light ion distribution. We have shown here how the basic features of the nonlinear DNIA shock waves are modified by the presence of the charge fluctuating dust and the nonthermal nature of the positively charged light ions for the cylindrical and spherical geometries. It is shown that the developed shock heights (amplitudes) are different for different geometries and in the case of spherical geometry, the shock wave has much higher amplitude than that of the cylindrical geometry. The results, which have been obtained from this investigation, would be useful in understanding the properties of localized DNIA shock waves in laboratories and in space dusty plasmas.

REFERENCES

1. Nakamura Y., Bailung H., and Shukla P. K. (1999), Observation of ion-acoustic shocks in a dusty plasma, *Physical Review Letters*, **83**: 1602-1605
2. Luo Q. Z., D'Angelo N., and Merlino R. L. (1999), Experimental study of shock formation in a dusty plasma, *Physics of Plasmas*, **6**: 3455-3458.
3. Nakamura Y. and Sharma A. (2001) Observation of ion-acoustic solitary waves in a dusty plasma. *Physics of Plasmas,* **8**: 3921-3935.
4. Shukla P. K. (2000), Dust ion-acoustic shocks and holes, *Physics of Plasmas,* **7**: 1044-1046.
5. Popel S. I., Gisko A. A., Golub A. P., Losseva T. V., Bingham R. and Shukla P. K. (2000), Shockwaves in charge-varying dusty plasmas and the effect of electromagnetic radiation, *Physics of Plasmas,* **7**: 2410-2416.
6. Mamun A. A. and Shukla P. K. (2002), The role of dust charge fluctuations on nonlinear dust ion acoustic waves, *IEEE Transactions on Plasma Science*, **30**:720-724.
7. Shukla P. K. and Mamun A. A. (2003), Solutions, shocks and vortices in dusty plasmas, *New Journal of Physics*, **5**: 17.1-17.37.
8. Shukla P. K. (2003), Nonlinear waves and structures in dusty plasmas, *Physics of Plasmas*, **10**: 1619-1627.
9. Eliasson B. and Shukla P.K. (2005) Formation of large-amplitude dust ion-acoustic shocks in dusty plasmas. *Physics of Plasmas,* **12**: 024502(1-4).
10. Mamun A.A., Shukla P.K. and Eliasson B. (2009) Arbitrary amplitude dust ion-acoustic shock waves in a dusty plasma with negative and positive ions. *Physics of Plasma,* **16**: 114503-114504.
11. Shukla P.K. (1992) Low-frequency modes in dusty plasmas. *Physica Scripta,* **45**: 504-507.

12. Mendis D. A. and Rosenberg M. (1994), Cosmic Dusty Plasma, *Annual Review of Astronomy and Astrophysics,* **32**: 418-463.
13. Bliokh P. V. and Yarashenko V. V. (1985), Electrostatic waves in Saturn's rings, *Soviet Astronomy*, **29**: 330-336 (English Translation.).
14. Northrop T. G. (1992), Dusty plasmas, *Physica Scripta*, **45**: 475-490.
15. Shukla P. K. and Mamun A. A. (2002), Introduction to Dusty Plasma Physics, *Institute of Physics Publishing, Bristol, U.K.*
16. Shukla P. K. and Silin V. P. (1992), Dust ion acoustic wave, *Physica Scripta*, **45**: 508.
17. Popel S. I., Golub A.P., and Losseva T. V. (2001), Weakly dissipative dust-ion-acoustic solitons, *Journal of Experimental and Theoretical Physics*, **74**: 336-401.
18. Popel S. I. (2004), Dust acoustic and dust ion acoustic nonlinear structures: Theory and Experiments, *Journal of Plasma and Fusion Research*, **6**: 421-424.
19. Kim S. H. and Merlino R. L. (2006), Charging of dust grains in a plasma with negative ions, *Physics of Plasmas*, **13**: 052118 (1-7).
20. Merlino R. L. and Kim S. H. (2006), Charge neutralization of dust particles in a plasma with negative ions, *Applied Physics Letters*, **89**: 091501.
21. Barkan A., D'Angelo N. and Merlion R. L. (1996), Experiments on ion-acoustic waves in dusty plasmas, *Planetary and Space Science*, **44**: 239-242.
22. Merlino R.L. and Goree J. (2004) Dust vortex modes in a nonuniform dusty plasma. *Physics Today,* **57**: 32-39.
23. Das G.C., Sharma J. and Roychoudhury R.J. (2001) Some aspects of shock-like nonlinear acoustic waves in magnetized dusty plasmas. *Physics of Plasmas,* **8**: 74-81.
24. Mamun A.A. and Shukla P.K. (2002) Cylindrical and spherical dust ion-acoustic solitary waves. *Physics of Plasmas,* **9**: 1468-1470.
25. Ghosh S. and Bharuthram R. (2008) Ion acoustic solitons and double layers in electron-positron-ion plasma with dust particulates. *Astrophysics and Space Science*, **314**: 121-127.
26. Das G.C., Sharma J. and Talukdar M. (1998) Dynamical aspects of various solitary waves and double layers in dusty plasma. *Physics of Plasmas,* **5**: 63-69.
27. Rosenberg M. and Merlino R.L. (2007) Ion acoustic instability in a dusty negative ion plasma. *Planetary and Space Science*, **55**: 1464-1469.
28. Alinejad H. (2010) Dust ion-acoustic solitary and shock waves in dusty plasma with no-thermal electrons. *Astrophysics and Space Science,* **327**: 131-137.
29. Duha S.S. and Mamun A.A. (2009) Dust ion-acoustic waves due to dust charge fluctuation. *Physics Letter A,* **373**: 1287-89.
30. Duha S.S. (2009) Dust negative ion acoustic shock waves in dusty multi-ion plasma with positive dust charging current. *Physics of Plasmas,* **16**: 113701-113705.
31. Mamun A.A., Cairns R.A. and Shukla P.K. (2009) Dust negative ion acoustic shock waves in a dusty multi-ion plasma. *Physics Letter A,* **373**: 2355 - 2359.
32. Sayeed F. and Mamun A.A. (2007) Solitary potential in a four-component dusty plasma. *Physics of Plasma* **14**: 014501-014504.
33. Mamun A.A. (2008) Dust electron-acoustic shock waves due to dust charge fluctuation. *Physics Letter A,* **372**: 4610-4613.

34. Shukla P.K. (2000) Dust ion-acoustic shocks and holes, *Physics of Plasmas* **7**: 1044-1046.
35. Moslem W.M. (2006) Dust ion-acoustic solitons and shocks in dusty plasma. *Chaos, Solitons and Fractals,* **28**: 994-999.
36. Popel S.I., Golub A.P., Losseva T.V., Ivlev A.V., Khrapak S.A. and Morfill G. (2003) Weakly dissipative dust-ion-acoustic solitons. *Physical Review E,* **67**: 056402-056407.
37. Mamun A.A. and Shukla P.K. (2002) The role dust charge fluctuations on nonlinear dust ion acoustic waves. *IEEE Transactions on Plasma Science,* **30**: 720-724.
38. Paul A., Mandal G., Mamun A.A., and Amin M.R. (2011) Effects of non-thermal ions on dust-ion-acoustic shock waves in a dusty electronegative plasma. *IEEE Transactions on Plasma Science,* **39**: 1254-1258.
39. Washimi H. and Taniuti T. (1966) Propagation of ion-acoustic solitary waves of small amplitude. *Physical Review Letter,* **17**: 996-998.
40. Das G.C., Dwivedi C.B., Talukdar M. and Sharma J. (1997) A new mathematical approach for shock wave solution in a dusty plasma. *Physics of Plasmas,* **4**: 4236-4239.
41. Mamun A.A. and Shukla P.K. (2001) Spherical and cylindrical dust acoustic solitary waves. *Physics Letter A,* **290**: 173-175.
42. Mamun A.A. (1999) Arbitrary amplitude dust-acoustic solitary structures in a three-component plasma. *Astrophysics and Space Science,* **268**: 443

Journal of Science and Technology in the Tropics (2012) 8: 53-59

Structure-activity relationships of anthraquinone derivatives from *Morinda citrifolia* as inhibitors of colorectal cancer cells

V.Y. M. Jong[1,2], G. C. L. Ee[1,*], M.A. Sukari[1] and Y.H. Taufiq-Yap[1]
[1] Chemistry Department, Faculty of Science, Universiti Putra Malaysia,
43400 UPM Serdang, Selangor, Malaysia
[2] School of Chemistry and Environmental Studies, Faculty of Applied Science,UniversitiTeknologi MARA Malaysia, JalanMeranek, 94300 Kota Samarahan Campus, Kuching, Sarawak, Malaysia
(*E-mail: gwen@science.upm.edu.my)

Received 08-03-2012; accepted13-03-2012

Abstract The structure-activity relationship for a series of anthraquinone compounds from *Morinda citrifolia* were carried out to clarify the structural requirement for inhibition of HT-29 cancer cell line by these compounds. The anthraquinones are damnacanthal**(1)**, nordamnacanthal**(2)**, 2-Ethoxy-1-hydroxyanthraquinone **(3)**, rubiadin**(4)**, 1-hydroxy-2-methylanthraquinone **(5)** and rubiadin-1-methyl ether **(6)**. Comparison of these related anthraquinones indicated the formyl and ethoxy substituent groups were crucial for the inhibition of the cancer cells in the MTT assay.

Keywords *Morinda citrifolia* – anthraquinones – cytotoxicity – HT-29

INTRODUCTION

Morinda citrifolia was first discovered as a medicinal plant in Southeast Asia and the subcontinent and is widely used for this purpose. Different parts of the plant, which include fruits, leaves, bark, and roots, have been shown to contain various biologically active compounds [1]. Some of the active components identified in this plant are terpenoids, alkaloids, and anthraquinones, to name a few [1]. Of particular interest in this study are the anthraquinones extracted from the roots, which has been found to possess therapeutic properties such as antiviral [2,3], anti-bacterial [4,5], as well as anti-cancer activities [6,7]. Our detailed chemical studies on the roots of *M.citrifolia* led to the isolation and identification of six anthraquinones which are damnacanthal(1), nordamnacanthal(2), 2-ethoxy-1-hydroxyanthraquinone (3), rubiadin(4), 1-hydroxy-2-methylanthraquinone (5) and rubiadin-1-methyl ether (6). These compounds were tested for their cytotoxic activities using HT-29 cell line.

EXPERIMENTAL

Plant material

The roots of *M.citrifolia* were collected from Wakaf Bharu, Kelantan, Peninsular Malaysia.The plant material (Voucher Specimen no. UiTM3004) was identified and authenticated by a plant taxonomist at Forestry Research Centre (FRC), Sarawak

General

Infrared spectra were measured using the universal attenuated total reflection (UATR) technique on a Perkin-Elmer 100 Series. EIMS were recorded on a Shimadzu GCMS-QP5050A spectrometer. NMR spectra were obtained using a Unity INOVA 500MHz NMR/ JEOL 400MHz FT NMR spectrometer using tetramethylsilane (TMS) as internal standard. Ultra violet spectra were recorded in $CHCl_3$ on a Shimadzu UV-160A, UV-Visible Recording Spectrophotometer. Melting points were measured using Leica Galen III microscope, equipped with Testo 720 temperature recorder.

Extraction and isolation

Solvent extraction on the roots of *M.citrifolia* (0.5 kg) yielded 9.6 g of chloroform extract. The chloroform extract was purified using chromatotron by eluting with solvents (hexane, chloroform, ethyl acetate or methanol) or solvent mixtures with increasing polarity. This gave six anthraquinones (Fig. 1): damnacanthal**(1)**, nordamnacanthal**(2)**, 2-ethoxy-1-hydroxyanthraquinone **(3)**, rubiadin**(4)**, 1-hydroxy-2-methylanthraquinone **(5)** and rubiadin-1-methyl ether **(6)**.

Damnacanthal(1): Pale yellow needles with a melting point of 209 -210 °C [lit. [8]. 211-212 °C].UV (EtOH) λ_{max} nm (log ε): 254 (0.33), 261 (0.35), 390 (0.19).IR ν_{max} cm^{-1}(KBr): 3745, 2924, 1648, 1589, 1464, 1282, 1190. EI-MS m/z (rel. int.): 282 (25), 254 (100), 225 (38), 208 (17.5), 139 (34). ^{1}H NMR (300 MHz, $CDCl_3$): δ 12.27 (s, 1H, OH-3), δ 10.46 (s, 1H, 2-CHO), δ 8.28 (d, *J* = 7.3 Hz, 1H, H-5), δ 8.23 (d, *J* = 8.2 Hz, 1H, H-8), δ 7.82 (t, *J* = 7.3 Hz, 1H, H-6), δ 7.76 (t, *J* = 7.3 Hz, 1H, H-7), δ 7.66 (s, 1H, H-4), δ 4.11 (s, 3H, 1-OCH_3).^{13}C NMR (100 MHz, $CDCl_3$): δ 195.6 (2-CHO), δ 181.9 (C-10), δ 180.2 (C-9), δ 166.7 (C-1), δ 166.7 (C-3), δ 141.9 (C-2), δ 134.9 (C-6), δ 133.8 (C-7), δ 132.7 (C-5a), δ 132.7 (C-8a), δ 127.5 (C-5), δ 127.2 (C-8), δ 118.4 (C-9a), δ 117.8 (C-4a), δ 113.2 (C-4), δ 64.8 (1-OCH_3).

Nordamnacanthal(2): Orange-yellow solid with a melting point of 217 -218 °C[lit. [9]. 218-220 °C]. UV (EtOH) λ_{max} nm (log ε): 420 (0.24), 290 (0.35), 246

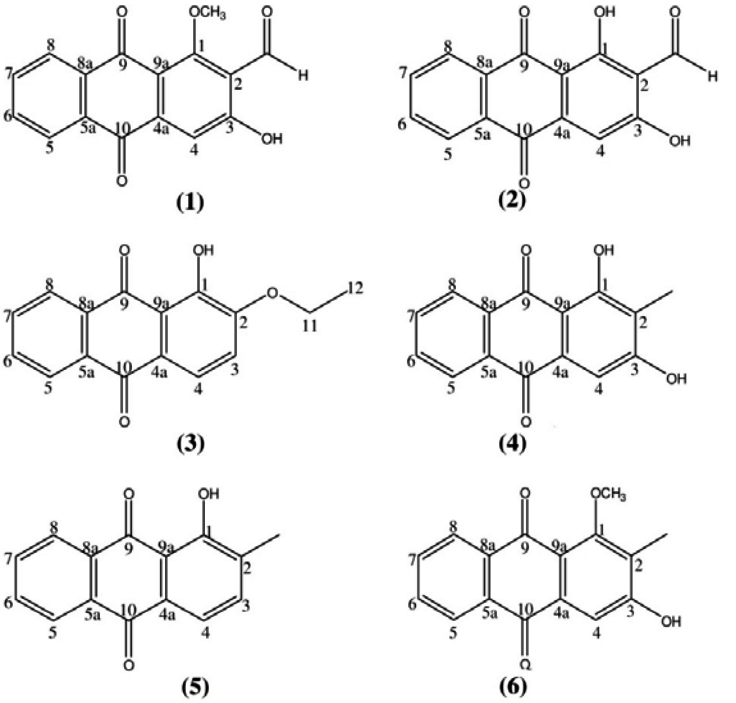

Figure 1. Anthraquinones obtained from *Morinda citrifolia*.

(0.37). IR ν_{max} cm^{-1} (KBr): 3776, 2921, 1663, 1569, 1454, 1345, 1268.EI-MS m/z (rel. int.): 268 (61), 240 (100), 212 (20), 184 (16), 138 (16), 77 (19). ^{1}H NMR (300 MHz, $CDCl_3$): δ 14.06 (s, 1H, OH-1), δ 12.68 (s, 1H, OH-3), δ 10.50 (s, 1H, 2-CHO), δ7.84 (m, 1H, H-6), δ7.84 (m, 1H, H-7), δ 8.32 (dd, *J* = 7.3, 1.8 Hz, 1H, H-5), δ 8.32 (dd, *J* = 7.3, 1.8 Hz, 1H, H-8), δ 7.34 (s, 1H, H-4). ^{13}C NMR (100 MHz, $CDCl_3$): δ 193.9 (2-CHO), δ 186.8 (C-9), δ 181.4 (C-10), δ 169.2 (C-3), δ 168.1 (C-1), δ139.5 (C-4a), δ134.7 (C-7),δ 134.8 (C-6),δ 133.3 (C-5a), δ 133.3 (C-8a), δ 127.8 (C-5), δ 127.0 (C-8), δ 112.1 (C-9a), δ 109.4 (C-4), δ 109.1 (C-2).

2-Ethoxy-1-hydroxyanthraquinone (3): Yellow solid with a melting point of 123-125°C [lit. [10]. 123-125 °C].UV(EtOH) λ_{max} nm (log ε): 412.0 (0.24), 302.5 (0.37), 209 (0.62).IR ν_{max} cm^{-1} (KBr): 3424, 1660, 1434, 1430 1313, 1019, 951. EI-MS m/z (rel. int.): 296 (48), 252 (41), 251 (100), 224 (77), 222 (35), 207 (10), 194 (18), 139 (69). ^{1}H NMR (400 MHz, $CDCl_3$): δ 13.30 (s, 1H, OH-1), δ 8.33 (dd, *J* = 7.4, 2.8 Hz, 1H, H-5), δ 8.25 (dd, *J* = 7.4, 2.8 Hz, 1H, H-8), δ 8.19 (d, *J* = 6.4 Hz, 1H, H-3), δ 7.97 (dd, *J* = 7.4, 2.8 Hz, 1H, H-6), δ 7.97 (dd, *J* = 7.4, 2.8 Hz, 1H, H-7), δ 7.81 (d, *J* = 6.4 Hz, 1H, H-4),δ 4.37 (s, 3H, H-11), δ 1.36 (s, 3H, H-12). ^{13}C NMR (100 MHz, $CDCl_3$): δ 189.2 (C-9), δ 181.9 (C-10), δ 164.5 (C-2), δ 161.8 (C-1), δ 138.1 (C-3), δ 136.1 (C-4a), δ 135.3 (C-6), δ 134.8 (C-7), δ 133.4 (C-5a),

δ 133.3(C-8a), δ 127.1 (C-5), δ 127.0 (C-8), δ 115.2 (C-9a), δ 117.9 (C-4), δ 61.2 (C-11), δ 13.7 (C-12).

Rubiadin(4): Yellow needles with a melting point of 289 -290 °C [lit. [11]. 290-291 °C].UV (EtOH) λ_{max} nm (log ε): 412.0 (0.24), 302.5 (0.37). IR ν_{max} cm^{-1} (KBr): 3397, 2925, 1663, 1586, 1436, 1339, 1122.EI-MS m/z (rel. int.): 254 (100), 238 (11), 226 (11), 207 (11), 152 (13), 76 (15), 64 (25). ^{1}H NMR (400 MHz, $CDCl_3$): δ 13.20 (s, 1H, OH-1), δ 8.25 (d, *J* = 7.3 Hz, 1H, H-8), δ 8.17 (d, *J* = 7.3 Hz, 1H, H-5), δ 7.87 (dd, *J* = 7.3, 1.8 Hz, 1H, H-6), δ 7.87 (dd, *J* = 7.3, 1.8 Hz, 1H, H-7), δ 7.32 (s, 1H, H-4), δ 2.13 (s, 3H, 2-CH_3).^{13}C NMR (100 MHz, $CDCl_3$): δ 187.0 (C-9), δ 182.1 (C-10), δ 163.3 (C-1), δ 163.0 (C-3), δ 134.4 (C-6), δ 134.3 (C-7), δ 133.6 (C-5a), δ 133.5 (C-8a), δ 132.4 (C-4a), δ 126.9 (C-5), δ 126.5 (C-8), δ 118.1 (C-2), δ 107.4 (C-4), δ 7.4 (2-CH_3).

1-hydroxy-2-methylanthraquinone (5): Yellow solid with a melting point of 180-181°C [lit. [12]. 182-182.5 °C].UV (EtOH) λ_{max} nm (log ε): 312.0 (0.39). IR ν_{max} cm^{-1} (KBr): 3747, 2931, 1668, 1454, 1278. EI-MS m/z (rel. int.): 238 (100), 237 (31), 181 (32), 152 (28), 76 (29). ^{1}H NMR (400 MHz, $CDCl_3$): δ 13.20 (s, 1H, OH-1), δ 8.30 (dd, *J* = 6.4, 2.8 Hz, 1H, H-5), δ 8.23 (dd, *J* = 6.4, 2.8 Hz, 1H, H-8), δ 7.92 (d, *J* = 6.9, 2.3 Hz, 1H, H-6), δ 7.92 (d, *J* = 6.9, 2.3 Hz, 1H, H-7), δ 7.68 (d, *J* = 6.4, 2.8 Hz, 1H, H-3), δ 7.68 (d, *J* = 6.4, 2.8 Hz, 1H, H-3), δ 2.33 (s, 3H, 2-CH_3). ^{13}C NMR (100 MHz, $CDCl_3$): δ 189.2 (C-9), δ 181.8 (C-10), δ 160.9 (C-1), δ 137.5 (C-3), δ 135.0 (C-7), δ 134.6 (C-2), δ 134.3 (C-6), δ 131.2 (C-4a), δ 133.9 (C-5a), δ 133.3 (C-8a), δ 127.0 (C-5), δ 126.7 (C-8), δ 118.8 (C-4), δ 115.2 (C-9a), δ 15.2 (2-CH_3).

Rubiadin-1-methyl ether (6): Yellow solid with a melting point of 280-281°C [lit. [9]. 283 °C].UV (EtOH) λ_{max} nm (log ε): 311.0 (0.36), 303.0 (0.37), 287.0 (0.44). IR ν_{max} cm^{-1} (KBr): 3309, 2927, 1670, 1568, 1483, 1335, 1296, 1119.EI-MS m/z (rel. int.): 268 (100), 253 (46), 250 (33), 225 (12), 222 (17), 194 (14), 197 (8), 181 (20), 165 (23), 152 (29), 139(19), 115(13), 76(31). ^{1}H NMR (400 MHz, $CDCl_3$): δ 8.19 (d, *J* = 5.8 Hz, 1H, H-5), δ 8.14 (d, *J* = 5.8 Hz, 1H, H-8), δ 7.84 (t, *J* = 5.8 Hz, 1H, H-6), δ 7.79 (t, *J* = 5.8 Hz, 1H, H-7), δ 7.56 (s, 1H, H-4), δ3.86 (s, 3H, 1-OCH_3), δ 2.22 (s, 3H, 2-CH_3). ^{13}C NMR (100 MHz, $CDCl_3$): δ 183.1 (C-9), δ 180.7 (C-10), δ 161.8 (C-1), δ 160.9 (C-3), δ 135.1 (C-4a), δ 134.3 (C-6), δ 133.1 (C-7), δ 132.6 (C-5a), δ 132.4 (C-8a), δ 126.8 (C-5), δ 126.6 (C-5), δ 126.1 (C-8), δ 115.2 (C-9a), δ 118.7 (C-2), δ 108.9 (C-4), δ 60.5 (1-OCH_3), δ 8.7 (2-OCH_3).

Cancer cell line culture

The human cancer cell line, HT-29 was used. This cell line was obtained from the American Type Culture Collection, USA. The cancer cells were cultured in their

respective media supplemented with 5% Fetal Bovine Serum (FBS), 100 IU mL^{-1} penicillin and 100 µg mL^{-1} streptomycin. The cultures were maintained at 37 °C in an incubator with 5% CO_2.

Cytotoxicity and MTT assay

Cells were seeded in a 96 well microplate at 3 × 105 cells mL^{-1} and then incubated at 37 °C in 5% CO_2 atmosphere. After 24 hours, the medium was removed and replaced with fresh medium containing test compounds at various concentrations (serial dilution) between 0 and 30 µg mL^{-1}. 72 hours later, the cells were tested with the MTT (3-[4,5-dimethylthioazol-2yl]-2-5-diphenyltetrazolium bromide) assay to evaluate the viability through its metabolic activity. 20 µL of MTT (5 mg mL^{-1}) in PBS solution was added to each well. Then, the plates were further incubated for 3 hours in the dark. During incubation period, viable cells convert MTT to a water-insoluble formazan dye. The plates were then centrifuged (Centrifuged 5810R, Eppendorf) at 400 × g and 4 °C. All the remaining supernatant was then removed and 100 µL of dimethylsulphoxide (DMSO, Fisher Scientific) was added to each well. The plates were reincubated, as done earlier, but for an hour to dissolve the crystals of formazan formed. The formation of the dye is proportional to the number of viable cells, which was detected using a microplate spectrophotometer (µQuant Universal Microplate Spectrophotometer, BIOTEK instrument, Inc) at wavelength of 570 nm. The mean absorbance for each compound concentration was expressed as a percentage of control untreated well absorbance and plotted versus compound dose. IC_{50} values represent the concentration that reduced the mean absorbance at 570 nm to 50% of those in the untreated control wells.

RESULTS AND DISCUSSION

Anthraquinones are known to be a homogeneous group of constituents in the *Morinda* species. Anthraquinone derivatives, including emodin, physcion, aloe-emodin, rhein, and chrysophanol, are nowadays well recognized as important biologically active components [13]. In this report, the anthraquinones tested include modified and rearranged anthraquinone groups. They reveal an interesting trend of cytotoxic effect on HT-29 cell line with IC_{50} values between 4.5 and 10.0 µg mL^{-1}. However, these cytotoxic results show significant dissimilarity in inhibition effects probably due to the nature of the substituents and the substitution pattern of the anthraquinone skeleton. Structurally, these include damnacanthal**(1)**, nordamnacanthal**(2)**, 2-ethoxy-1-hydroxyanthraquinone **(3),** as well as rubiadin**(4)**, 1-hydroxy-2-methylanthraquinone **(5)** and rubiadin-1-methyl ether **(6)**. The cytotoxic results of these compounds are summarized in Table 1.

Table 1. Cytotoxic activities of (1-6) against HT-29 cell line.

Compound	IC_{50} µg mL^{-1}
	HT-29
Damnacanthal**(1)**	10.0
Nordamnacanthal**(2)**	8.1
2-Ethoxy-1-hydroxyanthraquinone **(3)**	4.5
Rubiadin**(4)**	> 50.0
1-hydroxy-2-methylanthraquinone **(5)**	> 50.0
rubiadin-1-methyl ether **(6)**	> 50.0
[1]5-fluorouracil	3.7

[1]positive control of HT-29 cell line. Note:*IC_{50}< 5.0 µg mL^{-1} = strong inhibition activity; *5.0 ≤ IC_{50} ≤ 25.0 µg mL^{-1} = moderate inhibition activity; *IC_{50} > 25.0 µg mL^{-1} = weak inhibition activity [14].

It is interesting to observe that of the compounds tested, damnacanthal**(1)**, nordamnacanthal**(2)** and 2-ethoxy-1-hydroxyanthraquinone **(3)** are active cytotoxic compounds towards HT-29 (10.0, 8.1 and 4.5 µg mL^{-1}). This activity might be due to the formyl and ethoxyl moieties at the A-ring. The assays also indicated both damnacanthal**(1)** and nordamnacanthal**(2)** which have the formyl functional group at the A-ring of the structure exhibited a stronger cytotoxic activity when compared to that of **(4)** and **(6)** which are also 1,2,3-trisubstituted aromatic ring but carries a methyl group at position 2.

Hence, it is deduced that anthraquinones with the presence of formyl moieties at A ring is inclined to exhibit a prominent inhibitory activity. Furthermore, 2-ethoxy-1-hydroxyanthraquinone **(3)** also demonstrates strong cytotoxic properties towards HT-29 cell line with IC_{50} 4.5µg mL^{-1} when compared with 1-hydroxy-2-methylanthraquinone **(5)**. From the structure-activity relationship comparison, both compounds have a 1,2-disubstituted aromatic ring with a chelated hydroxyl group at C-1 but a ethoxyl substitution was attached at C-2 for compound **(3)** and a methyl group for 1-hydroxy-2-methylanthraquinone **(5)**. The methyl group substitution at C-2 position for compounds **(4)**, **(5)** and **(6)** tend to reduce the degree of inhibition effect towards the cell line. Thus, it is suggested that the formyl and ethoxyl groups are necessary requirements for the cytotoxic activity towards the HT-29 cell line.

In summary, the ethoxyl side chain and the presence of the formyl group at C-2 at A-ring of the anthraquinone derivatives contribute to the prominent inhibitory activity. Hence, it can be concluded that anthraquinones with formyl and ethoxyl side chain skeleton might be lead compounds for HT-29 cancer cell line.

Acknowledgements – We gratefully acknowledge financial support provided by the Fundamental Research Grant Scheme Malaysia (FRGS), staff of Forest Research Centre, Kuching, Sarawak for collection and identification of plant samples.

REFERENCES

1. Wang M.Y., West B.J., Jensen C.J., Nowicki D., Su C., Palu A.K. and Anderson G. (2002) *Morinda citrifolia*(Noni): A literature review and recent advances in Noni research. *Acta Pharmacologica Sinica* **23**: 1127-1141.
2. Koyama J., Moritaa I., Tagaharaa K., Mukainakab O.T., Tokudab H. and Nishinob H. (2001) Inhibitory effects of anthraquinones and bianthraquinones, Epstein-Barr virus activation. *Cancer Letters* **170**: 15-18.
3. Taloua J.R., Verbernea M.C., Muljonoa R.A.B., Tegelenc L.J.P., Bernala B.G., Linthorstb H.J.M., Wullemsc G.J., Bolb J.F. and Verpoortea R. (2001) Isochorismate synthase transgenic expression in *Catharanthus roseus* cell suspensions. *Plant Physiological and Biochemistry* **39:** 595-602.
4. Loy G., Cottiglia F., Garau D., Deidda D., Pompei R. and Bonsignore L. (2001) Chemical composition and cytotoxic and antimicrobial activity of *Calycotome villosa* (Poiret) Link leaves. *IlFarmaco* **56**: 433-436.
5. Babu K.S., Srinivas P.V., Praveen B., Kishore K.H., Murty U.S. and Rao J.M. (2003) Antimicrobial constituents from the rhizomes of *Rheum emodi*. *Phytochemistry* **62**: 203-207.
6. Sadeghi-Aliabadi H., Tabarzadi M. and Zarghi A. (2004) Synthesis and cytotoxic evaluation of two novel anthraquinone derivatives. *IlFarmaco* **59**: 645-649.
7. Hiramatsu T., Imoto M., Koyano T. and Umezawa K. (1993) Induction of normal phenotypes inras-transformed cells by damnacanthal from *Morinda citrifolia*. *Cancer Letters* **73**: 227-231.
8. Horie Y. (1956) Synthesis of damnacanthol. *Yakugaku Zasshi* **76**: 1448-1449.
9. Prista L.N., Roque A.S., Ferreira M.A. and Alves A.C. (1965) Chemical Study of *Morinda geminate*. I. Isolation of morindone, damnacanthal, nor-damnacanthal and rubiadin-1-methyl ether. *Garcia de Orta* **13**: 19-38.
10. Ee G.C.L., Wen Y.P., Sukari M.A., Go R. and Lee H.L. (2009) A new anthraquinone from *Morinda citrifolia* roots. *Natural Product Research* **23**: 1322-1329.
11. Chari V.M., Neelakantan S. and Seshadri T.R. (1966) Rubiadin. *India Journal of Chemistry* **4**: 330-331.
12. Locatelli M., Tammaro F., Menghini L., Carlucci G., Epifano F. and Genovese S. (2009) Anthraquinones profile and fingerprint of *Rhamnuss axatilis L.* from Italy. *Phytochemistry Letters* **2**: 223–226.
13. Savard J. and Brassard P. (1984) Reaction of ketene acetals-14. The use of simple mixed vinylketeneacetals in the annulation of quinones. *Tetrahedron* **40**: 3455-3464.
14. Ee G.C.L., Lim C.K. and Mawardi R. (2005) Structure-activity relationship of xanthones from *Mesua daphnifolia* and *Garcinia nitida*towards human estrogen receptor negative breast cancer cell line. *Natural Product Science* **11**: 220-224.

Journal of Science and Technology in the Tropics (2012) 8: 61-80

Rare earth minerals: occurrence, distribution and applications in emerging high-tech industries

Karen Wong Mee Chu[1] and Liang Meng Suan
Faculty of Engineering and Science, Universiti Tunku Abdul Rahman,
Kuala Lumpur, Malaysia
([1]E-mail: mcwong@utar.edu.my)

Received 21-03-2012; accepted 01-04-2012

Abstract Rare earths have been conventionally used in many areas for several decades especially in alloying and video applications. An interesting fact probably unaware by many is that the emergence of colour television is attributed to the discovery of red phosphors made from rare earth elements. These elements have been essential in various industrial areas for a long time although not widely known to the mass market. It is in part due to the quota imposed by the current world's largest supplier, China as well as the emerging high-tech industries requiring rare earths that propelled these elements to one of the world's most sought after commodity. However, the excessive pricing of these elements have reduced the demand somewhat and thus lowered the prices recently. This is due to the inability of the downstream industry, especially the electronic industries to absorb the high cost needed. This paper highlights occurrence and up-coming rare earths processing plants to cater for the market demand as well as provide an insight on the role of rare earth elements in emerging green technology and miscellaneous high-tech applications.

Keywords rare earths – occurrence – popularity – applications

INTRODUCTION

Rare earth elements are a set of 17 chemical elements in the periodic table, i.e. the 15 lanthanoids (lanthanides) plus scandium and yttrium (Fig.1). The latter two elements are classified as rare earths as these usually occur in the same ore deposit as lanthanoids and possess similar chemical properties. Despite their name, rare earth elements (with the exception of the radioactive promethium) are relatively plentiful in the Earth's crust, with cerium being the 25th most abundant element at 68 parts per million (similar to copper). However, because of their geochemical properties, rare earth elements are typically dispersed and not often found in concentrated and economically exploitable forms known as rare earth minerals, thus giving rise to the term 'rare earth'. The radioactive element promethium is too scarce in nature and can be considered as non-occurring [1, 2]. The element thorium is found together with rare earth elements in the common ore, monazite. Thorium can be separated by a relatively easy process while the others will remain grouped, to be extracted as metals or compounds for special purposes, thus the resulting high cost of rare earth metals [3]. The difficulty to extract the individual elements arises due to their similar chemical properties.

Rare earths can be classified into light rare earths (La-Sm) and heavy rare earths (Eu-Lu). The heavy rare earths europium, terbium and dysprosium are really scarce [4]. Most deposits are tilted towards light rare earths (constituting 97-99% of resource base). Deposits with high proportion of heavy rare earths (>20%) are rare and consequently more valuable. Table 1 shows rare earth element content and price of typical ores from two mines in 2007 [5]. In the first quarter of 2011, Nd price skyrocketed to USD 281.2/kg [6]. Rare earths can also be recovered from electronic scraps and from nuclear reprocessing, although the latter poses safety as well as economic issues.

COMPOSITION OF RARE EARTH

As a major manufacturer, the largest producer and consumer of rare earth elements is China. Being the lowest cost producer, about 94% of rare earth oxides and 97% of rare earth metals consumed worldwide originates from China. Domestic consumption is projected to exceed supply within 10 years.

Nurturing and protecting its rare earth production industry, China promises rare earth resources availability only if the production facilities are located in China, meant to attract industry, research, technology, manufacturing plants and jobs [7].

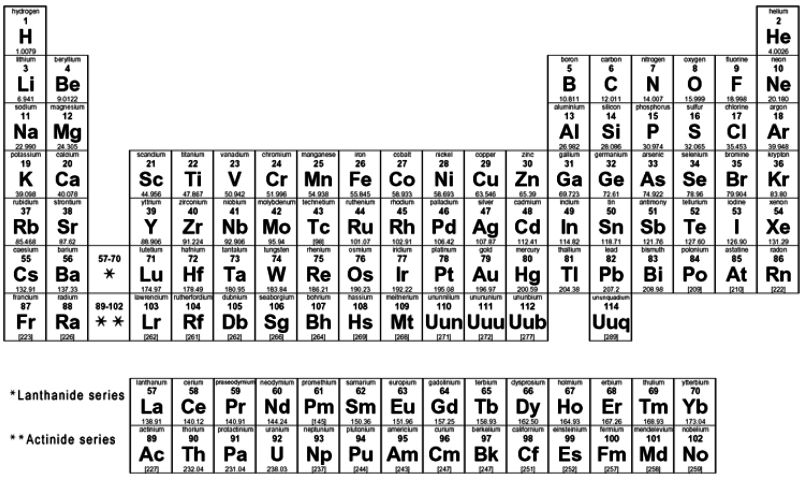

Figure 1. Periodic table – rare earth elements: Lanthanide series plus scandium (Sc) and yttrium (Y).

HOW CHINA EMERGED AS WORLD'S TOP RARE EARTH PRODUCER

The "Super 863" research and development program, named after its conception date in March 1986 involved 30,000 scientists and engineers including about 1000

Table 1. Rare earth element content and price [5].

Lanthanide	Bastnasite Mountain Pass (%)	Monazite Green Cove Springs (%)	Price 2007 ($/kg)
Cerium	49.3	43.7	50-65
Dysprosium	0.031	0.9	160
Erbium	-	-	165
Europium	0.11	0.16	1,200
Gadolinium	0.18	6.6	150
Holmium	-	0.11	750
Lanthanum	33.2	17.5	40
Lutetium	-	-	3,500
Neodymium	12	17.5	60
Praseodymium	4.3	5	75
Samarium	0.8	4.9	200-350
Terbium	0.016	0.26	850
Thulium	-	-	2,500
Ytterbium	-	0.21	4500

doctorate holders. A visionary 1992 outlook by China's late leader Deng XiaoPing is: "There is oil in the Middle East. There are rare earths in China. We must take full advantage of this resource." The program started in 1996 and claimed the achievement of 1500 unspecified technological breakthroughs.

After the launch of the Super 863 program in 1997, the Chinese Communist Party adopted the "16-character policy" in reference to the 16 Chinese characters that describe a four-sentence blueprint for China's ascendance on the world stage: "Combine the military with the civil. Combine peace and war. Give priority to military products. Let the civil support the military." This signals a possible future competition for the global rare earth resources as feed materials to a new green technologies industrial thrust [7].

RARE EARTH RESOURCE AND DISTRIBUTION

Rare earth deposits can be found in many parts of the world. Brazil is reputed to be the world's oldest rare earth producer, since 1884. The world distribution and production are as shown in Tables 2-5 [4]. Global rare earth resource and product distribution have been changing rapidly since 2009 due to the increasing importance of these materials and thus the intensive exploration and setting up of new mines and processing plants to produce more rare earth materials in response

to supply-demand gap caused by the export quota introduced by the world dominating supplier, China in recent years. Previously, the deposit at Mountain Pass was sufficient to supply the commercial needs of all cerium-based metals [3]. Table 6 shows rare earth element distribution in selected mines worldwide.

In Asia, 14 countries have rare earth deposits with Japanese companies setting up joint ventures with five of them, namely: Vietnam, India, Mongolia, Kazakhstan and Kyrgyzstan. There are plenty of rare earth reserves in Australia but no processing plants could be built due to environmental and economic factors. However, Lynas is establishing its processing plant in Gebeng, Malaysia. Another company, Arafura Resources Ltd is projected to produce heavy rare earth elements in 2013. In other regions, USA, Canada, Brazil and Africa are set to develop or accelerate their rare earths production [4].

Generally there are about 34 countries with rare earth deposits but there are only few which are economically viable to develop and mine. At present, about six countries can provide rare earths products with China topping the list at 94% and Russia, Estonia, USA, Malaysia and Brazil making up the rest (Table 2). Tables 7 and 8 list the current producers outside China and up-coming producers [4]. It was reported that there are currently about 200 projects on rare earth either at exploration stage, under preparation or exploitation, among which about 25 projects are prospective competitions for future rare earth supply [8,9].

Table 2. Rare earth supply in 2009 [4].

Country	Rare earth supply (tonne)	Rare earth supply (%)
China	129,400	94.23
India	2,700	1.97
Russia	2,500	1.82
USA	1,700	1.24
Brazil	650	0.47
Malaysia	380	0.28

Figure 2. Global rare earth resources [4].

Table 3. Global rare earth elements reserves 2009 [4].

Country	Rare earth element reserves (tonne)	Rare earth elements reserves (%)
China	36,000,000	36.52
CIS	19,000,000	19.27
USA	13,000,000	13.19
Australia	5,400,000	5.48
India	3,100,000	3.14
Brazil	48,000	0.05
Malaysia	30,000	0.03
Others	22 000 000	22.32

Table 4. Global rare earth elements reserves 2010 [4].

Country	Rare earth element reserves (tonne)	Rare earth elements reserves (%)
Brazil	52,597,000	37.01
China	36,000,000	25.33
CIS	19,000,000	13.37
Vietnam	14,800,000	10.42
Greenland	4,890,000	3.44
Canada	4,122,500	2.90
Australia	3,330,600	2.34
India	3,100,000,	2.18
USA	1,550,400	1.06
South Africa	1,254,000	0.88
Kenya	972,000	0.68
Kyrgyzstan	291,000	0.20
Turkey	130,500	0.09
Malawi	107,000	0.08
Brundi	1000	0.02

CONVENTIONAL USES OF RARE EARTH ELEMENTS

Rare earths had been used in many ordinary applications in the past before its recent emergence as a commodity with high strategic importance to many countries especially the industrially advanced countries. After extraction of thorium oxide from the typical ore monazite, the residual product after processing is known as mischmetal (German for mixed metal) which is a combination of about 50% cerium with lanthanum, deodymium and several other rare earth metals. Mischmetal is used in making aluminium alloys as well as some steels and iron. It opposes graphitization and produces a malleable iron when used in cast iron. It removes sulphur and oxides and completely degasifies steel. It is used for precipitation hardening in stainless steel. When added to magnesium alloys, mischmetal refines grains and give sound casting of complex shapes. It also provides heat resistance to magnesium castings [3].

Other conventional applications of rare earths include use as colorants in

glasses, especially neodymium glass which was used for colour television filter plates to produce truer colours and sharper contrasts in the pictures. Europium is added for the brilliant reds in television phosphors. In fact, the development of colour television took a long time due to the search for red phosphors. The first red emitting rare earth phosphor was introduced by Levine and Palilla as a primary colour in television in 1964 [10]. Neodymium is also used in magnesium alloys to increase high temperature strength. In fact, most of the rare earths can be used as colorant or as glass due to their unique optical properties. Dysprosium has the highest corrosion resistance among all mischmetals with good neutron-absorption ability and is used as nuclear reactor control rods, magnetic alloys and ferrites for microwaves. Samarium and gadolinium are also similarly used for neutron absorption in reactors. Thulium is used for radiographic applications.

RARE EARTH ELEMENTS IN THE NEW ERA

Although rare earths are still used for applications as mentioned above, they now play irreplaceable roles in the newly developed green technology, electronic industry, military and defense technology, and other emerging high-tech technologies. Examples include hybrid cars, wind turbines, lightings and displays, microprocessors, mobile communications, guided missiles, smart bombs, etc. These are considered to be rare earth-dependent technologies due to the non-availability of other alternative materials. In short, there are increasing downstream high-tech industry activities which are dependent on rare earth materials.

The successful application of rare earths in the above mentioned industries is largely attributed to their magnetism caused by their partially filled 4f shells. This property made rare earth elements crucial in the production of permanent magnets, catalytic cracking materials, luminescence materials, hydrogen storage materials, magnetic refrigeration materials, optical fiber, magneto-optical storage materials, giant magneto-resistance materials, lasers, superconductor materials and dielectric materials. They are widely used in applications in aerospace, aviation, information technology, electronic, energy resources, medical and health sectors, etc. Table 5 shows recent consumption areas of rare earth elements [5].

It is in fact the rapid development in modern science and technology that propelled rare earth elements to their current status as a group of highly-coveted commodity. This is of course also in part due to the recent market quota imposed by the largest rare earth producer, China. The revival of previous or the opening of rare earth mining which include: Mount Pass, Nolans Project (Central Australia), Hoidas Lake Project (Northern Canada), Mount Weld (Australia), Thor Lake (Northern Territories), Nebraska and Kvanefjeld (Greenland) are expected to cater for global rare earths supply as well as reduce the market monopoly by China.

Table 5. Global rare earth elements deposits 2010 [4].

Country	Rare earth element deposits (tonne)	Rare earth elements deposits (%)
Brazil	52,597,000	32.32
China	36,000,000	22.12
CIS	19,000,000	11.68
Vietnam	14,800,000	9.10
Australia	13,420,500	8.25
USA	11,771,600	7.23
Greenland	4,890,000	3.01
Canada	4,389,500	2.70
India	3,100,000	1.91
South Africa	1,254,000	0.77
Kenya	972,000	0.60
Kyrgyzstan	291,000	0.18
Turkey	130,500	0.08
Malawi	107,000	0.07
Brundi	1000	0.00

Table 6. Distribution of rare earth elements in selected deposits [4].

Atomic no.	Elements	Mountain Pass	Bayan Obo	Green Cove Spring	Lehat	Longnan	Xunwu	Bear Lodge	Strange Lake
57	La	33.8	23	17.5	1.2	1.8	43.3	30.4	4.6
58	Ce	49.6	50	43.7	3.1	0.4	2.4	45.5	12
59	Pr	4.1	6.2	5	0.5	0.7	7.1	4.7	1.4
60	Nd	11.2	18.5	17.5	1.6	3	30.2	15.8	4.3
62	Sm	0.9	0.8	4.9	1.1	2.8	3.9	1.8	2.1
63	Eu	0.1	0.2	0.2	-	0.1	0.5	0.4	0.2
64	Gd	0.2	0.7	6	3.5	6.9	4.2	0.7	2.5
65	Tb	-	0.1	0.3	0.9	1.3	-	0.1	0.3
66	Dv	-	0.1	0.9	8.3	7.5	-	0.1	8.2
67	Ho	-	-	0.1	2	1.6	-	-	1.7
68	Er	-	-	-	6.4	4.9	-	-	4.9
69	Tm	-	-	-	1.1	0.7	-	0.01	0.7
70	Yb	-	-	0.1	6.8	2.5	0.3	0.5	4
71	Lu	-	-	-	0.1	0.4	0.1	0.01	0.4
29	Y	0.1	-	2.5	61	65	8	0.01	52.7

Table 7. Current producers out of China [4].

Company	Location	Country	Current capacity (typ REO)	Target capacity after 2015 (typ REO)
Molycorp Minerals	Mountain Pass, CA	USA	3000	40000
Lovozersky Mining Company	Kamasurt Mine, Kola Peninsula	Russia	3000-4400	15000
Solikamsk Magnesium Works	Solikamsk Processing Plant, Urals	Russia		
Indian Rare Earths	Orissa, Tamil Nadu & Kerala	India	100	10000
Toyota/Sojitz/ Gov. Of Vietnam		Vietnam	1800-2000	>2000
Neo		Thailand		
Lynas/Malaysia	Gebeng, Malaysia	Malaysia		
Industrias Nucleares do Brasil S/A (INB)	Buena Norte	Brazil	1500	>1500
Total			9500-11000	>68500

Table 8. Up-coming producers [4].

Company	Location	Countries	2011-2013 Capacity (typ REO)	Target capacity after 2010 (typ REO)
Lynas Corp	Mount Weld, Western Australia & a processing plant in Gebeng, Malaysia	Australia	10500	21000
Rareco/ Great Western Minerals Group	Steenkramskaal, South Africa	South Africa/ Canada	3000	5000
Sumitomo/ Kazatomprom/ SARECO JV	Kazakhstan	Kazakhstan/Japan	3000	15000
Toyota/ Sojitz/ Govt. of Vietnam	Dong Pao, Vietnam	Vietnam/ Japan	300	5000
Toyota/ Indian Rare Earths	Orissa, India	India/ Japan	5000	10000
Mitsubishi/ Neo Material Technologies	Pitinga, Brazil	Japan/USA/ Canada /Brazil	500	1000
Alkaline Resources	Dubbo, NSW, Australia	Australia	2600	6000
Total			24900	63000

Table 9. Recent consumption areas of rare earths [5].

Usage area	China, 2007 (%)	USA, 2008 (%)
Permanent magnets	30.7	5.0
Metallurgical applications & alloys	15.2	29.0
Petrochemical, chemical catalysts	10.4	14.0
Glass polishing powders	10.2	-
Hydrogen storage alloys for batteries	8.5	-
Phosphors for fluorescent lighting, flat screen displays for computer monitors, colour televisions, radar, X-ray intensifying film	6.2	12.0
Glass & ceramic additives	4.5	6.0
Automotive catalysts, catalytic converters	3.7	9.0
Electronics	-	18.0
Petroleum refining catalysts	-	4.0

SPECIFIC AREAS OF APPLICATIONS

Rare earths magnets

Depletion of non-renewable natural resources resulted in ever-increasing prices of these commodities, affecting households and industries worldwide. Besides, non-renewable resources also produce emmisions harmful to both mankind and environment. Although alternative energy resources such as nuclear power can be tapped into, fear and controversy are attached to this group of power supply as proven by catastrophical hazards shown in the history. Therefore, generation of renewable energy which are sustainable with minimal risks to the entire nature has been identified as the solution to the above concerns.

WWS (wind, water, solar power) fulfill requirements that the global energy system remains clean even with large increases in population and economic activities in the long run. These technologies have essentially zero emissions of greenhouse gases and air pollutants as well as low impacts on wildlife, water and land pollution. There are also no significant waste-disposal or terrorism risks associated, and are based on primary resources that are indefinitely renewable or recyclable [11,12]. One way to implement these technologies will be through use of very strong permanent magnets.

Rare earth (RE)-based magnets are the strongest permanent magnet although these magnets are susceptible to brittleness and corrosion. This enables the production of lighter, smaller and more efficient electric motors and generators, leading to fuel economy as well as efficient energy generation. In the past decade or more, researches were carried out intermittenly on these magnets, mostly by Japanese researchers. A sensible intepretation to this would be that the Japanese are constantly sourcing sustainable energy resources besides their advanced state

of robotics industry. A search on literatures, however show that these intermittent researches have picked up significantly in the past two years. This is of course, a direct response due to the Fukushima nuclear plant incident, whereby it is realised that clean technology should be thoroughly explored.

There are two types of rare earth magnets, samarium-cobalt (Sm-Co) and the neodymium-based magnets. Magnetic field of rare earth magnets when compared to ferrite and ceramic magnets are: 1.4 Teslas for rare earth magnets and 0.5-1 Tesla for ferrite or ceramic magnets. Rare earth magnets have Curie temperatures below room temperature (in pure form magnetism only appears at low temperatures) and are able to form compounds with transition metals (Fe, Ni, Co) which have Curie temperatures above room temperature. Besides, they also possess very high magnetic anisotropy (easy to magnetize in one particular direction but resists being magnetized in any other direction).

Sintered NdFeB magnets have the highest values of the maximum energy product of any magnet, thus are suitable for use in motors for various applications [13]. It was in the early 1980s that General Motors used an alternative way to manufacture magnet, by using magnetic powder which could be mixed with rubber, injected into molds and sintered. The manufacturing of this magnet instead of using solid iron magnet requires the rare earth element, Nd. The use of powder requires less metal, thereby reducing overall weight of vehicles [1]. In effort to reduce vehicle emission as well as improve fuel efficiency, the reduction in overall weight of a vehicle is required. It was reported that a reduction of 10% in vehicle weight translates to a 5.5% improvement in fuel economy [14]. This can be achieved through innovative material modification of: car body skin [15], crank shaft, gears as well as motors [16]. Figure 3 shows usage of small motors in a vehicle [16].

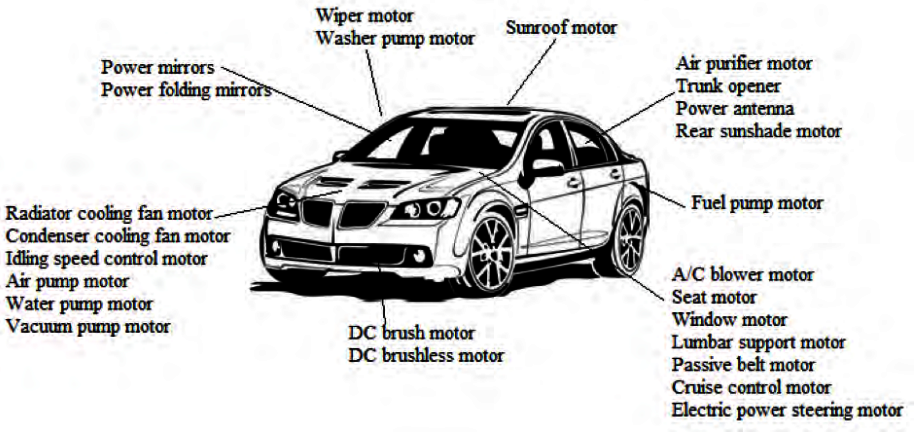

Figure 3. Small motors used in a vehicle [16].

Besides its applicability in motors for electrical, household and automotive usage, the NdFeB magnets are also currently targeted for use as gearless generators in wind turbines to convert the energy of the wind into electricity [4, 17].

Although gaining popularity and importance in hybrid vehicles especially, NdFeB magnets suffer demagnetization at operational temperatures of various motors which may reach as high as 746ºC [18] as well as being brittle and susceptible to corrosion. Additions of Ti [19], Cu, Al [20] as well as Ga, Zn, Sn, Co, W, Mo, Zr, V and Nb were carried out by some researchers to improve the magnetic properties of the NdFeB magnets. The magnetic properties of these magnets are strongly dependent on their microstructures, in particular the grain size of the $Nd_2Fe_{14}B$ phase and the grain boundary phases [21]. A team of researchers [13] claimed that heavy rare earth elements are coercivity-enhancing elements that act by increasing the anisotropy field of each grain (the $Nd_2Fe_{14}B$ phase) in the magnet by replacing Nd. Hu *et al*. (2008) researched on the effect of Co addition on the impact toughness of NdFeB magnets but the results were not very conclusive [22].

Rare earths in electronics and ICT

RE elements are used in video and audio devices, portable devices such as music players, cellphones, smartphones, tablets and laptops. These elements are only needed to be added in minute amounts in order to successfully cater to the purpose of application.

As mentioned in the conventional application of rare earths, these elements possess unique optical properties that enable them to reduce glare, filter out certain range of colours, etc and thus are used for display purposes. The rapid displacement of bulky television sets with their plasma, LCD and LED counterparts necessitates further exploration into phosphor substances, which can be produced by most rare earth elements. These substances are used in radar screens, glow-in-the-dark mechanisms, cathode ray tubes, plasma video display screens and sensors. Various researches to obtain better quality LEDs are listed in [23-32]. In aviation, aircraft instrument panel requires glare-free illumination which could be attained through use of rare earth glasses [33].

The thrust of rare earths onto the list of most needed commodity in electronics is largely due to the market trend and demand for portable devices. These devices not only need to be multi-functional but should also be trendy enough to attract certain target niches. Thus the VLSI needed for miniaturization requires high reliability (interconnections) to prevent failure caused by transporting, mishandling during consumer usage etc. The display screens of these devices also need to have high resolution with sharp contrast to attract the consumers of a rather costly technology that plays dual role: function plus aesthetics. Solders act as interconnection materials in an electronic package on chip as well as board level. As such, the reliability of

solder joint is critical because they provide electrical, thermal continuity as well as structural integrity [34].

The ban of toxic Pb (lead)-containing solders [35] which came into effect on 1 July 2006 by electronic packaging industries worldwide has intensified the search for suitable replacement materials for Pb-containing solders. Pb-free solders display inferior properties and reliability compared to Pb-containing solders. Numerous researches were carried out in the past few years, among which are doping of solders with rare earth elements [36-40]. Most of the published results reported that a small amount of rare earth elements can greatly enhance the properties of materials through grain refinement, formation of intermetallics and suppression of grain boundary sliding.

Rare earths in metallurgy and alloying

In metallurgy, RE elements are well known grain refiners and are usually added to materials as part of strengthening mechanism procedure. Rare earth elements are added to steels [41-43] to obtain desirable microstructures and properties through microstructure modification by the rare earth elements. When added to magnesium alloys rare earths aid in improving hot workability [44], mechanical properties [45-47], thermal fatigue behaviour [48] as well as corrosion resistance [49]. In aluminium alloys, the addition of rare earth elements led to grain refinement [15, 50, 51] which increases the hardness of these alloys. Tribology and mechanical properties of cast aluminium-silicon alloys are often controlled through microstructure modification by adding trace rare earth elements [52-54]. These are significant improvements since this category of alloys are usually used in engine blocks subjected to high temperature and abrasive conditions.

For corrosion protection and resistance purposes various contributions by the rare earth elements doping into alloys have been reported [55-59].

Rare earths in batteries

Certain alloys of rare earth elements have the ability to absorb hydrogen and store it as metal hydride, making these elements a must in the production of nickel metal hydride (NiMH) batteries [60]. NiMH batteries are mainly used in rechargeable AA and AAA batteries for domestic applications, power tools and hybrid electric vehicles. About 7% of a typical NiMH battery is made up of rare earth elements such as cerium, lanthanum, neodymium and praseodymium, making up to about 1 gram of rare earth metals per AAA battery, 60 grams for a household power tool and 2 kg for a hybrid electric vehicle battery [61].

Toyota pioneered the full hybrid mass produced passenger car with its Prius. A typical NiMH battery for a vehicle, with the size and performance of the Toyota Prius, uses between 12-20 kg of lanthanum containing some neodymium and

praseodymium in its overall construction. Additionally the battery uses up to five times as much nickel metal as it does lanthanum and a small amount of cobalt. Thus the manufacturing of a NiMH battery pack requires a lot of rare metals as well as a lot of engineering.

The difference between a NiMH battery and a lithium-ion battery is primarily that the NiMH battery has been used in over a million full hybrids, whereby most of the full hybrid cars built in the last decade primarily by Toyota, Honda, and Ford are still on the road and provide daily testimony to the reliability of the NiMH battery pack for full hybrid operation [62].

Although the current interest for rare earths use is now in NiMH batteries, rare earth elements are also added to other types of batteries such as redox flow battery [63] and lithium-ion batteries. It was reported that the doping of lithium-ion batteries with lanthanum resulted in reduction of crystal size to the nanoscale, increase of conductivity and diffusion rate of lithium ion. The results confirmed that rare earth doping is an effective method for improving electrochemical properties of the promising alternative cathode [64].

Rare earths in solar cell

Fossil fuels are still the main energy resources that drive the economies of the world today. Predicted exhaustion and limited resources of fossil fuels, combined with energy-hungry economies due to modernization and industrialization, coupled with the emission of environmental harmful greenhouse gases have stimulated development of sustainable renewable energy sources. Among many others, solar power is one of the most promising renewable energy sources as an alternative to our continued dependence on fossil fuels.

Conventional solar cells are manufactured with high purity and expensive silicon materials, using production methods that consumed high amounts of energy. For these reasons, silicon solar cells have not become very popular even though their conversion efficiency has reached between 15% and 20% [65, 66]. Gratzel *et al*. in 1991, had formulated in their lab an innovative solar cell based on dye-sensitized colloidal TiO_2 that is set to become a low-cost alternative to the conventional silicon-based solar cell [67]. Since the first introduction of dye-sensitized solar cell (DSSC) by the Gratzel's group, the improvement on conversion efficiency of DSSCs has been reported every year. Current focus and interest to extract higher conversion efficiency on DSSCs, aiming to overtake the best conversion efficiency achieved by silicon-based solar cell, falls in four major areas [68]: development of sensitizing materials; new anodic materials; use of various electrolytes; and modification of anodic materials.

To improve on the harvesting of incident light, thus increase the photocurrent of the DSSC, many sensitizing materials have been synthesized. However, the best of these sensitizing dyes can only absorb visible light in the wavelength

region of 300-800 nm, so most of the solar ultra-violet irradiation is unutilized [69]. If the ultraviolet irradiation can be transferred to visible light by conversion luminescence, and is reabsorbed by the dye in DSSC, more solar irradiation may be utilized with enhanced photocurrent. On the other hand, the DSSC photovoltage depends on the energy level of the electron in the anodic materials. If the energy level can be heightened by p-type doping on the anodic materials, the DSSC photovoltage will be increased.

Rare-earth-doped compounds as luminescence media have been the focus of extensive research lately and have wide application [70]. Among the many lanthanide ions, europium and samarium ions have been recognized as the most efficient down-converting materials that convert ultraviolet light to red and orange-red emissions, respectively [71, 72]. The use of these down-converting rare-earth materials as dopant was reported to have improved efficiency for the TiO_2 photoelectrodes.

A study on using rare-earth materials as dopant had demonstrated the improvement of the photoelectric performance of DSSC by introducing europium-doped yttria (Y_2O_3:Eu^{3+}) into the TiO_2 electrode [73]. Holmium doping on DSSC also leads to increased photocatalytic activity of TiO_2 by increasing the surface area of TiO_2 nanoparticles, and inhibit the growth of crystallite size and the anatase-rutile phase transformation [74]. Many other rare-earth materials used in the improvement of conversion efficiency in DSSC have been investigated, which include lanthanum (La), cerium (Ce), erbium (Er), promethium (Pr), gadolinium (Gd), neodymium (Nd) and samarium (Sm) [75].

RECOVERY OF RARE EARTHS ELEMENTS FROM SCRAPS/WASTE

Through the many uses of rare earths, there is bound to be scraps or waste of these materials after the projected lifespan of products or from completed processes utilizing rare earths as raw materials. Although not actively practiced on an industrial scale, there are some preliminary researches to recover or retrieve rare earth elements from used materials as detailed in [76-78].

On a positive note, Umicore of Belgium and Rhodia of France have jointly developed a process for the recycling of rare earth elements from NiMH rechargeable batteries. The process can service the entire range of NiMH batteries – from portable applications to batteries used in hybrid electric vehicles. Recovery of rare earth materials was expected to have begun by end of 2011. The process will be applied to NiMH cells treated at Umicore's new battery recycling plant in Hoboken. Following the separation of nickel and iron from the rare earths, the company will process the rare earths into a high-grade concentrate that will be refined and formulated into rare earth materials at Rhodia's plant at La Rochelle.

This is reported to be the first industrial process involving NiMH batteries [61].

This provides the insight that it may be possible to recycle these commodities in the future for sustainability and minimize harm to the living and environment due to excessive mining and processing activities. It may also maintain commodity prices at a reasonable level as there would be sufficient supply. This implicates that rare earths elements are potential candidates not only as purveyor for green technology applications but also fulfill the conditions of clean technology. Application of clean technology includes recycling, renewable energy, green transportation as well as any energy conserving practices with minimal pollution to the environment. Besides being environmental friendly, these applications should fulfill or even improve the operational performance, productivity and efficiency in their respective areas of applications. Prospects of recycling and recovery of rare earth elements will certainly close the loop in the rare earth production cycle.

POPULARITY AND RESEARCH TREND IN RARE EARTHS

Currently, global energy consumption is mainly derived from non-renewable natural resources which are getting scarce on top of the ever-increasing prices of these commodities. To conserve natural resources, there are increasing calls and implementations on clean technology. Application of clean technology includes recycling, renewable energy, green transportation as well as any energy conserving practices with minimal pollution to the environment. Besides being environmental friendly, these applications should fulfill or even improve the operational performance, productivity and efficiency in their respective areas of applications.

It is indisputable that by looking at areas of application of rare earth elements these elements are crucial in the development of green technology. As the petroleum price hit a record high in 2008 [7], there is much demand for hybrid vehicles, which can run at mileage of 20.4km/liter for city driving. However, there was a shortage of these vehicles due to shortage of rechargeable NiMH batteries requiring the use of lanthanum. It was reported that China is the world leader in electric batteries and wind turbine manufacturing and with increased internal demand, its export of rare earth elements decreased to 30,000 tons in 2009 compared with 45,000 tons in 2008 and 60,000 tons in 2002.

It is noted that most researches on magnets in the past decade has been carried out by Japanese researchers. This observation is not surprising considering that Japan is heavily reliant on alternative energy resources. However, an analysis on research trends in REs shows that today China is the top country in terms of RE research when compared among China, Japan and USA [79]. This is a direct consequence from the fact that China currently supplies 97% of the global RE,

especially the heavy REs. Magnets researches have been carried out since the 1990s but these were in no way comparable to the intensity research in other areas. The researches on magnets start to pick up again in this two years, possibly due to the awareness of the danger of nuclear technology as power resource as well as the increasing application of clean technology.

REFERENCES

1. Ragheb M. and Tsoukalas L. (2010) The Future Thorium Energy Economy Google Campus. Proceedings of the 2nd Thorium Energy Alliance Conference, Mountain View, California, USA, March 29-30, 2010.
2. Xu G. (1995) Rare earths (in Chin.). *China Metallurgical Industry Press* **2**.
3. Brady G., Clauser H. and Vaccari J. (1997) *Materials Handbook*, 14th edn, Mc-Graw Hill.
4. Chen Z. (2011) Global rare earth resources and scenarios of future rare earth industry. *Journal of Rare Earths* **29(1)**: 1–6.
5. Hedrick J.B. (2007) *Minerals Yearbook.*
6. China Rare Earth Industry Report, 2011-2012 - new market research report, London 3/16/2012 11:03 AM GMT (TransWorldNews): http://www.transworldnews.com/1033170/c1/china-rare-earth-industry-report-2011-2012-new-market-research-report
7. Walmer M.J., Liu P. and Dent (2009) Current status of permanent magnet industry in the United States. *Proceedings of 20th International Workshop on Rare earth permanent magnets and their applications, 8-10 September, 2009*, Crete, Greece.
8. Chegwidden J. and Kingsnorth D. (2010) Rare earths: facing the uncertainties of supply. *The Sixth International Rare Earths Conference, Hong Kong, China, November 2010.*
9. Watanabe Y. (2010) Japan's search for alternative rare earths supply. *The Sixth International Rare Earths Conference, Hong Kong, China, November 2010.*
10. Levine A.K and Palilla F.C. (1964) A new, highly efficient red-emitting cathodoluminescent phosphor (YVO_4:Eu) for color television. *Applied Physics Letters* **5 (6)**: 118-120.
11. Jacobson M.Z. and Delucchi M.A. (2011) Providing all global energy with wind, water and solar power, Part I: Technologies, energy resources, quantities and areas of infrastructure, and materials. *Energy Policy* **39**: 1154–1169.
12. Jacobson M.Z. (2009) Review of solutions to global warming, air pollution, and energy security. *Energy and Environmental Science* **2**:148-173.
13. Oono N., Sagawa M., Kasada R., Matsui H. and Kimura A. (2011) Production of thick high-performance sintered neodymium magnets by grain boundary diffusion treatment with dysprosium-nickel-aluminium alloy. *Journal of Magnetism & Magnetic Materials* **323**: 297–300.
14. Morita A. (1998) Aluminium alloys for automotive applications. *Aluminium Alloys* **1**: 25–32.
15. Daud A.R. and Wong K.M.C (2004) The effect of cerium additions on dent

resistance of Al–0.5Mg–1.2Si–0.25Fe alloy for automotive body sheets. *Materials Letters* **58(20):**2545–2547.

16. Honkura Y. (2006) Automotive motor innovation with anisotropic bonded magnet-MAGFINE. *Proceedings of the 19th International Workshop on Rare Earth Permanent Magnets & Their Applications*: 231–239.
17. Pinilla M, and Martinez S. (2011) Optimal design of permanent-magnet direct-drive generator for wind energy considering the cost uncertainty in raw materials. *Renewable Energy*: 1-10.
18. Satoh H., Akutsu A., Miyamura T. and Shinoki H. (2004) Development of traction motor for fuel cell vehicle. *SAE Technical Paper Series*: 1-9.
19. Spyra M. and Leonowicz M. (2008) Improvement of the magnetic properties of low-neodymium magnets by minor addition of titanium. *Journal of Magnetism & Magnetic Materials* **320**: 46–50.
20. Ni J., Ma T., and Yan M. (2011) Changes of microstructure & magnetic properties of Nd-Fe-B sintered magnets by doping Al-Cu. *Journal of Magnetism & Magnetic Materials* **323**:2549–2553.
21. Saito T. (2010) Electrical resistivity and magnetic properties of Nd–Fe–B alloys produced by melt-spinning technique. *Journal of Alloys & Compounds* **505**: 23–28.
22. Hu Z.H., Lian F.Z., Zhu M.G. and Li W. (2008) Effect of Co on the thermal stability and impact toughness of sintered Nd Fe B magnets. J*ournal of Magnetism & Magnetic Materials* **320**: 2364–2367.
23. Rao Y.X., Zhou H.X. and Li Y. (2011) Pr^{3+}-doped Li_2SrSiO_4 red phosphor for white LEDs. *Journal of Rare Earths* **29(3):**198–201.
24. Yu H., Gao G., Kong L., Li G., Gan S. and Hong G. (2011) Synthesis and luminescence properties of a novel red-emitting phosphor $SrCaSiO_4$: Eu^{3+} for ultraviolet white light-emitting diodes. *Journal of Rare Earths* **29(5)**: 431–435.
25. Bednarkiewicz A., Wawrzynczyk D., Nyk M. and Samoć M. (2011) Tuning red-green-white up-conversion color in nano $NaYF_4$:Er/Yb phosphor. *Journal of Rare Earths* **29(12):**1152–1156.
26. Guan L., Jin L., Guo S., Liu Y., Li X., Guo Q., Yang Z. and Fu G. (2010) Luminescent properties of Eu^{3+}-doped $BaZrO_3$ phosphor for UV white light emitting diode. *Journal of Rare Earths* **28(1)**: 292–294.
27. Guan L., Wang Y., Chen W., Jin L., Li X., Guo Q., Yang Z. and Fu G. (2010) Fabrication and luminescent properties of red phosphor M3BO6:Eu^{3+}(M=La,Y) *Journal of Rare Earths* **28(1)**: 295–298.
28. Huang J., Zhou L., Liang Z., Gong F., Han J. and Wang R. (2010) Promising red phosphors LaNbO4:Eu^{3+}, Bi^{3+} for LED solid-state lighting application. *Journal of Rare Earths* **28(3)**: 356–360.
29. Zhou L., Huang J., Yi L., Gong M. and Shi J. (2009) Luminescent properties of $Ba_3Gd(BO_3)$ 3:Eu^{3+} phosphor for white LED applications. *Journal of Rare Earths* **27(1)**: 54–57.
30. Chen L., Jiang Y., Yang G., Zhang G., Xin X. and Kong D. (2009) New red phosphor (Y,Gd,Lu)BO3: Eu^{3+} for PDP applications. *Journal of Rare Earths* **27(2):** 312–315.
31. Zhang A., Pan Q., Jia H., Liu X. and Xu B. (2012) Synthesis, characteristic and intramolecular energy transfer mechanism of reactive terbium complex in white light emitting diode. *Journal of Rare Earths* **30(1)**: 10–16.

32. Shi L., Li Y., Cao H., Guan Y. and Ma Y. (2012) Synthesis of novel europium complexes and their photoluminescence properties. *Journal of Rare Earths* **30(1)**: 17–20.
33. He D., Yu C., Cheng J., Li S. and Hu L. (2011) Energy transfer between Gd^{3+} and Tb^{3+} in phosphate glass. *Journal of Rare Earths* **29 (1)**: 48–51.
34. Yang X. and Nassar S. (2005) Effects of lanthanum addition on corrosion resistance of hot-dipped galvalume coating. *Mechanics of Materials* **37**: 801–814.
35. Zeng K. and Tu K.N. (2002) Six cases of reliability study of Pb-free solder joints in electronic packaging technology. *Materials Science & Engineering R* **38**: 55–105.
36. Wang J., Xue S., Han Z., Yu S., Chen Y., Shi Y. and Wang H. (2009) Effects of rare earth Ce on microstructures, solderability of Sn–Ag–Cu and Sn–Cu–Ni solders as well as mechanical properties of soldered joints *Journal of Alloy and Compounds* **467**: 219–226.
37. Lin H. and Chuang T. (2010) Effects of Ce and Zn additions on the microstructure and mechanical properties of Sn–3Ag–0.5Cu solder joints. *Journal of Alloy and Compounds* **500**: 167–174.
38. Chen Z., Shi Y., Xia Z. and Fan Y. (2002) Study on the microstructure of a novel lead-free solder alloy SnAgCu-RE and its soldered joints. *Journal of Electronic Materials* **31(10)**: 1122–1128.
39. Zhao X., Zhao M., Cui X., Xu T. and Tong M. (2007) Effect of cerium on microstructure and mechanical properties of Sn-Ag-Cu system lead-free solder alloys. *Transactions of Nonferrous Metals Society of China***17**: 805–810.
40. Wu C., Yu D., Law C. and Wang L. (2004) Properties of lead-free solder alloys with rare earth element additions. *Materials Science & Engineering R* **44**: 1–44.
41. Wu Y. and Yan M. (2011) Effects of lanthanum and cerium on low temperature plasma nitrocarburizing of nanocrystallized 3J33 steel. *Journal of Rare Earths* **29(4)**:383–387.
42. Hao F., Liao B., Li D., Liu L., Dan T., Ren X. and Yang Q. (2011) Effects of rare earth oxide on hardfacing metal microstructure of medium carbon steel and its refinement mechanism. *Journal of Rare Earths* **29 (6)**: 609–613.
43. Wang X. and Chen W. (2010) Influence of cerium on hot workability of 00Cr25Ni7Mo4N super duplex stainless steel. *Journal of Rare Earths* **28(2)**: 295–300.
44. Ma M., He L., Li X., Li Y. and Zhang K. (2011) Hot workability of Mg-9Y-1MM-0.6Zr alloy. *Journal of Rare Earths* **29(5)**: 460–465.
45. Yang M., Qin C., Pan F. and Zhou T. (2011) Comparison of effects of cerium, yttrium and gadolinium additions on as-cast microstructure and mechanical properties of Mg-3Sn-1Mn magnesium alloy. *Journal of Rare Earths* **29(6)**: 550–557.
46. Wang Z., Xu Y., Wang Z., Cheng J., Kang B. and Zhu J. (2011) Solidification behavior, microstructure and tensile properties of ZK60-Er magnesium alloys. *Journal of Rare Earths* **29 (6)**:558–561.
47. Dong H., Wang L., Wu Y. and Wang L. (2011) Preparation and characterization of Mg-6Li and Mg-6Li-1Y alloys. *Journal of Rare Earths* **29(7)**: 645–649.
48. Zhang Q., Li Q., Jing X. and Zhang X. (2010) Microstructure and mechanical properties of Mg-10Y-2.5Sm alloy. *Journal of Rare Earths* **28(1)**: 375–377.

49. Bayani H. and Saednoori E. (2009) Effect of rare earth elements addition on thermal fatigue behaviors of AZ91 magnesium alloy. *Journal of Rare Earths* **27(2)**: 255–258.
50. Daud A. and Wong K. (2003) The effect of Ce, La and Zr additions on the hardness of an as-cast AA6016 alloy for automotive applications.*The National Symposium on Science & Technology*, 27-30 July 2003.
51. Wong K. and Daud A. (2004) The mechanical properties of a 6XXX alloy containing cerium. *Proceedings of the First Metallurgy Seminar, 27 Nov 2004*, Bangi:119–124.
52. Harun M., Talib I. and Daud A. (1996) Effect of element additions on wear property of eutectic aluminium-silicon alloys. *Wear***194**: 54–59.
53. Shi W., Gao B., Tu G., Li S., Hao Y. and Yu F. (2010) Effect of neodymium on primary silicon and mechanical properties of hypereutectic Al-15%Si alloy. *Journal of Rare Earths* **28(1)**: 367–370.
54. Hou D., Li D., Han L. and Ji L. (2011) Effect of lanthanum addition on microstructure and corrosion behavior of Al-Sn-Bi anodes. *Journal of Rare Earths* **29(2)**: 129–132.
55. Lin G., Zhou Y., Zeng J., Zou Y., Liu J. and Sun L. (2011) Influence of rare earth elements on corrosion behavior of Al-brass in marine water. *Journal of Rare Earths* **29(7)**: 638–644.
56. Kiyota S., Valdez B., Stoytcheva M., Zlatev R. and Bastidas J. (2011) Anticorrosion behavior of conversion coatings obtained from unbuffered cerium salts solutions on AA6061-T6. *Journal of Rare Earths* **29(10)**: 961–968.
57. Sun H., Wang H. and Meng F. (2011) Study of corrosion protection of the composite films on A356 aluminum alloy. *Journal of Rare Earths* **29(10)**: 991–996.
58. Yun A., Feng L. and Wang Z. (2010) Influence of yttrium addition on properties of Mg-based sacrificial anode. *Journal of Rare Earths* **28(1)**: 393–395.
59. Yang D., Chen J., Han Q. and Liu K. (2009) Effect of lanthanum addition on corrosion resistance of hot-dipped galvalume coating. *Journal of Rare Earths* **27(1)**: 114–118.
60. Molycorp website, accessed 28 February 2012 <http://www.molycorp.com/*GreenElements*/RareEarthsManyUses/BatteryTechnologies.aspx>.
61. Editorial board, *Recycling International, 17 June 2011: Rare earth metals extracted from rechargeable batteries*, <http://www.recyclinginternational.com/recycling-news/3692/e-waste-and-batteries/belgium-france/rare-earth-metals-extracted-rechargeable-batteries>.
62. Lifton J. (2012) accessed 28 February <https://www.gplus.com/consumer-vehicles/insight/peugeot-expands-use-of-rare-earth-based-batteries-with-first-diesel-hybrid-42278>.
63. Xie Z., Zhou D., Xiong F., Zhang S. and Huang K. (2011) Cerium-zinc redox flow battery: Positive half-cell electrolyte studies. *Journal of Rare Earths*, **29(6)**: 567–573.
64. Luo S., Tian Y., Li H., Shi K., Tang Z. and Zhang Z. (2010) Influence of lanthanum doping on performance of $LiFePO_4$ cathode materials for lithium-ion batteries. *Journal of Rare Earths* **28(3)**: 439–442.
65. Li B., Wang L.D., Kang B.N., Wang P. and Qiu Y. (2006) Review of recent progress

in solid-state dye-sensitized solar cells. *Solar Energy Materials and Solar Cells* **90**: 549-573.

66. Gunes, S. and Sariciftci N.S. (2008) Hybrid solar cell. *Inorganica Chimica Acta Volume* **361**: 581-588.
67. O'Regan B. and Gratzel M. (1991) A low cost, high efficiency solar cell based on dye-sensitized colloidal TiO_2 films. *Nature* **535**: 737-740.
68. Zalas M., Walkowiak M. and Schroeder G. (2011) Increase in efficiency of dye-sensitized solar cells by porous TiO_2 layer modification with gadolinium-containing thin layer. *Journal of Rare Earths* **29(8)**: 783–786.
69. Gratzel M. (2001) Review article photoelectrochemical cells. *Nature* **414**: 338-344.
70. Wang W., Widiyastuti W., Ogi T. and Lenggoro I. (2007) Correlations between Crystallite/Particle Size and Photoluminescence Properties of Submicrometer Phosphors. *Chemistry of Materials* **19**: 1723-1730.
71. Saif M. (2007) Luminescence based on energy transfer in silica doped with lanthanide titania ($Gd_2Ti_2O_7$:Ln^{3+}) [$Ln^{3+} = Eu^{3+}$ or Dy^{3+}]. *Journal of Photochemistry and Photobiology A: Chemistry.* **205**: 145–150.
72. Li H.Y., Wu J., Huang W., Zhou Y.H., Li H.R., Zheng Y.X. and Zuo J.L. (2009) Synthesis and photoluminescent properties of five homodinuclear lanthanide ($Ln^{3+} = Eu^{3+}$, Sm^{3+}, Er^{3+}, Yb^{3+}, Pr^{3+}) complexes. *Journal of Photochemistry and Photobioogy. A: Chemistry.* **208:**110–116.
73. Wu J., Xie G., Lin J., Lan Z., Huang M. and Huang Y. (2010) Enhancing photoelectrical performance of dye-sensitized solar cell by doping with europium-doped yttria rare-earth oxide. *Journal of Power Sources* **195**: 6937–6940.
74. Shi J.W., Zheng J.T. and Wu P. (2009) Preparation, characterization and photocatalytic activities of holmium-doped titanium dioxide nanoparticles. *Journal of Hazardous Materials* **161**: 416–422.
75. Xu A.W., Gao Y. and Liu H.Q. (2002) The preparation, characterization, and their photocatalytic activities of rare-earth-doped TiO_2 nanoparticles. *Journal of Catalysis*. **207**: 151–157.
76. Kim J., Byeon M., Kang W., Kwang T. and Cho W. (2011) Recovery of cerium from glass polishing slurry. *Journal of Rare Earths* **29(11)**: 1075–1078.
77. Xu T., Zhang X., Lin Z., Lu B., Ma C. and Gao X. (2010) Recovery of rare earth and cobalt from Co-based magnetic scraps. *Journal of Rare Earths* **28(1)**: 485–488.
78. Zhao F., Hu Z. and Che L. (2010) Recovery of rare earth and cobalt from Co-based magnetic scraps. *Journal of Rare Earths* **28(1)**: 523–524.
79. Adachi G., Imanaka N. and Tamura S. (2010) Research trends in rare earths: A preliminary analysis. *Journal of Rare Earths* **28(6)**: 843–846.